Justus-Liebig-University Giessen
Faculty 08 (Biology and Chemistry)
Institute for Animal Physiology
Department of Animal Physiology and Molecular Biomedicine

JUSTUS-LIEBIG-UNIVERSITÄT GIESSEN

Visualization of the secondary olfactory pathway in *tubb2b* promoter-driven transgenic *Xenopus laevis* larvae

Dissertation

for the degree of Doctor rerum naturalium

(Dr. rer. nat.)

Submitted by

Daniela Daume

Dean: Prof. Dr. Holger Zorn

1st Reviewer: Prof. Dr. Ivan Manzini

2nd Reviewer: Prof. Dr. Reinhard Lakes-Harlan

“Alles was wir in Worte fassen können,
können wir hinter uns lassen.”

Sokrates

Table of contents

Abstract

The olfactory system of vertebrates consists of an olfactory epithelium containing olfactory sensory neurons that send axons to the olfactory bulb (OB), where they are connected to interneurons and projection neurons (PNs) via structures called glomeruli. PNs are the first relay station of olfactory information processing and are directly connected with their axons to higher brain regions. Among vertebrates the morphology, molecular characteristics, position in the OB, and axonal projections of PNs vary. In the olfactory system of larval *Xenopus laevis*, two odor-processing streams with different molecular and functional characteristics exist. Those streams terminate in a lateral and medial glomerular cluster within the ventral OB. It is not known whether these streams are continuous within PNs and higher olfactory processing centers. In this work, I analyzed the morphology of lateral and medial PNs and compared their structure as well as axonal projection pattern. For the visualization of neurons in the forebrain I used transgenic *tubb2b*-Katushka *Xenopus laevis* tadpoles. In this transgenic line the *tubb2b* promoter drives the expression of the fluorescent protein Katushka. The *tubb2b* promoter expresses class II β-tubulin protein, which is part of microtubules in neurons of the frog. Although the *tubb2b* promoter is used in different transgenic frog lines, a thorough investigation of the expression pattern of *tubb2b* has not been done. Therefore, I performed a detailed analysis of the expression pattern of *tubb2b* in the whole forebrain including the olfactory system of larval *Xenopus laevis* at cellular resolution. I found that *tubb2b*-dependent fluorescence is not present in all neurons and thus cannot be used as a pan-neuronal marker. *tubb2b*-dependent fluorescence is present in the OB, parts of the basal ganglia, the amygdaloid complex, pallium, optic nerve, preoptic area, hypothalamus, prethalamus and thalamus. In the OB, *tubb2b*-dependent fluorescence is present in axons of olfactory sensory neurons from the nose, cells in the mitral cell layer, fibers of the extra bulbar olfactory system, but not in interneurons. I used the *tubb2b*-dependent expression to target PNs in the mitral cell layer of the OB for sparse cell electroporation. I labelled lateral and medial PNs and 3D reconstructed them for a detailed morphological analysis. I found that both PN populations share many morphological characteristics, but differ in the number of dendritic tufts. I then injected dye into the whole lateral and medial PN population to trace their axons and observed that lateral PNs have a different axonal projection pattern than medial PNs. Finally, I

performed functional multiphoton calcium imaging in *tubb2b*-GCaMP6s transgenic *Xenopus* larvae and was able to identify the lateral and central amygdala as higher olfactory processing centers. Together, this present work provides the first description of the larval secondary olfactory pathway in *Xenopus laevis* and a detailed map of the expression pattern of *tubb2b* in the larval forebrain.

Zusammenfassung

Das Riechsystem von Vertebraten besteht aus einem Riechepithel mit sensorischen Neuronen, die Axone in den olfaktorischen Bulbus (OB) senden und dort mit Interneuronen und Projektionsneuronen (PNs) über Strukturen, die Glomeruli genannt werden, verbunden sind. PNs sind die erste Verschaltungsstation olfaktorischer Informationsweiterleitung und sind auf direktem Wege mit ihren Axonen an höhere Hirnregionen gebunden. Unter Vertebraten variieren die Morphologie, molekulare Charakteristika, Position im OB und axonale Projektionen der PNs. Im olfaktorischen System von *Xenopus laevis* existieren zwei Duftstoff-Verarbeitungsbahnen mit unterschiedlichen molekularen und funktionalen Merkmalen. Diese Bahnen enden im lateralen und medialen glomerulären Cluster innerhalb des ventralen OB. Es ist nicht bekannt, ob sich diese Bahnen auch unter den PNs und höheren Hirnregionen weiterziehen. In dieser Arbeit habe ich die Morphologie von lateralen und medialen PNs analysiert und deren Struktur sowie axonale Projektionsmuster verglichen. Zur Visualisierung der Neurone im Vorderhirn habe ich transgene *tubb2b*-Katushka *Xenopus laevis* Kaulquappen verwendet. In dieser transgenen Linie steuert der *tubb2b*-Promotor die Expression des fluoreszierenden Proteins Katushka. Der *tubb2b*-Promotor exprimiert das Klasse II β-tubulin, welches Teil der Mikrotubuli in Neuronen des Frosches ist. Obwohl der *tubb2b*-Promotor oft in verschiedenen transgenen Frosch Linien verwendet wird, wurde bisher noch keine genaue Untersuchung des Expressionsmusters von *tubb2b* gemacht. Deshalb habe ich eine detaillierte Analyse auf zellulärer Ebene des Expressionsmusters von tubb2b im gesamten Vorderhirn, inklusive des olfaktorischen Systems von larvalen *Xenopus laevis* vorgenommen. Ich fand heraus, dass *tubb2b*-abhängige Fluoreszenz nicht in allen Neuronen zu finden ist und demnach nicht als pan-neuronaler Marker verwendet werden kann. *tubb2b*-abhängige Fluoreszenz befindet sich im OB, Teilen der Basalganglien, dem

amygdaloiden Komplex, Pallium, optischen Nerv, der präoptische Region, dem Hypothalamus, Präthalamus und Thalamus. Im OB befindet sich *tubb2b*-abhängige Fluoreszenz in Axonen der olfaktorischen sensorischen Neurone aus der Nase, Zellen in der Mitral-Zell-Schicht, Fasern des extrabulbären olfaktorischen Systems, jedoch nicht in Interneuronen. Für meine Einzel-Zell-Elektroporation in die Mitral-Zell-Schicht des OB konnte ich die *tubb2b*-abhängige Expression nutzen um PNs gezielt zu finden. Ich färbte laterale und mediale PNs und 3D rekonstruierte diese für eine detailliertere morphologische Analyse. Ich fand heraus, dass beide PN Populationen viele gleiche morphologische Merkmale teilen, sich aber in der Anzahl dendritischer Büschel unterscheiden. Dann habe ich Farbstoff in die gesamte laterale und mediale PN Population injiziert, um deren Axone zu verfolgen und beobachtete, dass laterale PNs ein anderes axonales Projektionsmuster besitzen als mediale PNs. Abschließend habe ich funktionelle Multiphotonen Kalzium Messungen in transgenen *tubb2b*-GCaMP6s *Xenopus* Larven gemacht und es war mir möglich die laterale und zentrale Amygdala als höhere olfaktorische Verarbeitungszentren zu identifizieren. Zusammenfassend zeigt die vorliegende Arbeit eine erste Beschreibung des larvalen sekundären olfaktorischen Verarbeitungswegs in *Xenopus laevis* und eine detaillierte Karte des Expressionsmusters von *tubb2b* im larvalen Vorderhirn.

Publication Information

My results about the pattern of *tubb2b*-dependent fluorescence in the larval *Xenopus laevis* forebrain is published in the journal “Frontiers of Neuroanatomy” (Daume et al., 2022).

Please note that figures 13-15 are identical with the figures 3-5 of the published manuscript. Figure 1 of the manuscript is shown here in two separate figures (Figures 11 and 12). Figure 2 of the manuscript is shown as Figure 25 in the discussion.

Publication:

Daume, D., Offner, T., Hassenklöver, T., and Manzini, I. (2022). Patterns of *tubb2b* promoter-driven fluorescence in the forebrain of larval *Xenopus laevis*. *Front. Neuroanat.* 16, 1–13. doi:10.3389/fnana.2022.914281.

Abbreviations

1-9, α, β, γ, δ	Projection fields of axons from the olfactory organ
Acc	Nucleus accumbens
ac	Anterior commissure
BST	Bed nucleus of the stria terminalis
CeA	Central amygdala
DP	Dorsal pallidum
Dp	Dorsal pallium
DC	Dorsal glomerular cluster
EBOS	Extrabulbar olfactory system
Hyp	Hypothalamus
LA	Lateral amygdala
LC	Lateral glomerular clusters
lfb	Lateral forebrain bundle
Lp	Lateral pallium
MeA	Medial amygdala
MC	Medial glomerular cluster
MOE	Main olfactory epithelium
Mp	Medial pallium
OB	Olfactory bulb
ON	Olfactory nerve
OpN	Optic nerve
p 1-3	Prosomeres 1-3
PN	Projection neuron
POA	Preoptic area
Str	Striatum
Th	Thalamus
V	Ventricle
Vp	Ventral pallium

Introduction

Olfaction

Olfaction is the sensation of chemical substances, called odorants, from a distant environment. Odorants are recognized and interpreted by the olfactory system (Farbman, 1992; Manzini et al., 2022; Manzini & Schild, 2010). Unlike gustation, olfaction does not require physical contact to enable the detection of chemicals (Eisthen & Polese, 2007). During evolution, the olfactory system has adapted to many kinds of environmental niches especially a terrestrial versus aquatic life (Ache & Young, 2005; Weiss et al., 2021a). Although, the olfactory systems are highly conserved across phyla (Ache & Young, 2005; Eisthen, 2002; Weiss et al., 2020a). Vertebrate olfactory systems share many general features and usually contain three main subsystems (Eisthen & Polese, 2007).

The vertebrate olfactory system

The main olfactory system, the vomeronasal system and the terminal nerve are the three olfactory subsystems known in vertebrates (Eisthen & Polese, 2007). The vomeronasal system is exclusive for tetrapods and is responsible for the detection of odorants as well as pheromones. Its sensory neurons are located in the vomeronasal organ and synaptically connect to mitral cells in the accessory olfactory bulb (AOB; Figure 1; Baxi et al., 2006; Eisthen & Polese, 2007). The terminal nerve is part of the cranial nerves and modulates activity in the olfactory epithelium. No sensory activity has been recorded from the terminal nerve (Eisthen & Polese, 2007; Oka, 1992; Wirsig-Wiechmann et al., 2002). The main olfactory system consists of a main olfactory epithelium (MOE; Figure 1), located in the nostril, which is connected via the olfactory nerve to the olfactory bulb (OB) in the forebrain (Figure 1; Eisthen & Polese, 2007). Sensory neurons are able to detect odorants and are located in the MOE. Axons of these cells project into the OB and terminate in functional units called glomeruli (Eisthen & Polese, 2007). Glomeruli act as functional units that connect arriving neurons from the nose with projection neurons (PNs) and interneurons of the bulbar network. PNs forward the olfactory information further to higher processing centers

(Figure 1) in the brain, where odorant induced physiological and behavioral changes are mediated (Eisthen & Polese, 2007; Manzini et al., 2014).

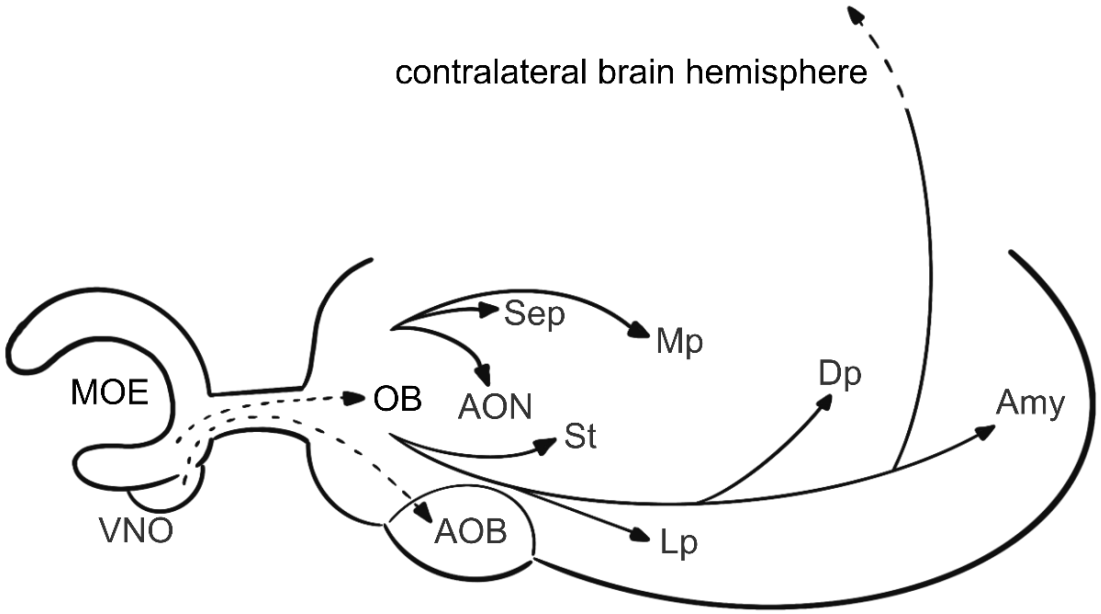

Figure 1: The vertebrate olfactory system. Schematic overview of the general morphology of the olfactory systems among vertebrates from a ventral view. The main olfactory epithelium (**MOE**) and vomeronasal organ (**VNO**) are connected to the olfactory bulb (**OB**) and accessory olfactory bulb (**AOB**) via the olfactory nerve. OB neurons project to higher brain regions in the telencephalon, such as the anterior olfactory nucleus (**AON**), septum (**Sep**), medial pallium (**Mp**), striatum (**St**), lateral pallium (**Lp**), dorsal pallium (**Dp**), amygdala (**Amy**) and to the contralateral brain hemisphere. Adapted from (Eisthen & Polese, 2007).

The olfactory system of the African clawed frog *Xenopus laevis*

Among anuran amphibian, the African clawed frog *Xenopus laevis* belongs to the family of primitive, tongueless frogs called pipidae. *Xenopus* has long been an important research animal and especially studies of *Xenopus* larvae gained more popularity in the last years (Davidson & Lowery, 2022; Hawkins et al., 2017; He et al., 2022; Manzini, 2015; Offner et al., 2020). The olfactory system is of special interest, because it retains its ability to regenerate new cells throughout the whole life of the

animal, from a pool of residing stem cells (Brann & Firestein, 2014; Graziadei & Dehan, 1973; Graziadei & Monti Graziadei, 1983; Hawkins et al., 2017; Schwob, 2002) and in *Xenopus* tadpoles the olfactory system is exceptionally good accessible (Hassenklöver & Manzini, 2014; Manzini & Schild, 2010). *Xenopus laevis* is a secondary aquatic frog and lives mainly in water. While adult frogs are also able to move on land (Measey, 2016), the tadpoles live fully aquatic. In their metamorphosis, when they develop from the tadpole to the adult frog, their body undergoes massive changes and so does the olfactory system (Burd, 1991; Dittrich et al., 2016; Hansen et al., 1998; Higgs & Burd, 2001; Reiss & Burd, 1997b, 1997a; Reiss & Eisthen, 2008; Weiss et al., 2021b). The olfactory system of the premetamorphic larvae consists of one olfactory epithelium (main olfactory epithelium: MOE, Figure 2), connected to the principal cavity and has a connection to the ventral OB via the olfactory nerve (Figure 2; Hansen et al., 1998; Higgs & Burd, 2001; Reiss & Burd, 1997b). The premetamorphic olfactory system is separated into two odor-processing streams (yellow and cyan, Figure 2; Gliem et al., 2013). Spatially, the premetamorphic principal cavity is partially segregated. Laterally (Figure 2; cyan), olfactory sensory neurons in the MOE respond to the stimulation with amino acids, while medially (Figure 2; yellow), olfactory sensory neurons respond to alcohols, aldehydes and ketones (Gliem et al., 2013). Each stream contains different G-proteins of different signal transduction cascades. It is assumed, that due to their molecular characteristics, lateral olfactory sensory neurons are microvillous and medial olfactory sensory neurons are ciliated. This segregation is also present and even more distinct at the level of the OB (Figure 2; Gliem et al., 2013). Axon terminals of olfactory sensory neurons form several glomerular clusters in the ventral OB (Figure 3; Gaudin & Gascuel, 2005). Nine larger and four smaller clusters were found in the premetamorphic OB (Figure 3; Gaudin & Gascuel, 2005). The lateral clusters in the OB responded to the stimulation with amino acids while the medial clusters responded to alcohols, aldehydes and ketones (Gliem et al., 2013).

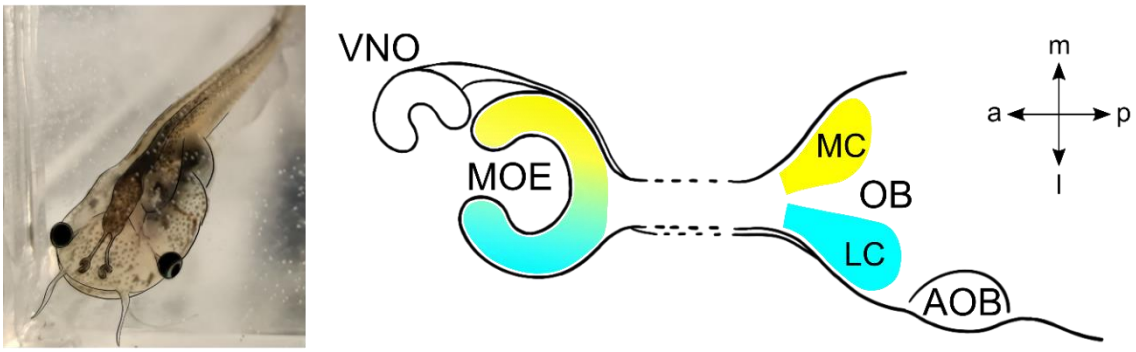

Figure 2: The olfactory system of premetamorphic *Xenopus laevis.* Image of a *Xenopus laevis* tadpole at stage 50-52 (Nieuwkoop & Faber, 1994)with a scheme showing its olfactory system (left brain hemisphere). The main olfactory epithelium (**MOE**) and vomeronasal organ (**VNO**) are located in the nostrils. The olfactory bulb (**OB**) and accessory olfactory bulb (**AOB**) are located anteriorly in the forebrain. The larval MOE and OB contain two olfactory processing streams (cyan: lateral stream; yellow: medial stream). Lateral clusters (**LC**). Medial cluster (**MC**).

During metamorphosis, a second cavity is formed, called the middle cavity, and contains a second olfactory epithelium (Hansen et al., 1998; Higgs & Burd, 2001). Sensory neurons of the middle cavity also form a connection to the OB, but connect with projection neurons in the dorsal part of the OB (Projection field 9, Figure 3; Gaudin & Gascuel, 2005; Reiss & Burd, 1997a). This newly formed cavity takes over the function of the principal cavity, by sensing waterborne odorants, while the principal cavity remodels to be able to detect airborne odorants (Hansen et al., 1998; Higgs & Burd, 2001; Reiss & Burd, 1997a, 1997b; Reiss & Eisthen, 2008; Weiss et al., 2021a). The two odor-processing streams of premetamorphic larvae remain present after metamorphosis in the ventral OB (Weiss et al., 2021b).

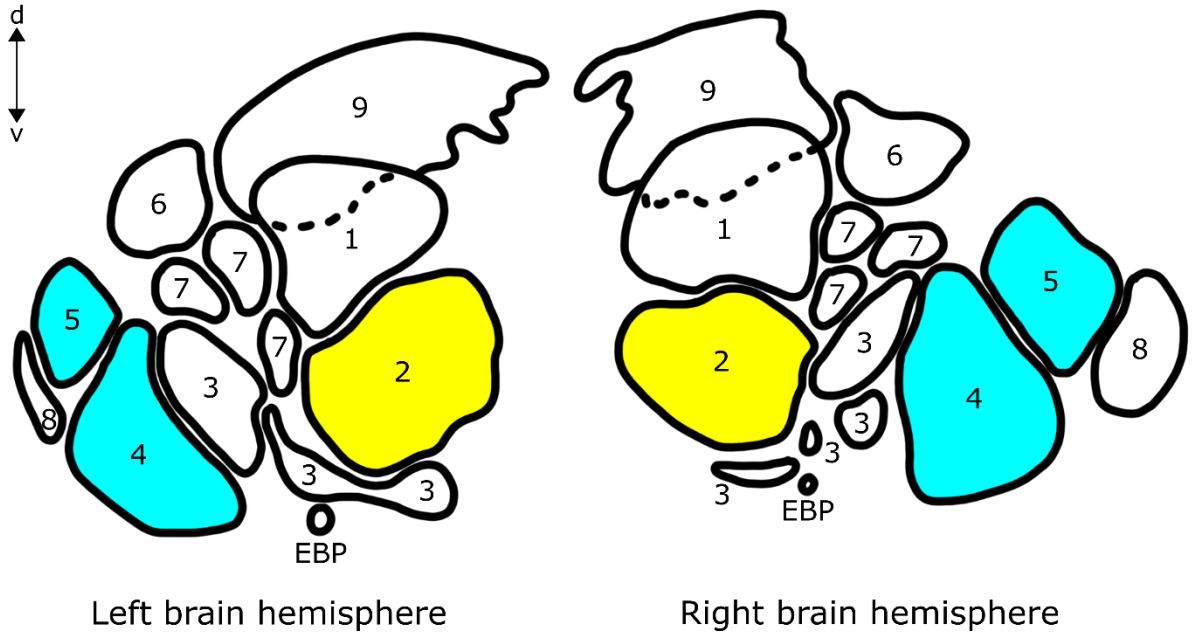

Figure 3: Schematic overview of the glomerular clusters in the OB of larval *Xenopus laevis* at stage 50. Scheme of a coronal section trough all projection fields (glomerular clusters) described by (Gaudin & Gascuel, 2005). Lateral clusters are shown in cyan (Projection fields 4 and 5) and the medial cluster is shown in yellow (Projection field 2). Projection field 1 is the dorsomedial glomerular cluster, Projection field 3, 6 and 7 are the intermediate glomerular clusters, Projection field 8 is the AOB and Projection field 9 is the dorsal glomerular cluster. Extrabulbar projections (**EBP**). Dorsal (**d**). Ventral (**v**). Projection fields 1-9 (**1-9**). Figure adapted from (Gaudin & Gascuel, 2005).

In the anuran olfactory system, the OB is the first relay station of olfactory information processing and can be separated into six different cell layers (Figure 4 A and B; Byrd & Burd, 1991; Moreno et al., 2008; Nezlin & Schild, 2000). The most anterior part of the OB contains the ON and glomerular layer (gl). In this section, sensory neurons from the nose enter the OB and form glomeruli together with dendrites of interneurons and PNs (Byrd & Burd, 1991; Nezlin & Schild, 2000). The gl is followed by the mitral cell layer (mcl) as well as the external and internal plexiform layer. In anuran and other frogs, the mcl and the external plexiform layer are not clearly disjunct and cell types that are specific for a certain layer in other vertebrates, here occur also in another cell layer (Byrd & Burd, 1991; Hoffman, 1963; Nezlin & Schild, 2000; Scalia et al., 1991a). The most posterior part of the OB is the granule cell layer (gcl), which contains interneurons called granule cells (Byrd & Burd, 1991; Nezlin & Schild, 2000).

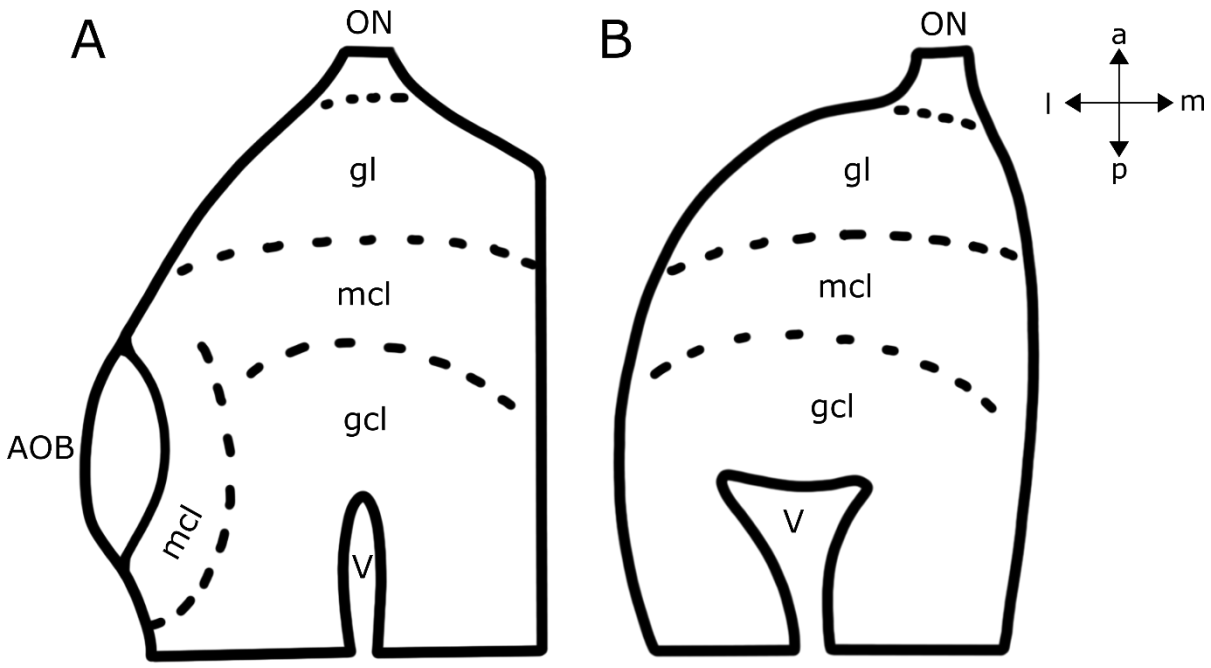

Figure 4: Cell layers of the premetamorphic *Xenopus laevis* OB. Schematic overview of two horizontal sections of the OB from a ventral view (left brain hemisphere). **A** Horizontal section of the main OB and accessory olfactory bulb (**AOB**). **B** Horizontal section of the main OB. Glomerular layer (**gl**). Mitral cell layer (**mcl**). Granule cell layer (**gcl**). Olfactory nerve (**ON**). Ventricle (**V**). Anterior (**a**). Posterior (**p**). Lateral (**l**). Medial (**m**). Adapted from (Nezlin & Schild, 2000).

Olfactory projection neurons

PNs are the main output neurons of the vertebrate olfactory bulb. They directly connect sensory neurons of the nose with cortical neurons in the brain (Eisthen & Polese, 2007; Lodovichi, 2021; Manzini et al., 2022; Nagayama et al., 2014; G. M. Shepherd, 1972). The structure of PNs can vary among different vertebrate species (Dryer & Graziadei, 1994; Eisthen & Polese, 2007; Fuller et al., 2006; Igarashi et al., 2012; Imai, 2014; Imamura et al., 2020; Miyasaka et al., 2014; Nagayama et al., 2010; Zeppilli et al., 2021). In mammals, different classes of PNs are known, like the mitral and tufted cells in mice (Figure 5; Imai, 2014; Imamura et al., 2020; Nagayama et al., 2014). Mitral cells and tufted cells show different morphological properties and can be separated into subtypes based on different molecular characteristics (Nagayama et al., 2014; Zeppilli et al., 2021). Mitral cells are located in the mitral cell layer and extend their basal dendrites into the deeper/inner external plexiform layer. Tufted cells in

comparison are located in the external plexiform layer and project their basal dendrites into the superficial/outer external plexiform layer. Primary dendrites of both mitral and tufted cells are in contact with glomeruli in the gl (Figure 5; Nagayama et al., 2014).

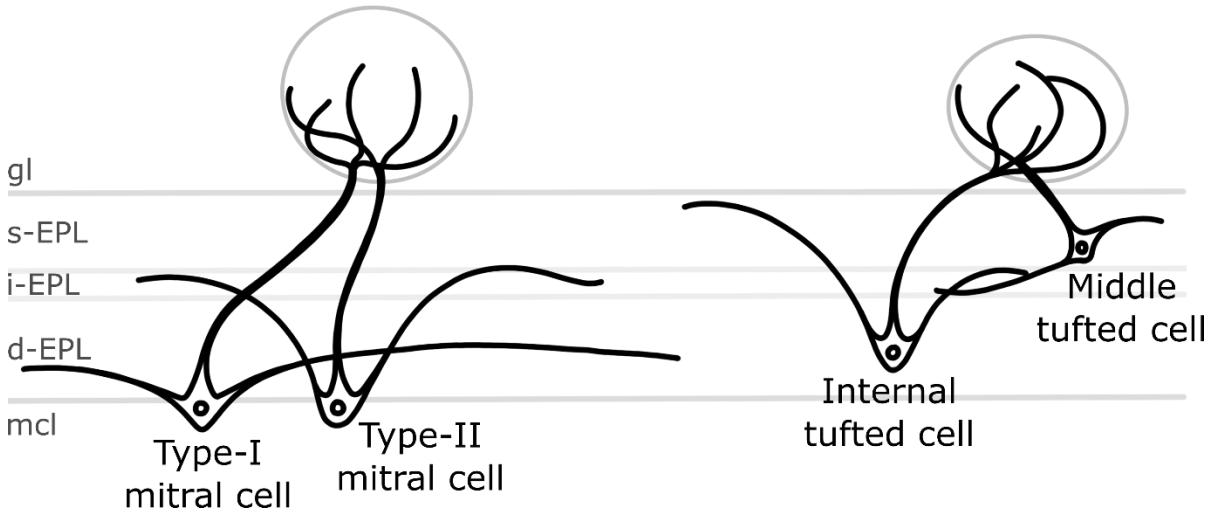

Figure 5: Different types of olfactory output neurons in mammals. Olfactory output neurons in mammals are divided in mitral (left side) and tufted cells (right side). Mitral cells are subdivided into type I and type II mitral cells. Tufted cells are subdivided into internal and middle tufted cells. Glomerular layer (**gl**). Superficial/outer external plexiform layer (**s-EPL**). Inner external plexiform layer (**i-EPL**). Deeper-external plexiform layer (**d-EPL**). Mitral cell layer (**mcl**). Adapted from (Nagayama et al., 2014).

In another vertebrate, the teleost fish *Danio rerio*, mitral cells are the main output neurons. While tufted cells are not present, two other types of output neurons, ruffed and terminal ganglion cells, have been found (Fuller et al., 2006). Three mitral cell subtypes, based on different transcriptional promoters, and two mitral cell groups, based on the number of dendrites, are known from zebrafish (Fuller et al., 2006; Miyasaka et al., 2009, 2014). Fuller et al., 2006 categorized zebrafish mitral cells into unidendritic and multidendritic mitral cells (Figure 6). Unidendritic mitral cells contain only one dendrite that arises from the soma while multidentritic mitral cells have more than one dendrite that arises from the soma (Figure 6; Fuller et al., 2006).

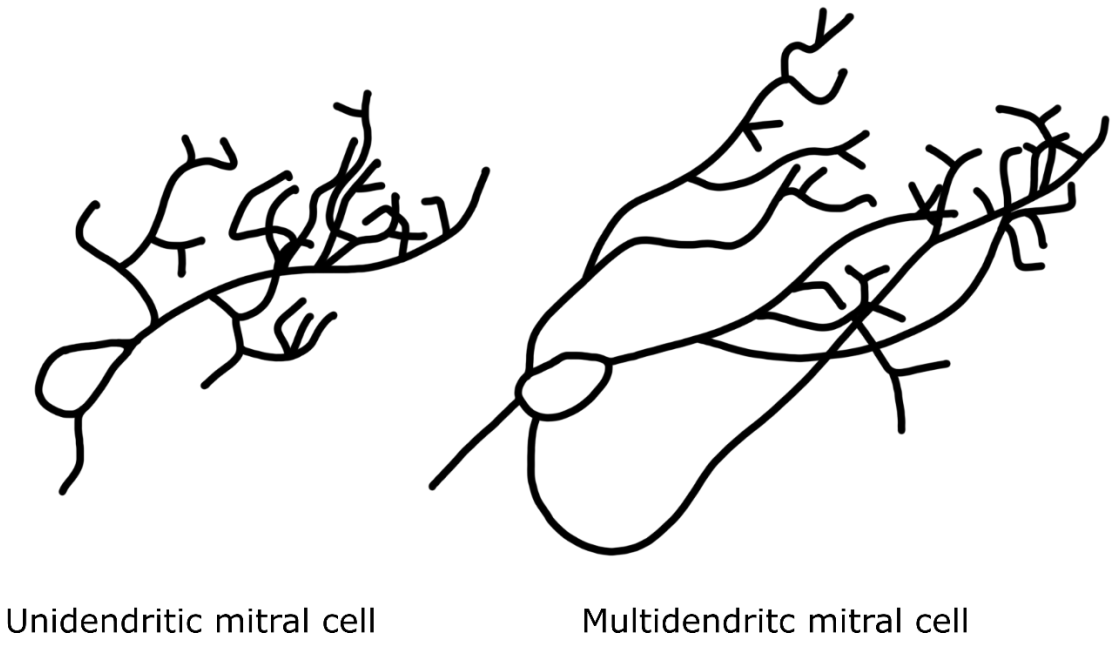

Figure 6: Mitral cells of the zebrafish *Danio rerio*. Scheme of two types of olfactory PNs in the zebrafish OB. Mitral cells in *Danio rerio* are subdivided into unidendritic (left side) and multidendritic (right side) mitral cells. Adapted from (Fuller et al., 2006).

Although some frog and salamander species possess cells with similarities to tufted cells, mainly mitral cells have been found in amphibians (Eisthen & Polese, 2007; Jiang & Holley, 1992; Scalia et al., 1991a). Two groups of PNs were described in the frog *Rana ridibunda* that differ in the structure of the dendritic tree (Figure 7; Jiang & Holley, 1992). One group has similarities to mammalian superficial/middle tufted cells, due to the close position of the somata to the glomerular layer and a widespread dendritic tree (right cells, Figure 7). The second group has more similarities with mammalian deep tufted mitral cells, because their somata are located more posteriorly and the dendritic tree is more linear (left cell, Figure 7; Jiang & Holley, 1992). In *Xenopus laevis*, cells with similarities to tufted cells have been found close to the glomerular layer and mitral cell shaped neurons were described in the mitral cell layer (Nezlin et al., 2003). After metamorphosis, a new group of PNs is formed, which connects to the new glomerular cluster in the dorsal OB. These PNs differ in size, length of dendrites and number of dendritic tufts from the ventral PN population (Weiss et al., 2021b). Nonetheless, a detailed description of *Xenopus laevis* olfactory PNs, especially of the tadpoles, is still missing.

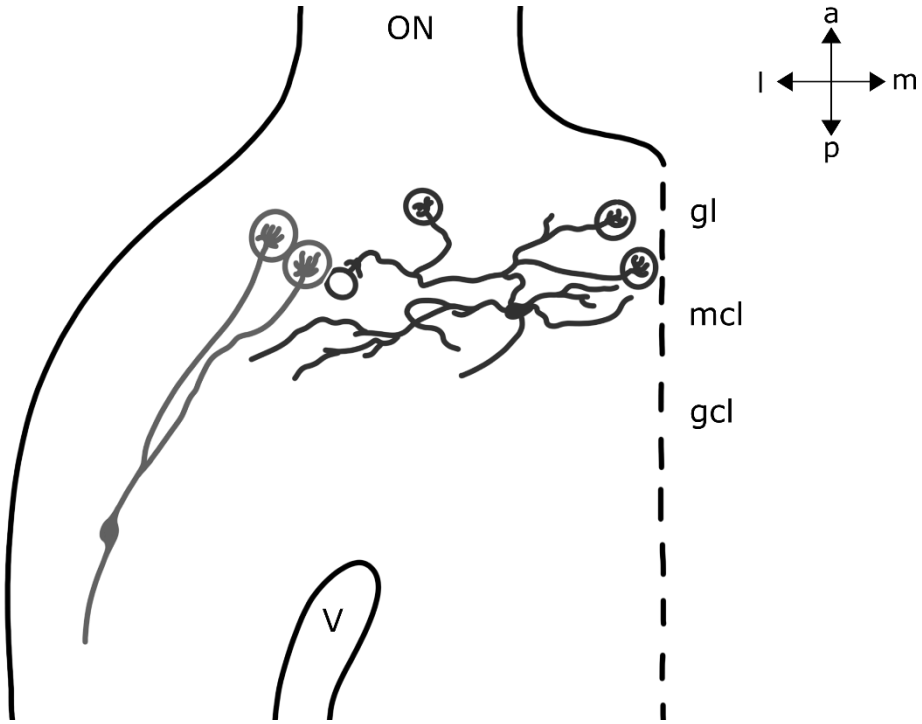

Figure 7: Olfactory PNs in the OB of the frog *Rana ridibunda.* Schematic overview of the OB (left brain hemisphere) including two types of olfactory PNs. Glomerular layer (**gl**). Mitral cell layer (**mcl**). Granule cell layer (**gcl**). Olfactory nerve (**ON**). Ventricle (**V**). Anterior (**a**). Posterior (**p**). Lateral (**l**). Medial (**m**). Adapted from (Jiang & Holley, 1992).

Higher olfactory processing centers

PNs are connected with their axons to higher brain regions. Thereby different subtypes of PN in vertebrates often show different projection patterns and connections to different brain regions (Igarashi et al., 2012; Miyasaka et al., 2009, 2014; Nagayama et al., 2010). In the mammalian olfactory cortex, main target regions by olfactory PNs are the piriform cortex, anterior olfactory cortex and olfactory tubercle (Nagayama et al., 2010). Mitral cells project their axons to the entire olfactory cortex and tufted cells to the anterior olfactory cortex (Haberly & Price, 1977; Nagayama et al., 2010; Scott et al., 1980). It is assumed, that mitral cells are involved in the creation of an accurate odor image, while tufted cells support monitoring the environment in order to respond with a certain behavior to surrounding stimuli (Nagayama et al., 2010). Thereby, mitral cells only convey very strong signals and tufted cells are able to convey strong as well as weak signals (Igarashi et al., 2012). Mitral and tufted cells also show different response latencies after receiving a signal. Mitral cells respond after ~ 250 – 300 ms

and tufted cells already after ~ 110 ms. This shows that tufted cells could have a critical role in fast behavioral response, while mitral cells are more important for a finer and more difficult odor discrimination (Igarashi et al., 2012). Similar observations have also been made in the zebrafish *Danio rerio* (Miyasaka et al., 2009, 2014).

In frogs, olfactory PNs are connected with brain regions in the telencephalon (Moreno et al., 2005; Northcutt & Royce, 1975; Scalia et al., 1991b). The telencephalon is divided into the pallium (dorsal) and subpallium (ventral; Hoffman, 1963; Northcutt, 1974), containing regions like the basal ganglia and the amygdaloid complex (Brox et al., 2004; Marín, González, et al., 1997; Marín, Smeets, et al., 1997; Moreno & González, 2003, 2004). In adult *Xenopus laevis,* the main target region of main OB PNs is the lateral amygdala (LA; Moreno et al., 2005; Moreno & González, 2004). The LA is located in the ventral pallium, a region between the lateral pallium and the subpallium (Moreno & González, 2004). A few projections from main OB PNs have been observed to target the medial amygdala (MeA; (Moreno et al., 2005). In frogs, this region is located in the subpallium and primarily targeted by PNs of the AOB (Moreno et al., 2005; Scalia, 1972; Scalia et al., 1991b). Intra-amygdaloid connections between the LA and the MeA and their mutual projections to the hypothalamus suggest, that projections from the main OB and AOB are not strictly segregated (Moreno et al., 2005; Moreno & González, 2003, 2004). It is assumed, that the anuran amygdaloid complex is an intermediate center for processing a variety of stimuli. Especially the association of odors and pheromones with attractive and aversive stimuli might have a major role. Consequently, the amygdaloid complex would be involved in emotional memory (Moreno et al., 2005).

tubb2b promoter-driven transgenic *Xenopus laevis*

In the past years, the creation and use of transgenic *Xenopus laevis* has gained more popularity and offers new possibilities for the use of *Xenopus* as a research model (Horb et al., 2019; Love et al., 2011; Offner et al., 2020). One commonly used promoter to study the nervous system is the class II β-tubulin promoter *tubb2b* (Horb et al., 2019; Love et al., 2011). Unlike in frog *Xenopus laevis*, where class II β-tubulin is expressed in neurons (Moody et al., 1996; Oschwald et al., 1991; Richter et al., 1988), other vertebrates instead possess class III β-tubulin (Katsetos et al., 1993, 2003;

Latremoliere et al., 2018; M. K. Lee, Rebhun, et al., 1990; M. K. Lee, Tuttle, et al., 1990; Moody, 1989; Moody et al., 1996). The promotor *tubb2b* is used in transgenic lines such as tubb2b:GCaMP6s Rno.elas:GFP (NXR; Cat# 0.0107; Horb et al., 2019) and tubb2b:Katushka cryga:Venus (EXRC; Cat# 202; Love et al., 2011). In transgenic tubb2b:GCaMP6s Rno.elas:GFP, *tubb2b* drives the expression of the genetically encoded calcium indicator GCaMP6s (Horb et al., 2019), which is used to measure neuronal activity in the nervous system (Chen et al., 2013; Offner et al., 2020). Offner et al., 2020 show that measurements of the activity of individual cells is possible even in regions like the OB and amygdaloid complex (Offner et al., 2020). Using the mentioned transgenic lines is already an advantage; however, detailed information about the explicit activity pattern of the *tubb2b* promoter in *Xenopus laevis* has not been shown yet.

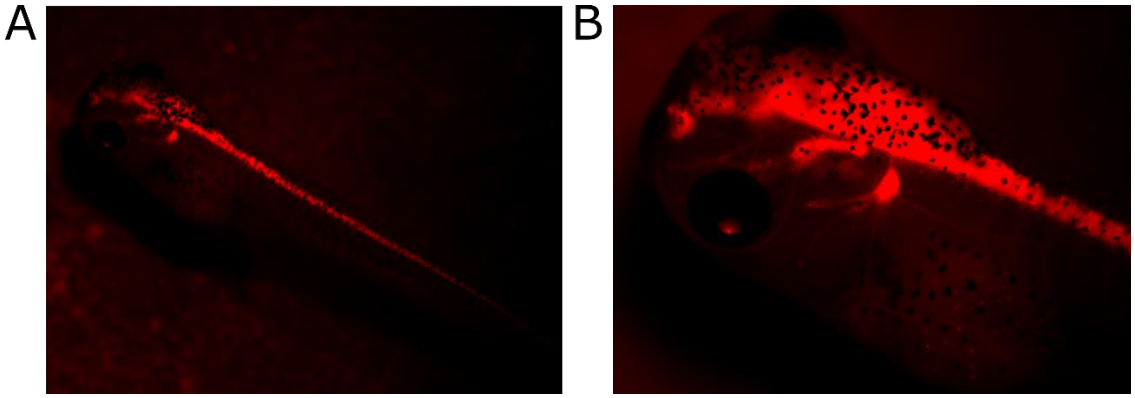

Figure 8: Transgenic NBT-Katushka γ-cry Venus *Xenopus laevis* larvae. A *Xenopus laevis* tadpole with red fluorescence in the nervous system. **B** Head of *Xenopus laevis* tadpole with red fluorescence in the brain. Find the images on the website of the Xenopus Resource Center *https://xenopusresource.org/* under X.la Tg lines #202.

This work aims to study the secondary olfactory pathway of larval *Xenopus laevis* for the first time, with special focus on the two odor processing streams found in the primary olfactory pathway (Gliem et al., 2013) and with the use of transgenic *tubb2b* promoter-driven *Xenopus laevis*. Additionally, a thorough study of this specific transgenic line was intended, to have a detailed map of regions with *tubb2b*-dependent fluorescence in the forebrain and olfactory system of the premetamorphic tadpole.

Material and Methods

Animals

For my experiments I used the following transgenic larval *Xenopus laevis* lines: NBT-Katushka γ-cry Venus [Xla.Tg(tubb2b:Katushka; cryga:Venus)^{EXCR}; (Love et al., 2011)], custom bred NBT-Katushka pax6-GFP [Xla:Tg(tubb2b:Katushka;cryga:Venus; pax6:GFP;CMV:DsRED)^{Manzini}] as well as tubb2b-GCaMP6s Rno.elas-GFP [Xla.Tg(tubb2b:GCaMP6s; Rno.elas:GFP)^{NXR}; (Horb et al., 2019)]. All animals were raised in the animal husbandry at the Institute of Animal Physiology of the Justus-Liebig-University Gießen, Germany. Transgenic NBT-Katushka pax6-GFP frogs were naturally bred from transgenic NBT-Katushka γ-cry Venus and pax6-GFP CMV-DsRED [Xla.Tg(pax6:GFP;CMV:DsRED)^{Papal}; (Hartley et al., 2001)] *Xenopus laevis*. In all experiments, I used tadpoles of developmental stages 48 – 52 (ca. 7 to 17 days after fertilization at 22-24°C; Nieuwkoop & Faber, 1994). The tadpoles were kept in water tanks of 1,8 – 7,5 l at a water temperature of 19 – 22 °C and were fed daily with a mixture of spirulina and chlorella algae (Dose Aquaristik). All animal handling procedures were performed following the guidelines of laboratory animal research of the Institutional Care and Use Committee of the Justus-Liebig-University Gießen (649_M).

Whole mount preparation and tissue slicing

Whole mount preparation

For all experiments, I anesthetized each animal in 0.02% MS-222 solution (ethyl 3-aminobenzoate methanesulfonate; TCI Germany), dissolved in tap water (ph adjusted to 7.4 – 7.6). After complete anesthesia all animals were killed by severing the spinal cord at the level of the brainstem with fine scissors. In all experiments, I dissected tissue blocks containing the whole olfactory system and forebrain. For immunohistochemical stainings, injections and sparse cell electroporation, I removed the palatial tissue that is covering the ventral side of the forebrain. For all calcium

imaging experiments, I specifically removed tissue above the target brain regions, which were located either on the ventral, lateral or dorsal side of the telencephalon. During the sample preparation, I kept the tissue moist with frog ringer solution (98 mM NaCl, 2 mM KCl, 1 mM $CaCl_2$, 2 mM MgCl, 5 mM Na-pyruvate, 5 mM glucose, 10 mM HEPES, pH 7.8, osmolarity of 230 mOsmol/l). All samples were collected in frog ringer solution for further experiments.

Tissue slicing

To visualize the location of *tubb2b*-positive brain regions in the larval forebrain, I performed coronal slices of the whole forebrain of transgenic NBT-Katushka γ-cry Venus and NBT-Katushka pax6-GFP tadpoles. Before slicing, I fixated the samples in 4% formaldehyde (Carl Roth) for 1 h. Afterwards, the samples were washed with PBS (137 mM NaCl, 2.7 mM Kcl, 8 mM Na_2HPO_4, dissolved in purified water, pH 7.4) three times for 15 min. I then embedded the samples in 5% of low-melting point agarose (Sigma-Aldrich) to be able to perform precise cuts. Using a half-automatic vibratome (Leica VT1200S; Leica Biosystems) I sliced the forebrain into 300-µm-thick coronal slices, which were collected for immunohistochemical stainings in PBS.

Immunohistochemistry

Transgenic NBT-Katushka γ-cry Venus forebrain slices were additionally immunohistochemically stained to have landmarks for specific brain regions. Therefore, I chose Pax7 (Bandín et al., 2013, 2014), calretinin (CR; Castro et al., 2008; Milán & Puelles, 2000; Morona & González, 2013; Porteros et al., 1997) and tyrosine hyrdroxlase (TH; Boyd & Delaney, 2002; González et al., 1994; Milán & Puelles, 2000) since their locations are well described in *Xenopus laevis* and cover all main forebrain areas. For a detailed analysis of the olfactory bulb, I stained whole mount preparations of transgenic NBT-Katushka γ-cry Venus with antibodies against CR, TH and additionally HuC/D to label all mature neurons. I also performed immunohistochemical stainings with all slices and whole mount preparations of transgenic NBT-Katushka pax6-GFP larvae, to enhance the signal of Katushka and GFP for better visualization.

As explained above all samples were dissected and some were cut into coronal slices prior to the immunohistochemical stainings. All samples were then permeabilized with PBST (PBS containing 0.2% Triton-X100; Carl Roth) three times for 15 min at room temperature (RT). I then incubated the samples with PBST containing 2% normal goat serum (NGS; MP Biomedicals) for 1 h at RT, to block unspecific binding sites. Afterwards, the samples were incubated with the primary antibodies (1:100; see Tab. 1) in PBST with 2% NGS for three days at 4°C.

Table 1: Primary Antibodies. PAX7 was deposited to the DSHB by Kawakami, A. (DSHB Hybridoma Product PAX7).

Primary Antibody	Cat#	Company	Clonality & Host species	Target
anti-tRFP	AB233	BioCat	Polyclonal, Rabbit	Katushka
anti-GFP	ab1218	Abcam	Monoclonal, Mouse	GFP
anti-Pax7	PAX7	DSHB	Monoclonal, Mouse	Pax7
anti-CR	6B3	Swant	Monoclonal, Mouse	Calretinin
anti-TH	22941	Immunostar	Monoclonal, Mouse	Tyrosine Hydroxylase
anti-HuC/D	A-21271	Thermo Fisher Scientific	Monoclonal, Mouse	HuC/D

The primary antibodies were washed off with PBS (three times for 15 min. at RT) and incubate with the secondary antibodies Alexa Fluor 594 goat anti-rabbit (Invitrogen, Thermo Fisher Scientific; 1:100) and Alexa Fluor 488 goat anti-mouse (Invitrogen, Thermo Fisher Scientific; 1:100) in PBS with 2% NGS for three days at 4°C. The secondary antibodies were washed off with PBS three times for 15 min. at RT and the samples were transferred to a recording chamber for multiphoton microscopy (A1R MP; Nikon).

Sparse cell electroporation

To study the morphology of olfactory projection neurons, I labeled single cells using sparse cell electroporation (Weiss et al., 2018). In all samples I electroporated the ventromedial and ventrolateral olfactory bulb. I used transgenic NBT-Katushka γ-cry Venus larvae for all electroporations to target structures in the olfactory bulb precisely and for a better orientation in the brain during microscopy.

For the electroporation, I dissected a tissue explant, as explained above, and transferred it to a petri dish, covered with a platinum grid for stabilization. Afterwards, I prepared electroporation micropipettes by pulling borosilicate glass capillaries (Resistance of 10-15 MΩ; BM150F-10P; BioMedical Instruments) and filled them with 3-5 µl of fluorophore coupled Alexa 488 dextran (3 mM diluted in frog ringer solution; Life Technologies, Thermo Fisher Scientific). The micropipettes were mounted to a micromanipulator connected to a Axoporator (800 A; Axon instruments, Molecular Devices) and positioned under an epifluorescence stereomicroscope (BX51WI; Olympus). Using the micromanipulator the region of interest was approached and a 500 ms train of square voltage pulses (50 V, single pulses 300 µs at 200–300 Hz) was applied to transfer dye into the surrounding neurons. All labelled neurons were imaged immediately with a multiphoton microscope (A1R MP; Nikon) at a wavelength of 780 nm.

Reconstruction and analysis of labeled neurons

To analyze morphological structures of olfactory projection neurons, I semi-automatically reconstructed the labeled single neurons from the recorded image stack with Vaa3D (Peng et al., 2010). With the soma as the root point, all branching- and endpoints of each PN was defined and translated into a hierarchical 3D tree-structure. Each PN contains at least one dendritic tuft and each segment of the neuron-tree is connected to one single parent segment. The reconstruction is generated by placing nodes along the neuron structure in the 3D space. The placement of the nodes depends on the image signal intensity. Interrupted structures of the cell, that happen for instance when gaps arise when a cell starts to undergo apoptosis (apoptotic

blebbing) cannot be traced by the program (see example in Supplementary Figure 1). To make sure all structures were correctly recognized by the program, I manually checked all cells and compared their reconstruction with the microscopic image. Structures that were not recognized by the program, where then added manually into the data set.

In this work, I specifically focused on the number of dendritic tufts, the number of branching- and endpoints and the number of stems that arise from the soma, in order to describe the basic structure and complexity of the neuron-tree. The number of dendritic tufts was determined with the DBSCAN algorithm (Density-based spatial clustering of applications with noise; Scikit learn machine learning package; Pedregosa et al., 2011; Weiss et al., 2020b) written for Python. Thereby, the algorithm classifies a structure as a tuft-cluster, when more than five branching- and endpoints accumulate in spatial proximity lower than 15 µm. Sparsely distributed branching points are classified as extraglomerular branching points and endpoints as blunt endings. The number of stems from soma is the number of neuron segments that are connected to the root point of the neuron-tree.

Bulk injection

To visualize and compare the axonal projections of olfactory PNs from the medial and lateral olfactory stream, I injected calcein AM (acetoxymethyl) dye into the ventromedial and ventrolateral olfactory bulb mitral cell layer. I here as well used transgenic NBT-Katushka γ-cry Venus *Xenopus* larvae for a precise application into the OB and analysis of the target brain regions. For the injection I dissected a tissue explant as explained above and transferred it to a petri dish filled with frog ringer solution. The sample was then covered with a platinum grid for stabilization and placed under an epifluorescence stereomicroscope (BX51 WI; Olympus). I diluted Calcein Green AM (Molecular Probes, Thermo Fisher Scientiftic) with 5 µl DMSO (Sigma-Aldrich) and 10 µl Pluronic F-127 (Molecular Probes, Thermo Fisher Scientific) in 35 µl frog ringer solution. Micropipettes were prepared from borosilicate glass capillaries (Resistance of 8-10 MΩ; BM150F-10P; BioMedical Instruments) and filled with 3-5 µl of Calcein Green AM. I mounted the micropipette to a micromanipulator which is connected to a custom made pressure application system. With the use of an

epifluorescence stereomicroscope (BX51 WI; Olympus) I carefully approached the region of interest within the OB. I then injected the dye using small pulses of air pressure. After injection, each sample was incubated for 2h at RT in complete darkness. The axonal projections were imaged by recording the whole forebrain with a multiphoton microscope (A1R MP; Nikon; wavelength of 780 nm).

Calcium imaging

To find out whether axons of olfactory PNs are functionally connected to regions in the forebrain, I performed whole mount calcium imaging experiments with transgenic tubb2b-GCaMP6s Rno.elas-GFP *Xenopus* larvae (Horb et al., 2019; Offner et al., 2020). To be able to measure odorant-induced cellular activity in whole mount preparations, we used fast resonant scanning of volumetric time-series of our multiphoton microscope (excitation wavelength of 900 nm; 35 image planes; lateral dimension: 509 x 509 µm, 512 x 512 pixels, frame rate: 1 Hz).

For each measurement a tissue explant was dissected (as explained above) and transferred to a petri dish, filled with frog ringer solution. The sample was covered with a platinum grid for stabilization and placed under the multiphoton microscope. For the application of the bath solution and stimuli, I used a gravity-fed perfusion system. Through a silicon tube the solutions are led into the recording chamber and removed by a syringe needle caudally to the preparation. The samples are constantly perfused with frog ringer solution (bath solution) during the experiment and the stimuli were applied during a constant flow.

The stimulus in all experiments was a mixture of odorants (OD; 50 µM dissolved in frog ringer solution; Gliem et al., 2013) containing the following substances: A mixture of amino acids, a mixture of alcohols, aldehydes and ketones, a mixture of amines and a mixture of bile acids (for details see Tab. 2).

Table 2: Odorant mixture ingredients. All chemicals were purchased from Sigma-Aldrich.

Mixture	Ingredients
Amino acids	L-valine, L-leucine, L-isoleucin, L-methionin, glycine, L-serine, L-threonine, L-cysteine, L-arginine, L-lysine, L-histidine, L-tryptophan, L-phenylalanine, L-alanine, L-proline
Alcohols, Aldehydes, Ketones	α-Terpineol, β-phenylethylalcohol, γ-phenylpropylalcohol, Citral, β-ionone
Amines	2-phenylethylamine, tyramine, butylamine, cyclohexylamine, hexylamine, 3-methylbutylamine, N,N-dimethylethylamine, 2-methylbutylamine, 1-formylpiperidine, 2-methylpiperidine, N-ethylcyclohexylamine, 1-ethylpiperidine, piperidine
Bile acids	Taurocholic acid, cholic acid, glycholic acid, deoxycholic acid

To find out, whether potential target regions in the posterior telencephalon respond to stimulation of the olfactory system, I first recorded the whole posterior telencephalon. The pallium was recorded from a dorsal view and the subpallium from a ventral view. I recorded each region for one minute total and applied the stimulus for 5 sec. after 30 sec. during the recording (see Figure 9). To ensure, that the recorded signal is based on olfactory stimulation, I repeated each measurement twice and as a control with both olfactory nerves transected.

Figure 9: Experimental settings for recordings of the whole posterior telencephalon. Application of odorant mixture for 5 sec. after 30 sec. during the measurement.

I additionally recorded every responding region at a higher magnification, to image the activity of single cells. In this experiment, I recorded for 8 min in total and applied the stimulus three times with an inter-stimulus interval of 2 min (first stimulus after 2 min. during the recording; Figure 10). To ensure, that the recorded signal is based on olfactory stimulation here as well, I repeated each measurement twice and with both olfactory nerves transected, as a control.

Figure 10: Experimental settings for recordings of single neurons. Application of odorant mixture for 5 sec. for three times with a interstimulus-interval of 2 min. during the measurement.

For processing and analyzing the calcium imaging data, I used the calcium imaging analysis toolkit CaImAn (Giovannucci et al., 2019). In all recordings I corrected the lateral drift using piecewise rigid motion correction (Pnevmatikakis & Giovannucci, 2017). Every recording has been denoised, deconvoluted and de-mixed (Giovannucci et al., 2019). I created fluoresence intensity difference maps to visualize stimulus-induced activity. For the recordings of the whole posterior telencephalon, I manually drew regions of interest (ROIs) around the pallium and subpallium using Fiji (http://fiji.sc/Fiji; Schindelin et al., 2012). ROIs for single cells were automatically created by CaImAn. I further manually selected single neurons for the final analysis, in case they fulfilled the following conditions:

1. The response signal is higher than three times the standard deviation of all baseline intervals.
2. The response signal took place within a 15 sec. time window after application start.

Finally, the raw fluorescent time traces of all recordings from the posterior telencephalon as well as all selected single neurons were baseline corrected, and absolute fluorescent changes were transformed into deltaF/F (after the protocol of Offner et al., 2023).

Image processing and data analysis

Image processing was performed with the open-source software Fiji (http://fiji.sc/Fiji; Schindelin et al., 2012). All images were recorded with a z-resolution of 1 µm and provided as a multidimensional image stack. Of all immunohistochemial stainings, whole mount preparations are shown as maximum projections of all planes of the

recorded z-stack and slices are shown as individual z-planes. Images of single neurons and tracing experiments are shown as a maximum projection of all planes from the z-stack. Images of the calcium imaging experiments are shown as individual z-planes. Due to the size of some images of the coronal brain slices, I stitched multiple image stacks together to create a full image of the whole forebrain slice (Preibisch et al., 2009). Some images of the immunohistochemical stainings were cropped, to show details. I linearly adjusted brightness and contrast in all images. In all images of tracing experiments and single-cell injections, I used the blue wavelength detector (400-492 nm) of the multiphoton microscope to record autofluorescence caused by tissue pigmentation. With the image calculator tool, I then mathematically subtracted autofluorescence-derived signals from all other emission channels. Cell counting was performed manually using the ImageJ ROI Manager. Mean counts are shown with standard deviation. In all images of whole posterior telencephalon calcium imaging, I applied a gaussian filter. I also tested for statistical significance between lateral and medial olfactory PNs with the Mann-Whitney U test (Mann & Whitney, 1947).

Results

This work was set out to analyze the secondary olfactory pathway in larval *Xenopus laevis*, with the use of transgenic *tubb2b* promoter-driven tadpoles. Therefore, it was necessary to first characterize the activity pattern of the *tubb2b* promoter in the olfactory system (OS) and forebrain. I prepared whole mount preparations of the OS and coronal slices of the whole forebrain of transgenic NBT-Katushka γ-cry Venus (n = 21) and NBT-Katushka pax6-GFP (n = 13) tadpoles. To describe the precise location of *tubb2b*-positive neurons, I additionally performed antibody stainings against Pax7 (n = 6), TH (n = 8) and CR (n = 15), which are well described proteins that are located in the main forebrain regions (Bandín et al., 2013, 2014; Boyd & Delaney, 2002; González et al., 1994; Milán & Puelles, 2000; Morona & González, 2013). The following publications were used to evaluate the location of *tubb2b*-dependent fluorescence in certain brain areas: olfactory bulb (Gaudin & Gascuel, 2005; Nezlin & Schild, 2000; Pinelli et al., 2004; Weiss et al., 2020a); telencephalon and diencephalon: (Bandín et al., 2014; González et al., 1994; Marín, González, et al., 1997; Marín, Smeets, et al., 1997; Moreno & González, 2003, 2004; Morona & González, 2013).

tubb2b promoter-driven fluorescence in the OS and forebrain of premetamorphic *Xenopus laevis* tadpoles

This chapter is published in Frontiers in Neuroanatomy, 2022 (Daume et al., 2022).

Olfactory system: Main olfactory epithelium and olfactory bulb

The OS of premetamorphic *Xenopus laevis* consists of an MOE (Figure 11 C) which is connected via the ON (Figure 11 C) to the OB in the forebrain (Manzini & Schild, 2010). The OB is located in the most anterior part of the telencephalon (Figure 12 I) and contains six different layers (Byrd & Burd, 1991; Manzini & Schild, 2010). In the MOE, I found that *tubb2b* is active in ORN cell bodies (Figure 11 A and B; magenta) and associated axons in the ON (Figure 12 F - G; Daume et al., 2022).

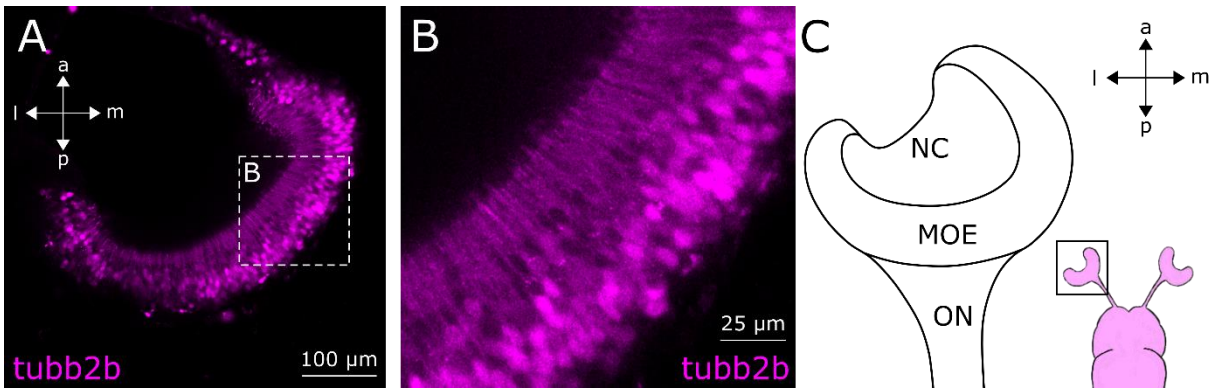

Figure 11: *tubb2b*-dependent fluorescence in the MOE. A Single focal plane of the left main olfactory epithelium (**MOE**; dorsal view). *tubb2b* is active in ORNs (magenta). **B** Close-Up of the MOE showing *tubb2b*-positive ORNs (magenta). **C** Scheme of the OS with a close-up of the left MOE and anterior part of the olfactory nerve (**ON**). Nasal cavity (**NC**). Adapted from Daume et al., 2022 Figure 1.

Axonal terminals of ORNs form nine large and four small glomerular clusters (projection fields) within the OB (projection fields 1 – 9, α, β, γ, δ; Figure 3) which are conserved structures among anurans (Gaudin & Gascuel, 2005; Weiss et al., 2020a). I observed that every projection field is innervated by *tubb2b*-positive axon terminals (Figure 12 A) as well as a bundle of fibers that bypasses the OB and projects caudally into the forebrain (Figure 12 F; white arrow; also shown in Daume et al., 2022). *tubb2b*-positive cells were scattered across the whole OB in close proximity to the glomerular clusters and within the mitral cell layer (Figure 12 B; Daume et al., 2022).

To find out whether *tubb2b*-activity is restricted to a specific cell type in the OB, I performed antibody stainings in NBT-Katushka γ-cry Venus transgenic larvae, against CR and TH as markers for interneurons and mitral cells (Boyd & Delaney, 2002; Castro et al., 2008; González et al., 1994; Morona & González, 2013; Porteros et al., 1997). I additionally used a custom bred transgenic line in which GFP is expressed under the *pax6* promoter (NBT-Katushka pax6-GFP) to visualize another subset of interneurons (Bandín et al., 2014) in combination with *tubb2b*-dependent fluorescence.

I detected CR-positive cells in the granule cells layer of the OB as well as the mitral cell layer (Figure 12 F; Daume et al., 2022). I detected no *tubb2b*-dependent fluorescence in CR-positive cells (Figure 12 F; Daume et al., 2022). TH-positive cells were located in the mitral cell layer and periglomerular layer and also here no both *tubb2b*- and TH-positive cells were present (Figure 12 G; Daume et al., 2022). *pax6*-

dependent fluorescence was present in the mitral cell layer of the main and accessory OB, were I found *tubb2b*-dependent fluorescence as well (Figure 12 C - E; Daume et al., 2022). Some *tubb2b*-positive cells also show *pax6* dependent fluorescence (Figure 12 D and E; Daume et al., 2022).

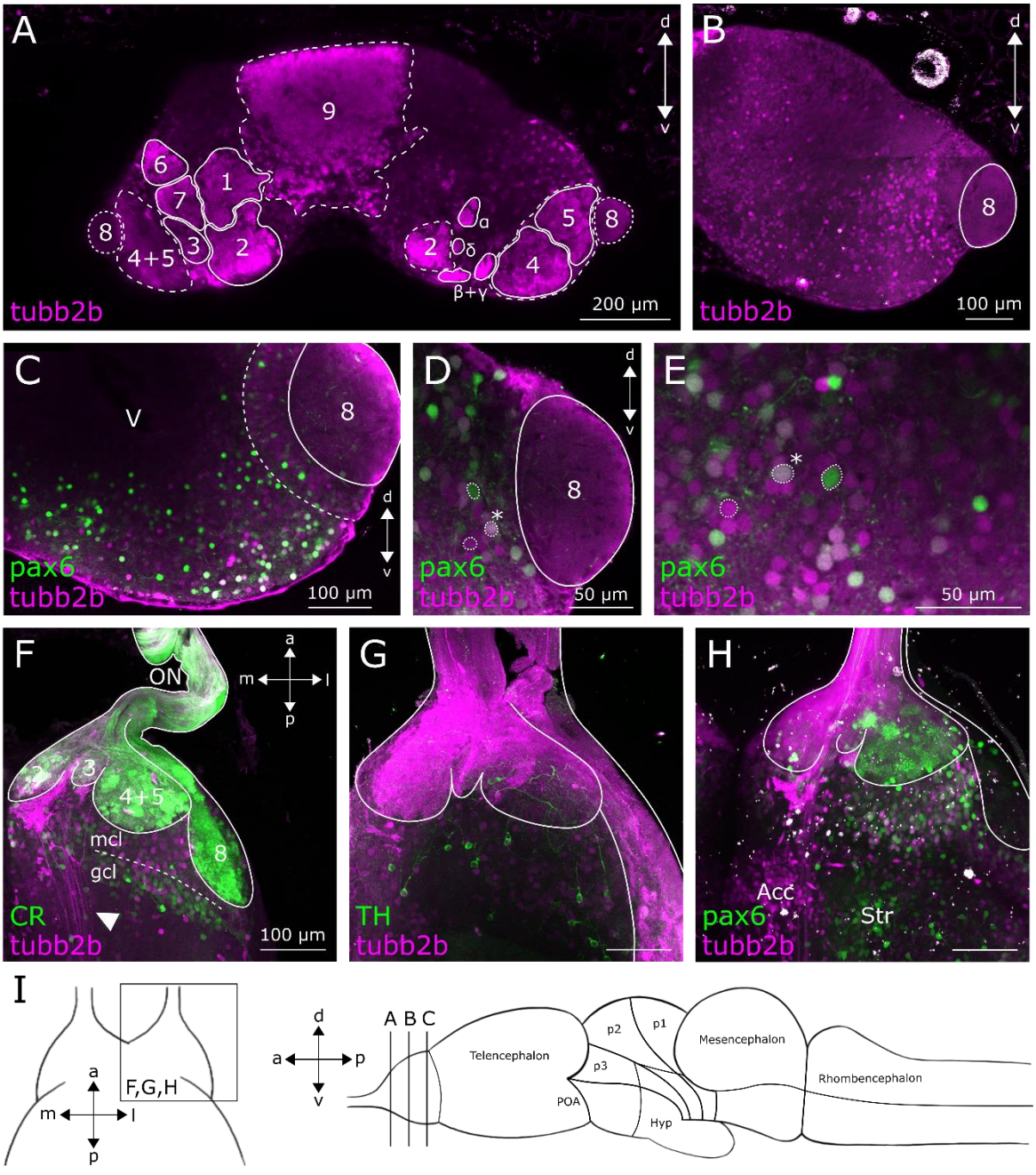

Figure 12: *tubb2b*-dependent fluorescence in the OB of larval *Xenopus laevis*. A Coronal slice of the OB (left and right brain hemisphere) of NBT-Katushka γ-cry Venus transgenic larvae. *tubb2b*-dependent fluorescence (magenta) in ORN axons terminating in all glomerular clusters (**projection fields 1 – 9 and α, β, γ, δ**; Gaudin & Gascuel, 2005). **B** Coronal slice of the OB in the right brain hemisphere of NBT-Katushka γ-cry Venus transgenic larvae.

tubb2b-depentent fluorescence (magenta) in the mitral cell layer of the main OB and accessory OB (**projection field 8**). **C – E** Coronal slices of the OB in the right brain hemisphere of NBT-Katushka pax6-GFP transgenic larvae. **C** *tubb2b*-dependent fluorescence (magenta) together with *pax6*-dependent fluorescence (green) in cells of the mitral cell layer. **D and E** Close-ups of the mitral cell layer of the main OB and accessory OB (**projection field 8**). Examples of single cells (encircled) with either *tubb2b*-dependent fluorescence (magenta), *pax6*-dependent fluorescence (green) or both *tubb2b*- and *pax6*-dependent fluorescence (*). **F – H** Maximum projection of the OB in the right brain hemisphere from a ventral view. **F** *tubb2b*-dependent fluorescence (magenta) is not present in calretinin positive cells (**CR**; green). In the intermediate OB *tubb2b*-positive fibers (white arrow) bypass OB structures and project posteriorly. **G** *tubb2b*-dependent fluorescence (magenta) is not present in tyrosine hydroxylase-positive cells in the OB (**TH**; green). **H** *tubb2b*-dependent fluorescence together with *pax6*-dependent fluorescence in the mitral cell layer of the OB. *tubb2b*-dependent fluorescence found in the nucleus accumbens (**Acc**) and *pax6*-dependent fluorescence found in the striatum (**Str**). **I** Scheme of the larval brain with approximate positions of the sections shown in A – C (lines) and whole mount preparation shown in F – H (box). Preoptic area (**POA**). Hypothalamus (**Hyp**). Nasal cavity (**NC**). Olfactory nerve (**ON**). Mitral cell layer (**mcl**). Granule cell layer (**gcl**). Ventricle (**V**). Dorsal (**d**). Ventral (**v**). Anterior (**a**). Posterior (**p**). Medial (**m**). Lateral (**l**). Adapted from Daume et al., 2022 Figure 1.

To find out, whether *tubb2b* is active in all mature neurons in the larval OB, I performed antibody stainings against the neuronal marker HuC/D in whole mount preparations of NBT-Katushka γ-cry Venus transgenic larvae. Compared to HuC/D, which is expressed in all cell layers of the OB (Figure 13 A and B; Daume et al., 2022), I found that *tubb2b* is active only in the mitral cell layer and in close proximity to projection fields 1-9 as well as α-δ (Figure 12 B and 13 A and C; Daume et al., 2022). To calculate the cell density of *tubb2b* and HuC/D positive cells in this brain region, I performed cell counting in the whole OB. I counted an average number of 6,517 ± 210 HuC/D positive cells (Figure 13 D; Daume et al., 2022) and an average number of 1,588 ± 191 *tubb2b* positive cells (Figure 13 D; Daume et al., 2022). This leads to an overall density of on average 24,4 % of *tubb2b* positive cells in comparison to HuC/D positive cells (Figure 13 D; Daume et al., 2022).

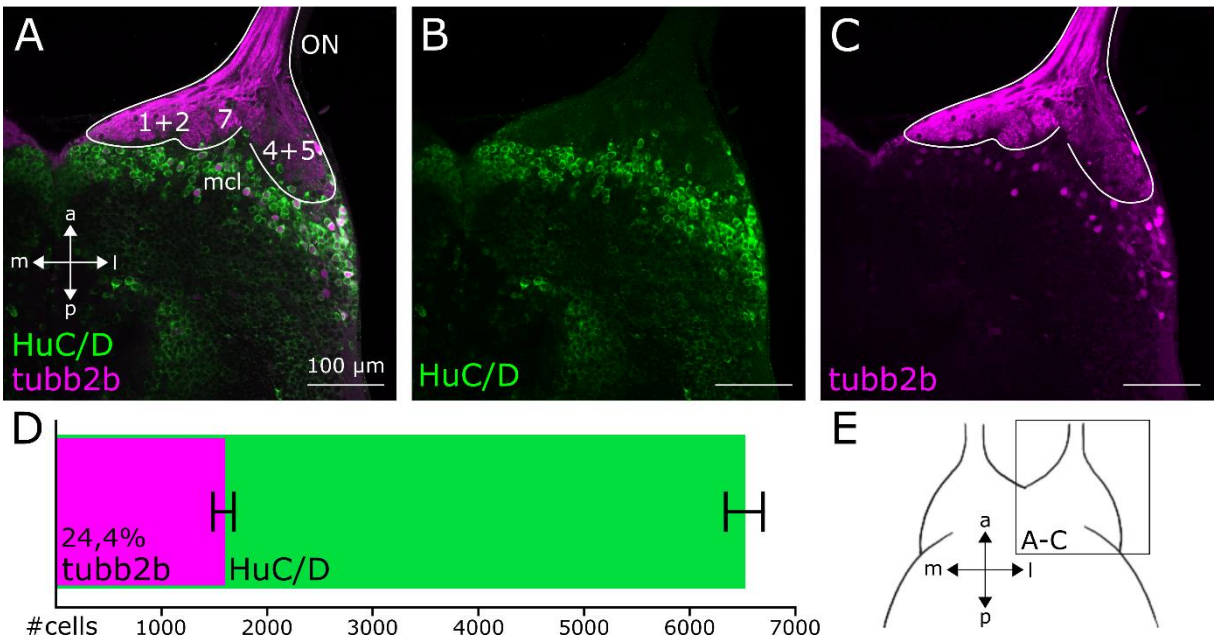

Figure 13: *tubb2b*-positive and HuC/D-positive neurons in the OB of premetamorphic *Xenopus laevis*. A - C Single focal plane of the OB of the right brain hemisphere (ventral view). **A** HuC/D-positive cells (green) are present in the whole OB. Some HuC/D-positive cells are also *tubb2b*-positive (magenta). **B** Pattern of HuC/D-positive cells in the larval OB. C Pattern of *tubb2b*-dependent fluorescence in the larval OB. **D** Cell density of HuC/D- (green) and *tubb2b*-positive (magenta) cells in comparison. Average number of: 1,588 ± 191 (n = 10) *tubb2b*-positive cells, 6,517 ± 210 (n = 3) HuC/D-positive cells. **E** Scheme of the larval anterior telencephalon with the OB (box). Olfactory nerve (**ON**). Anterior (**a**). Posterior (**p**). Medial (**m**). Lateral (**l**). Image from Daume et al., 2022 Figure 3.

Pallium and subpallium

In the anterior telencephalon, I observed that cells of the nucelus accumbens (Acc) are *tubb2b*-positive (Figure 12 H; Daume et al., 2022). I also found *tubb2b*-positive cells in the striatum (Str; Figure 14 A; Daume et al., 2022). Here, I also found *pax6*-positive cells (Figure 12 H; Daume et al., 2022). Posteriorly in the telencephalon, I found *tubb2b*-positive cells in the medial pallium (Mp; (Figure 14 A, B and E; Daume et al., 2022), Lp (Figure 14 B, D and E; Daume et al., 2022) and Vp (Figure 14 D and E; Daume et al., 2022). In the posterior telencephalon, *tubb2b*-dependent fluorescence was also present in the MeA (Figure 14 C, E and G; Daume et al., 2022), central amygdala (CeA; Figure 14 G and H; Daume et al., 2022), septum (S; Figure 14 C; Daume et al., 2022), dorsal pallium (Dp; Figure 14 B; Daume et al., 2022) and at the position of the lateral forebrain bundle (lfb; Figure 14 E; Daume et al., 2022). I additionally found *tubb2b*-positive cells in fibers of the optic nerve (OpN; (Figure 14 E,

F and H; Daume et al., 2022), fibers that project through the anterior commisure (ac; Figure 14 E and H; Daume et al., 2022) and cells of the preoptic area (POA; Figure 14 E and F; Daume et al., 2022) and hypothalamus (Hyp; Figure 15 B - D; Daume et al., 2022). I also observed *pax6*-positive cells throughout the telencephalon, which were present in the all areas of the pallium (Mp, Dp, Lp, Vp; Figure 14 B and D; Daume et al., 2022), parts of the amygdala (MeA and CeA; Figure 14 C, G and H; Daume et al., 2022), bed nucleus of the stria terminalis (BST; Figure 14 G and H; Daume et al., 2022), and fibers of the OpN (Figure 14 H; Daume et al., 2022). *pax6*-dependent fluorescence was most prominent at the level of the CeA (Figure 14 G and H; Daume et al., 2022).

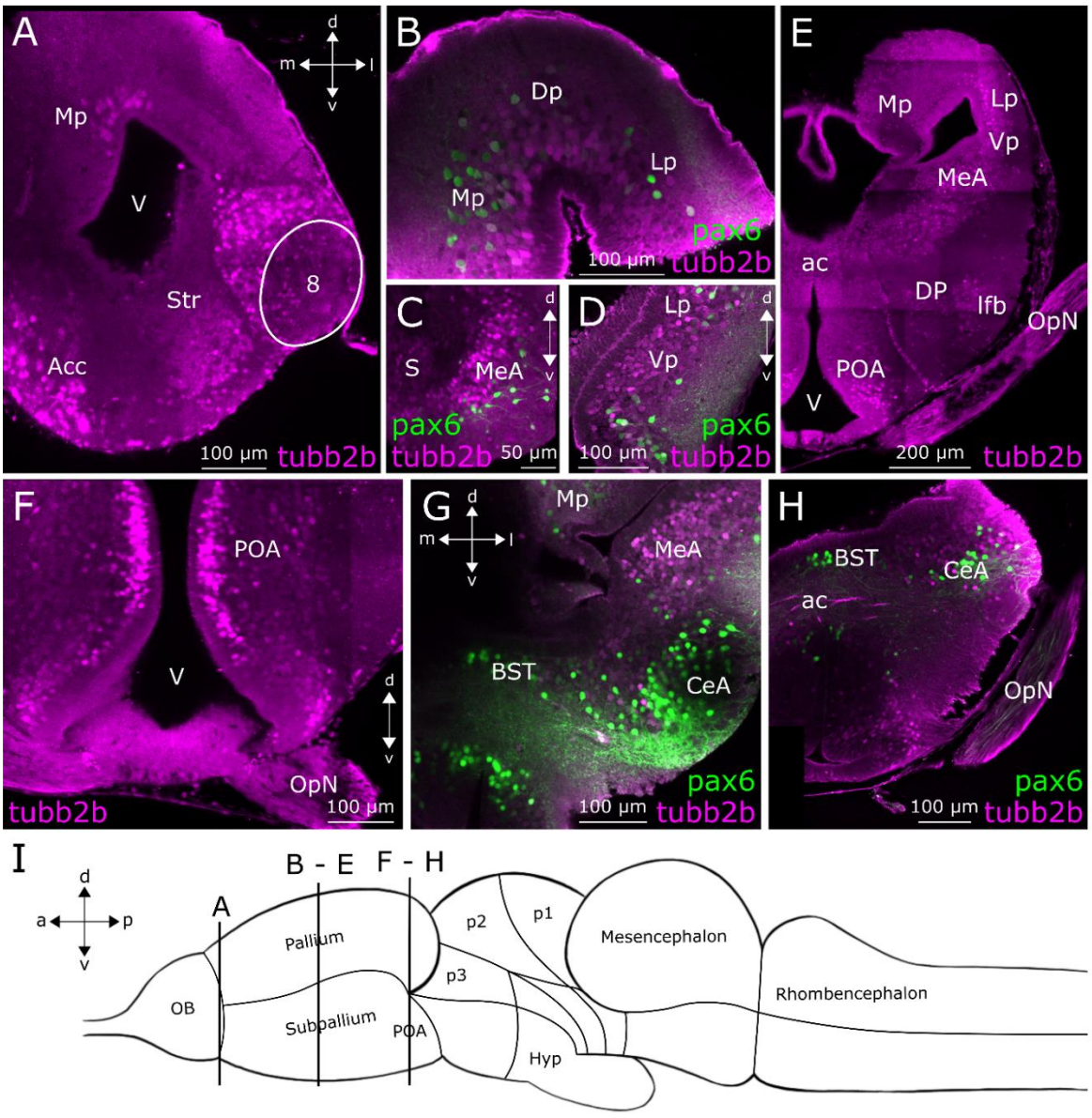

Figure 14: *tubb2b*-dependent fluorescence in the pallium and subpallium of premetamorphic *Xenopus laevis*. Coronal sections through the telencephalon containing all subpallial and pallial brain regions of transgenic NBT-Katushka γ-cry Venus (A, E and F) and NBT-Katushka pax6-GFP (B-D, G and H) larvae. **A** *tubb2b*-dependent fluorescence in the anterior telencephalon in cells of nucleus accumbens (**Acc**), striatum (**Str**), accessory OB (**projection field 8**) and medial pallium (**Mp**). **B – D** Close-ups of the intermediate telencephalon with *tubb2b*-dependent fluorescence in the dorsal pallium (**Dp**), ventral pallium (**Vp**), medial pallium (**Mp**), lateral pallium (**Lp**), septum (**S**), and medial Amygdala (**MeA**). *pax6*-dependent fluorescence in the Mp, Dp, Lp, Vp and MeA. **E** Sections through the intermediate telencephalon show *tubb2b*-dependent fluorescence in cells of the Mp, Lp, Vp, MeA, dorsal pallidum (**DP**), preoptic area (**POA**) and optic nerve (**OpN**). **F – H** Close-ups of the posterior telencephalon. **F** *tubb2b*-dependent fluorescence in cells of the POA and fibers of the OpN. **G and H** *tubb2b*-dependent fluorescence in the MeA and central amygdala (**CeA**) as well as fibers in the anterior commissure (**ac**) and OpN. *pax6*-dependent fluorescence in the bed nucleus of the stria terminalis (**BST**), CeA and fibers of the OpN. **I** Scheme of the larval brain with the approximate positions of the sections shown in A – H (lines). Hypothalamus (**Hyp**). Olfactory bulb (**OB**). Ventricle (**V**). Dorsal (**d**). Ventral (**v**). Anterior (**a**). Posterior (**p**). Lateral (**l**). Medial (**m**). Figure from (Daume et al., 2022) Figure 4.

Diencephalon

In the diencephalon, I detected *tubb2b*-positive cells within the subventricular zone of prosomeres 1-3 (p1-3; Figure 15 A - D; Daume et al., 2022). Within p2, I also found *tubb2b*-positive cells at the level of the thalamus (Th; Figure 15 B and C; Daume et al., 2022). At the level of the Th I also observed CR-positive cells, which were not *tubb2b*-positive (Figure 15 B and C; Daume et al., 2022). In the posterior part of p3 I detected Pax7-positive cells, which were also not *tubb2b*-positive (Figure 15 D; Daume et al., 2022).

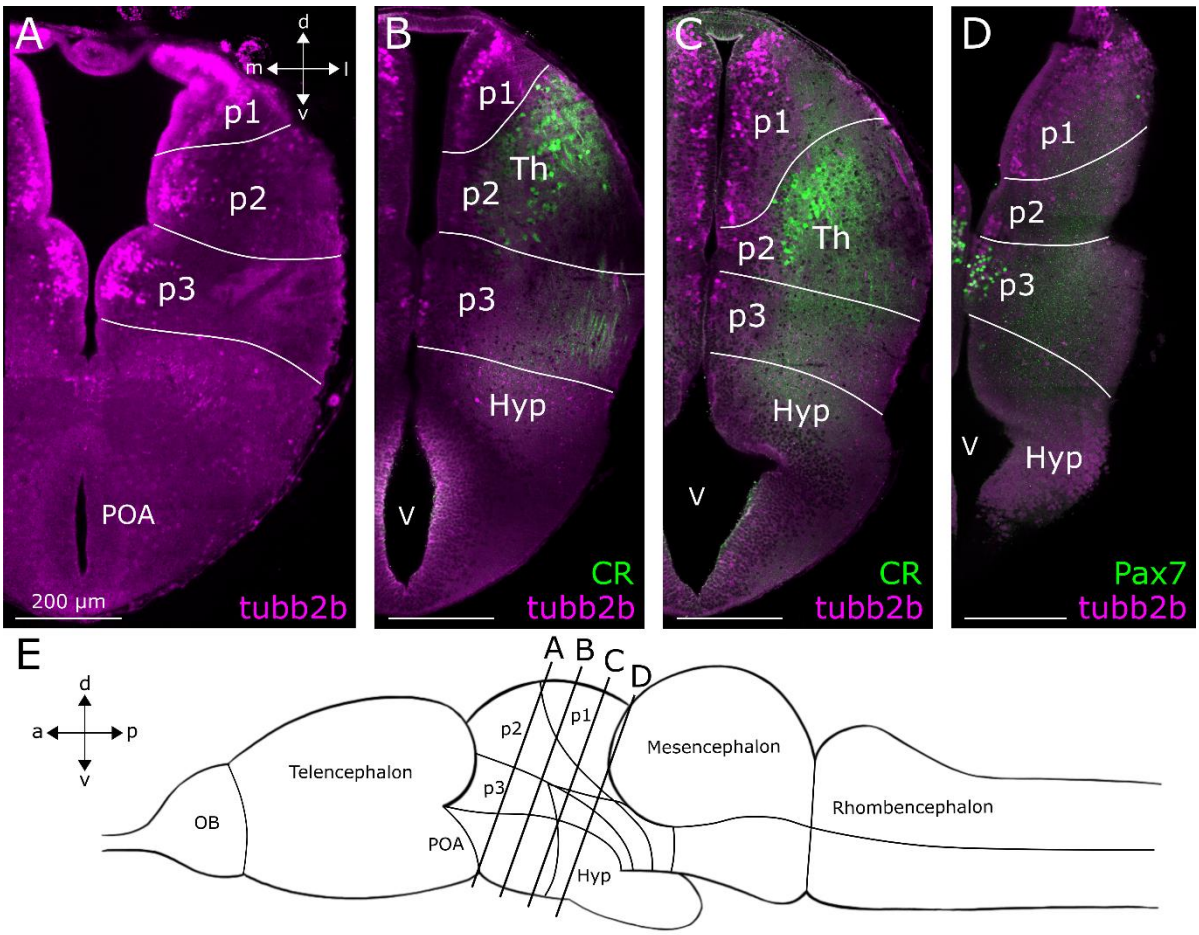

Figure 15: *tubb2b*-dependent fluorescence in the diencephalon of premetamorphic *Xenopus laevis*. Coronal sections through the diencephalon of transgenic NBT-Katushka γ-cry Venus tadpoles. **A** *tubb2b*-dependent fluorescence (magenta) is present in cells of prosomeres 1-3 (**p1-3**). **B and C** *tubb2b*-dependent fluorescence (magenta) is not present in calretinin-positive cell bodies and fibers (CR; green) within the thalamus (**Th**). **D** Pax7-positive cells in p3 are not *tubb2b*-positive. E Scheme of the larval brain with the approximate positions of the slices shown in A – D (lines). Olfactory bulb (**OB**). Hypothalamus (**Hyp**). Preoptic Area (**POA**). Ventricle (**V**). Dorsal (**d**). Ventral (**v**). Anterior (**a**). Posterior (**p**). Medial (**m**). Lateral (**l**). Figure from Daume et al., 2022 Figure 5.

Premetamorphic olfactory PNs of transgenic *Xenopus laevis*

With the knowledge of the activity pattern of *tubb2b* in transgenic *Xenopus laevis* larvae, I was able to study olfactory PN more precisely. I started with labelling single PNs with fluorophore-coupled dextran dye to study their morphology. Because we knew from past studies, that ORNs can be separated into a lateral and medial odor processing stream (Gliem et al., 2013), I specially focused on comparing lateral vs. medial PNs. In this experiment, the use of NBT-Katushka γ-cry Venus transgenic larvae (*tubb2b*-promoter driven) helped me to specifically target PNs during the injection process, but also to analyze their location within the OB during microscopy.

Lateral vs. medial PNs

During my project, I labelled and 3D reconstructed a total of 29 PNs in the premetamorphic OB of transgenic NBT-Katushka γ-cry Venus larvae using Vaa3D (Peng et al., 2010). These include a total of 15 lateral PNs and 14 medial PNs (Figure 16 B and C). These cells were compared in the number of dendritic tufts, neurites that originate from the soma, extra-glomerular branching points, and dendritic/ axonal blunt endings (Figures 17 and 18).

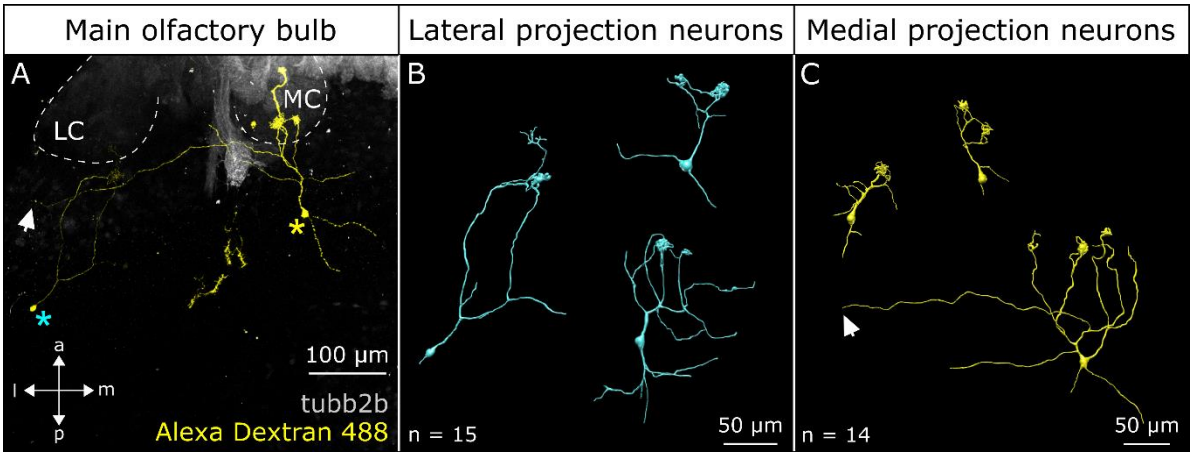

Figure 16: Medial and lateral olfactory PNs in the OB of larval *Xenopus laevis*. A Maximum projection of the OB (left brain hemisphere) of transgenic NBT-Katushka γ-cry Venus tadpoles with one labelled lateral (cyan asterisk) and one medial (yellow asterisk) single PN. The lateral PN is connected to the lateral clusters (LC) and the medial PN to the

medial cluster (MC). The medial PN shows a secondary dendrite projecting into the lateral mitral cell layer (white arrow). **B** Selection of three reconstructed lateral PNs showing structural varieties and size differences. **C** Selection of three reconstructed medial PNs with varieties in structure, like a long secondary dendrite (white arrow) and size. Anterior (**a**). Posterior (**p**). Lateral (**l**). Medial (**m).**

Dendritic tufts

I observed, that the reconstructed PNs had at least one and a maximum of three dendritic tufts (Figure 17 A). Medial PNs differ in their number of dendritic tufts from lateral dendritic tufts significantly (p = 0.0025). The majority of lateral PNs had one tufted dendrite (60%; Figure 17 A, cyan) while the majority of medial PNs had two tufted dendrites (64.3%; Figure 17 A, yellow). One-third of the lateral PNs had two tufted dendrites and 6.7 % had three tufted dendrites (Figure 17 A, cyan). In comparison, 21.4 % of medial PNs had one and 14.3 % three tufted dendrites (Figure 17 A, yellow).

Stems from soma

Counting the neurites originating from the soma, I detected between one and four neurites per cell (Figure 17 B). I found no significant difference in the number of soma stems between lateral and medial PNs (p = 0.399). With eight lateral (Figure 17 B, cyan) and seven medial (Figure 17 B, yellow) PNs the majority had two soma stems. Having four soma stems was second most common with four lateral (Figure 17 B, cyan) and six medial (Figure 17 B, yellow) PNs. Uneven numbers of soma stems were less common, as only one lateral PNs (Figure 17 B, cyan) had one soma stem, and two lateral (Figure 17 B, cyan) and one medial (Figure 17 B, yellow) PN had three soma stems.

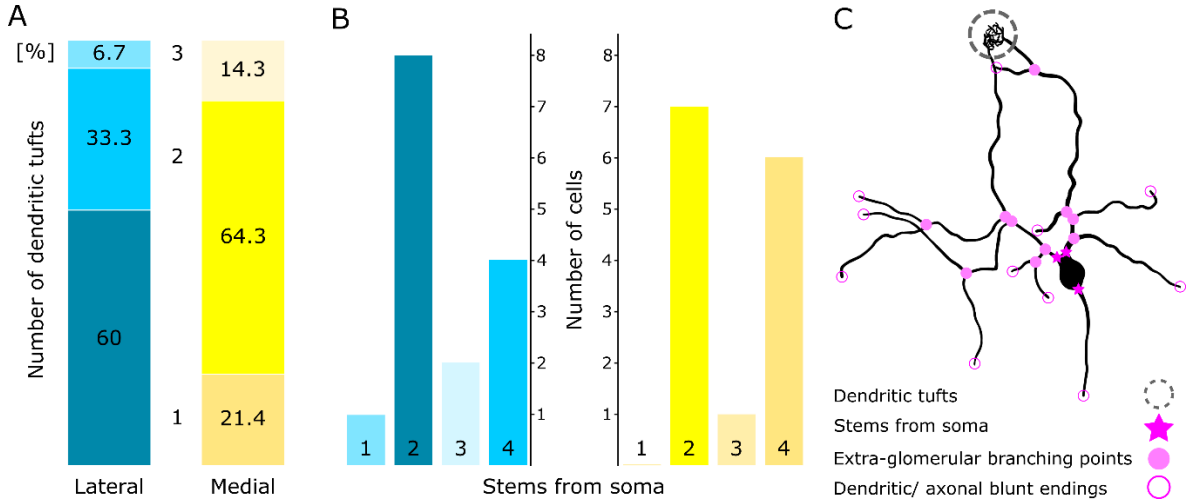

Figure 17: Lateral and medial PNs vary in the number of dendritic tufts but share a similar number of soma stems. A Lateral PNs (cyan; n = 15 cells) show a significantly different (p = 0.025) distribution [%] in the number of dendritic tufts then medial PNs (yellow; n = 14 cells). **B** Lateral (cyan) and medial (yellow) PNs are not significantly different (p = 0.399) in the number of stems from the soma, where both share a majority of either two or four stems. **C** Scheme of the structural characteristics of an example PN showing all analyzed elements of Figure 17 and 18.

Branching points

To measure how highly branched lateral and medial PNs are, I counted all branching points that are located outside of dendritic tufts (extraglomerular). Both cell groups have no significant difference in the number of extraglomerular branches ($p > 0.05$). I found four to 16 extraglomerular branches in lateral PNs (Figure 18 A; cyan) and four to 15 extraglomerular branches in medial PNs (Figure 18 A; yellow). I measured an average of 8 branches in both lateral (8 ± 3; Figure 18 A; cyan) and medial PNs (8 ± 4; Figure 18 A; yellow).

Blunt endings

To see how many dendrites do not end in tufted dendrites, I counted the number of blunt endings. Lateral PNs contain four to 17 blunt endings (Figure 18 B; cyan). In comparison, the number of dendritic tufts lays between one and three (Figure 17 A; cyan). Medial PNs possess two to 17 blunt endings (Figure 18 B; yellow). Both lateral

and medial PNs show an average number of eight blunt endings (Lateral PNs: 8 ± 3 blunt endings; Figure 18 B cyan; Medial PNs: 8 ± 4 blunt endings; Figure 18 B yellow). Again, lateral and medial PNs do not differ significantly from each other (p = 0.43).

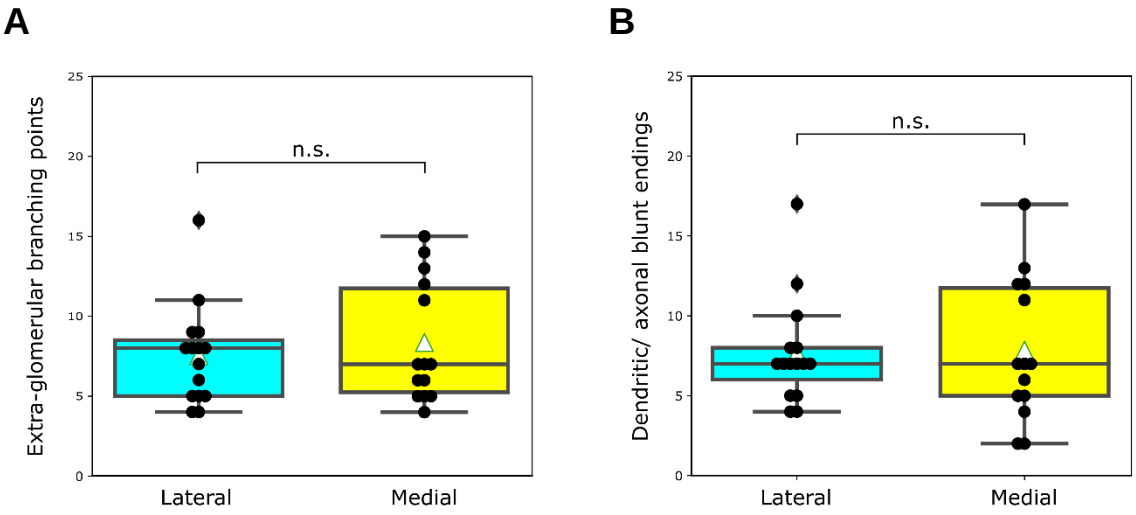

Figure 18: Lateral and medial PNs share a similar amount of extra-glomerular branching points as well as dendritic/ axonal blunt endings. A Number of extra-glomerular branching points of lateral (cyan) and medial (yellow) PNs. Lateral PNs have 4 to 16 extraglomerular branching points (Mean: 7,53; Standard deviation 3,01). Medial PNs have 4 to 15 extraglomerular branching points (Mean: 8,36; Standard deviation 3,66) **B** Number of dendritic/ axonal blunt endings of lateral (cyan) and medial (yellow) PNs. Lateral PNs have 4 to 17 dendritic/ axonal blunt endings (Mean: 7.67; Standard deviation: 3.33). Medial PNs have 2 to 17 dendritic/ axonal blunt endings (Mean: 7.86; Standard deviation: 4.47). Each black dot represents one PN.

Additionally, I observed, that within the medial PN population, a small group of cells has more extra-glomerular branches (20-25 branching points; Figure 18 A) and more blunt endings (10-20 blunt endings; Figure 18 B) that other medial PNs. I then tested statistically if this group is a separate cell population, but several tests showed no significant difference.

I also observed, that four medial PNs extend one or multiple secondary dendrites in the direction of the lateral OB (Figure 16 A and C, white arrow). To find out whether those dendrites stand out in their length compared to secondary dendrites of lateral PNs, I measured the distance from the soma to the endpoint of the longest secondary dendrite of lateral and medial PNs. I found that lateral and medial PNs do not differ significantly in the length of the longest dendrite (p = 0.14).

Axonal projection patterns

To study and compare axonal projections of the whole lateral and medial PN population, I injected Calcein dye into the lateral (n = 5; Figure 19 A - C) and medial (n = 5; Figure 19 D - F) mitral cell layer of the OB. In this experiment, I used transgenic NBT-Katushka γ-cry Venus larvae for a precise injection and further analysis under the microscope. I examined the axonal projections in whole mount preparations of the forebrain which were imaged from a ventral and lateral view (lateral view shown in Figure 19 B and E, 20 and 21).

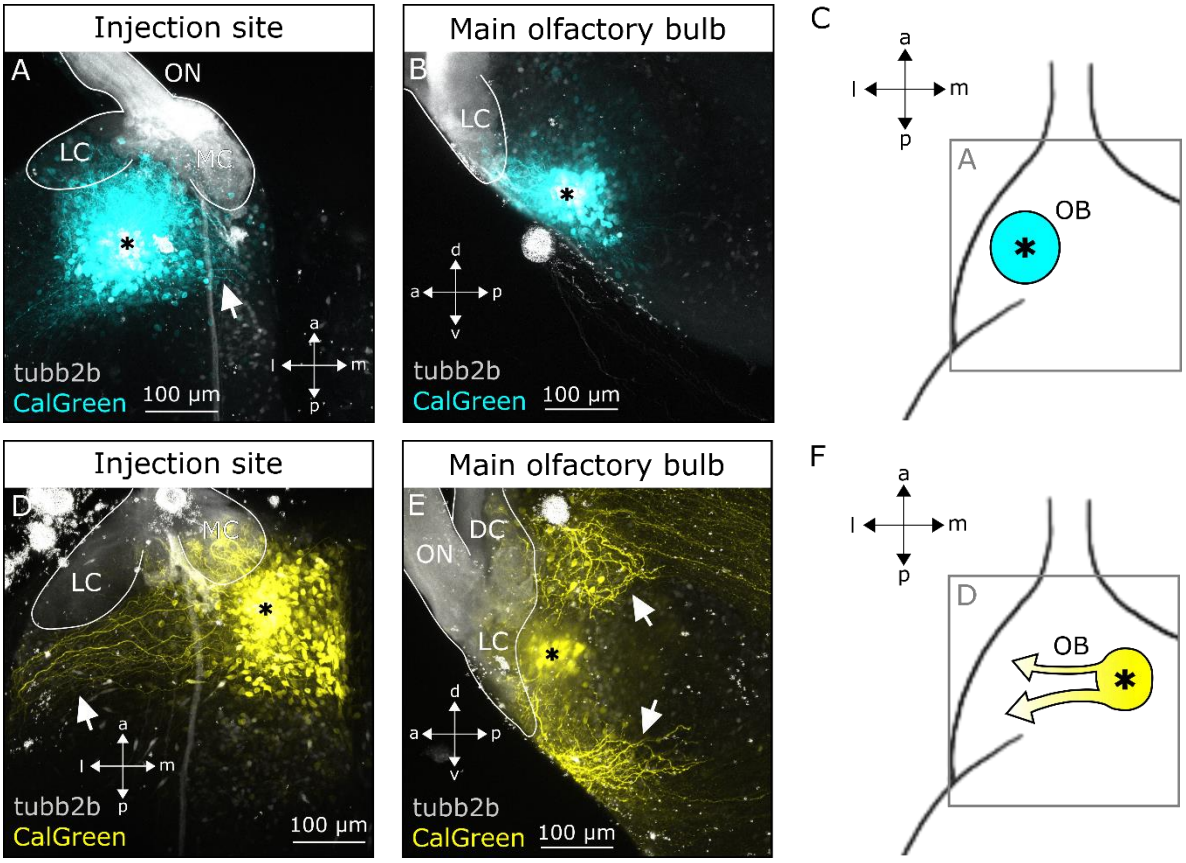

Figure 19: Injection site within the ventrolateral and ventromedial OB of transgenic *Xenopus laevis* larvae. A Maximum projection of the ventral OB (left brain hemisphere). Calcein Green injection (**CalGreen**) into the ventrolateral mitral cell layer (cyan; injection site: *). Dendrites of lateral neurons project towards the medial mitral cells layer (white arrow). **B** Maximum projection of the ventral OB from a sagittal view. Injection site (*) of CalGreen into the ventrolateral mitral cell layer (cyan). **C** Scheme of the ventral OB (left brain hemisphere) from a horizontal view showing the area of the Injection (*) shown in A. **D** Maximum projection of the ventral OB (left brain hemisphere) with CalGreen injection into

the ventromedial mitral cell layer (*; yellow). Dendrites of medial neurons project towards the lateral mitral cell layer (white arrow). **E** Maximum projection of the OB from a sagittal view showing the injection site within the ventromedial OB (*; yellow) and two bundles of dendrites from medial neurons, that projects ventrally and dorsally into the lateral mitral cell layer (white arrows). **F** Scheme of the ventral OB (left brain hemisphere) from a horizontal view showing the area of the injection (*) shown in D. The arrows indicate the two dendritic fiber bundles shown in E. Olfactory nerve (**ON**). Lateral glomerular clusters (**LC**). Medial glomerular cluster (**MC**). Dorsal glomerular clusters (**DC**). Olfactory bulb (**OB**). Lateral (**l**). Medial (**m**). Anterior (**a**). Posterior (**p**). Ventral (**v**). Dorsal (**d**).

Lateral PNs

Within the OB, lateral PNs possess short dendrites projecting towards the medial OB (Figure 19 A) and form two laterally located tracts with their axons (cyan; Figure 20 A, C and E). One axon bundle project dorsally towards the posterior telencephalon (Figure 20 A and E) and one ventrally (Figure 20 C and E). At the level of the Acc and Str, the axon bundles merge and form one large lateral tract (Figure 20 A, C and E). This lateral tract extends up to the ventral subpallium (Figure 20 D and E). I found no axonal projections towards the Dp (Figure 20 B and E), POA, Hyp and diencephalon.

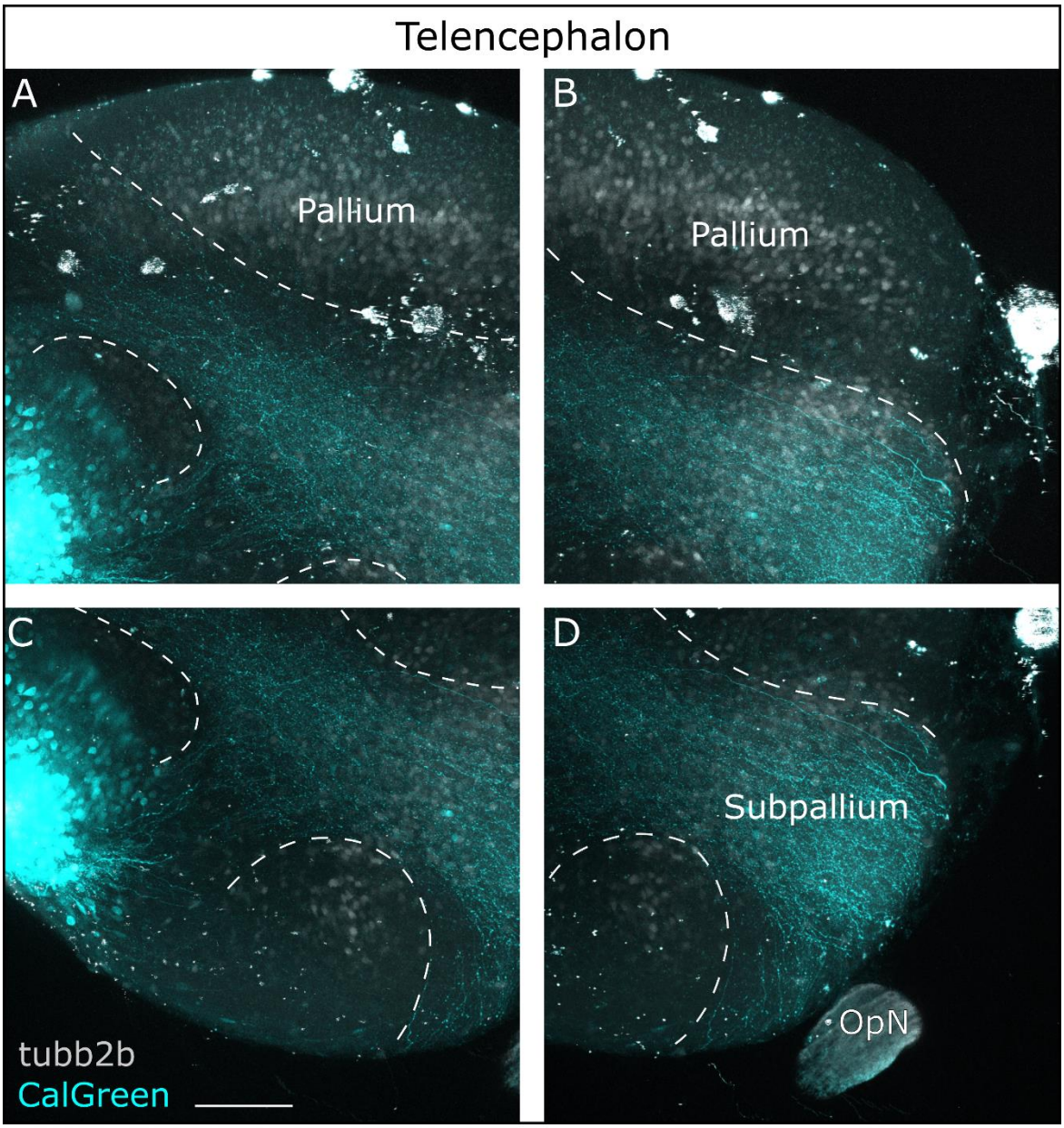
Telencephalon
A
Pallium
B
Pallium
C
D
Subpallium
OpN
tubb2b
CalGreen

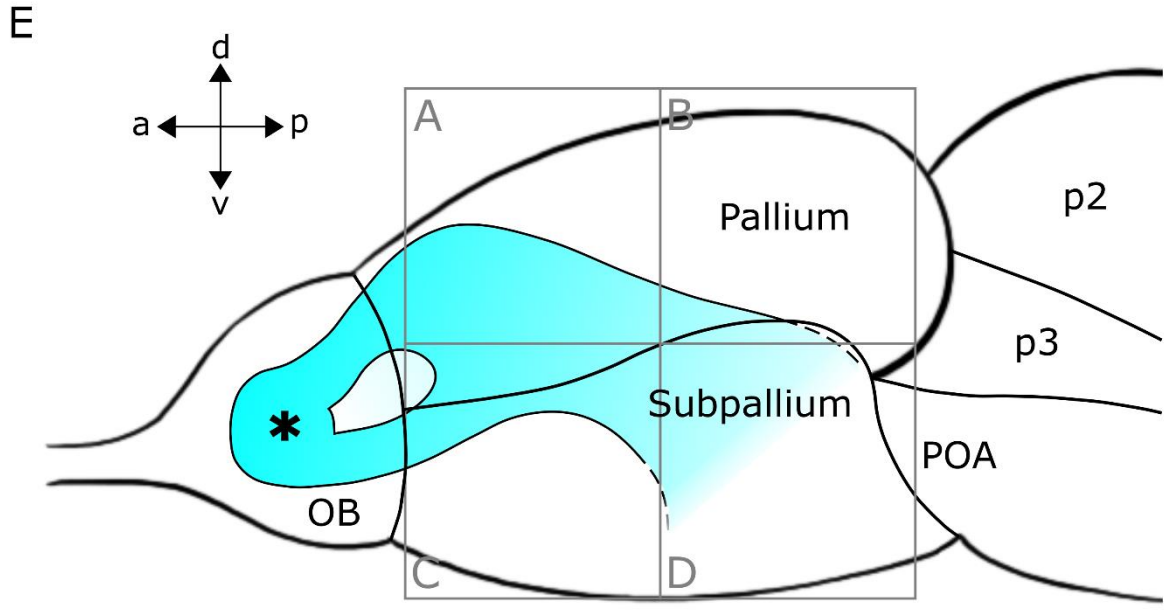
E
d
a
p
v
A
B
Pallium
p2
p3
Subpallium
POA
OB
C
D

Figure 20: Axonal projections of lateral PNs in larval transgenic *Xenopus laevis* OB target the posterior subpallium. A – D Maximum projections of the ventral telencephalon (left brain hemisphere) from a sagittal view. Axons of lateral PNs (cyan) form two distinct fiber bundles in the anterior telencephalon that converge in the anterior telencephalon (A and C). The converged fiber bundle projects posteriorly into the posterior subpallium (D). No axons have been observed that project to the dorsal pallium (B). **E** Scheme of the larval forebrain from a sagittal view showing all four areas shown in A – D. Dye injection site (*) and axonal projection pattern shown in cyan. Olfactory bulb (**OB**). Optic nerve (**OpN**). Preoptic area (**POA**). Prosomeres 2 & 3 (**p2 & p3**). Dorsal (**d**). Ventral (**v**). Anterior (**a**). Posterior (**p**).

Medial PNs

Medial PNs extend long secondary dendrites towards the lateral OB, but in comparison to lateral PNs, they split into two distinct bundles (Figure 19 E). One bundle targets the ventral side the lateral OB and the other one the dorsal side (Figure 19 E; white arrows). Axons of medial PNs form two distinct axon bundles projecting laterally through the dorsal and ventral telencephalon (Figure 21 A, C and E). In comparison to lateral PNs, those axon bundles do not fuse into one large tract, but both terminate in the posterior subpallium as well (Figure 21 D and E). Similar to lateral PNs, I found no axonal projections towards the Dp (Figure 21 B and E), POA, Hyp and diencephalon.

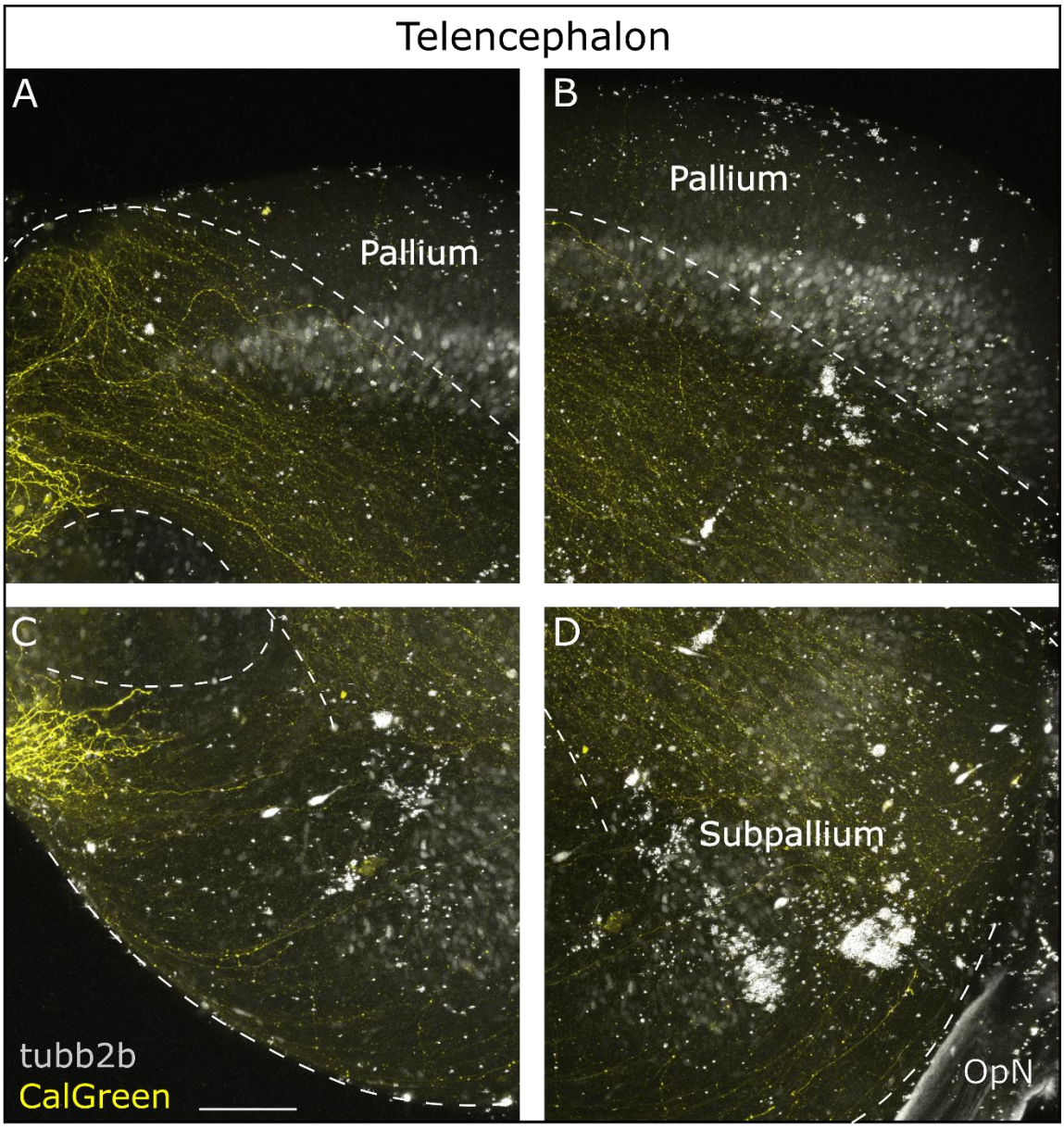
Telencephalon
A
Pallium
B
Pallium
C
tubb2b
CalGreen
D
Subpallium
OpN

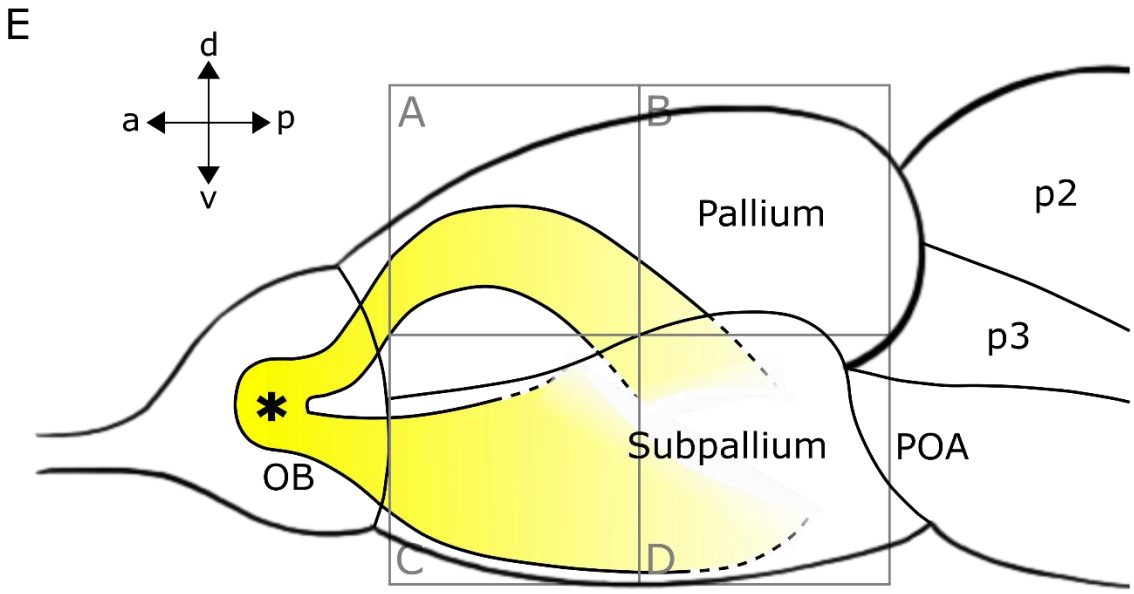
E
d
a
p
v
A
B
Pallium
p2
p3
*
OB
Subpallium
POA
C
D

Figure 21: Axonal projections of medial PNs in larval transgenic *Xenopus laevis* OB target the posterior subpallium via two separate axon bundles. A – D Maximum projections of the ventral telencephalon (left brain hemisphere) from a sagittal view. Axons of medial PNs (yellow) form two distinct fiber bundles in the anterior telencephalon that stay disconnected throughout the whole telencephalon. One fiber bundle project dorsally through the anterior telencephalon (A) and then towards the posterior subpallium (D). The second axon bundle projects ventrally (C) and ends in the posterior subpallium as well (D). No axons have been observed that project to the dorsal pallium (B). **E** Scheme of the larval forebrain from a sagittal view showing all four areas shown in A – D. Dye injection site (*) and axonal projection pattern shown in yellow. Olfactory bulb (**OB**). Optic nerve (**OpN**). Preoptic area (**POA**). Prosomeres 2 & 3 (**p2 & p3**). Dorsal (**d**). Ventral (**v**). Anterior (**a**). Posterior (**p**).

Odorant-induced responses in the posterior telencephalon

To find out whether potential target regions in the posterior telencephalon are functionally connected to olfactory PNs, I performed whole-mount calcium imaging experiments in transgenic tubb2b-GCaMP6s Rno.elas-GFP (*tubb2b*-promoter driven) *Xenopus* larvae.

In my first experiment, I applied a mixture of odorants to the olfactory epithelium while capturing the neuronal activity in the whole posterior telencephalon using multiphoton microscopy. I imaged the subpallium (n = 6) from a lateral view (Figure 23 A, B, E and F) and the pallium (n = 7) from a dorsal view (Figure 23 C and D). To ensure, that the measured responses are reproduceable, all measurements were repeated multiple times.

I identified two major regions in the subpallium and pallium, which responded to the odorant mixture stimulation (Figure 23 H and I). In the subpallium, epithelial odorant mixture application induced robust responses in the CeA (Figure 23 A, B, E, F and H). Within the pallium, the most prominent responses were recorded in the LA (Figure 23 C, D and I). After olfactory nerve transection in both cases no response was present after odorant mixture stimulation (Figure 23 H and I).

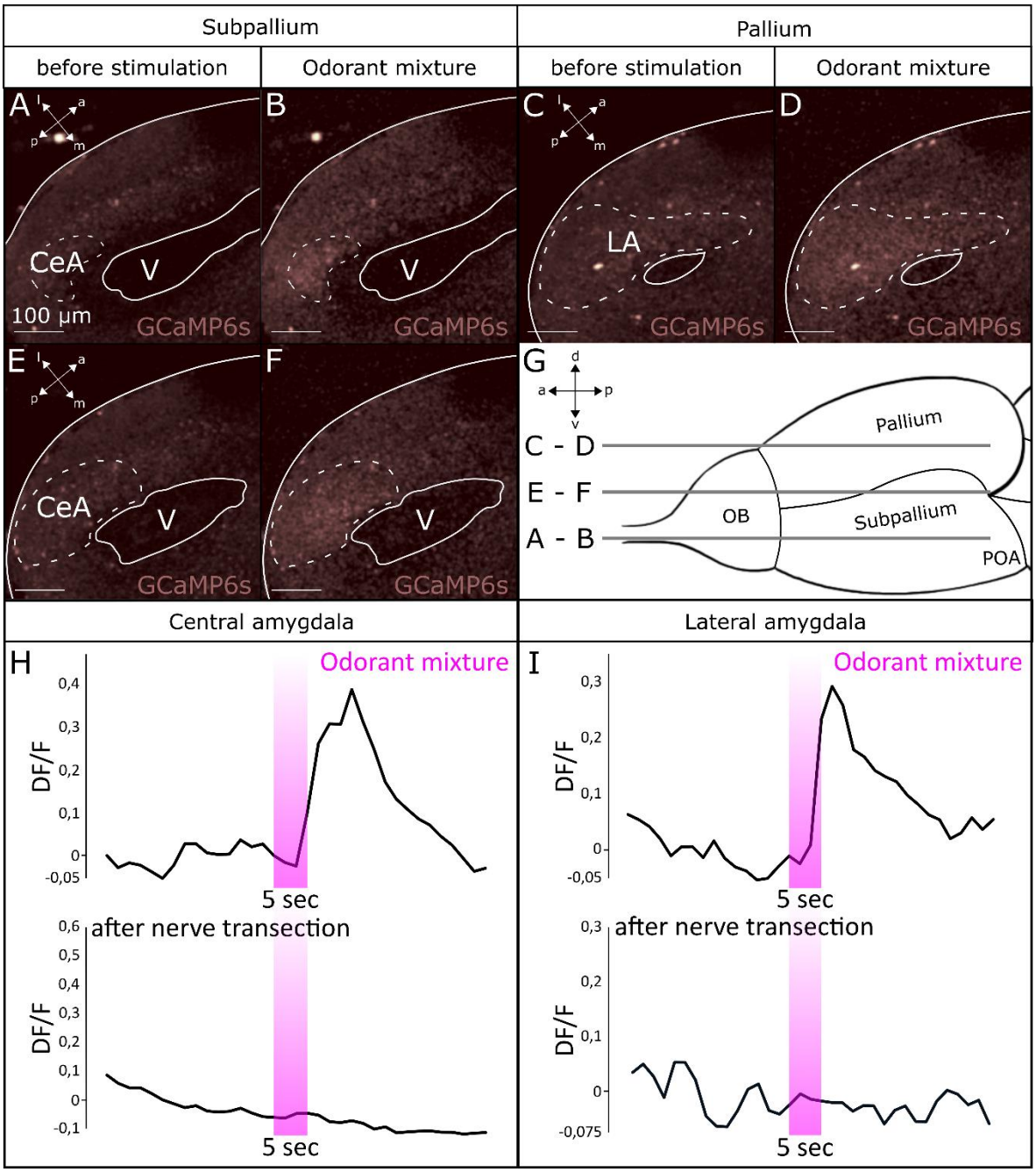

Figure 23: Odorant-induced changes in calcium-dependent fluorescence in the subpallium and pallium of larval *Xenopus laevis*. A – F Microscopic images of one focal plane of the whole posterior telencephalon (subpallium: A, B, E and F; pallium: C and D) of tubb2b-GCaMP6s Rno.elas-GFP *Xenopus* larvae. Epithelial odorant mixture application induced a robust increase of Ca^{2+}-dependent fluorescence in the CeA (B and F) and LA (D). **G** Scheme of the larval telencephalon from a sagittal view showing the approximate positions of the focal planes shown in A – F (lines). **H and I** Time course of odorant-induced intracellular Ca2+ changes in the CeA (H; upper graph) and the LA (I; upper graph). The time period of epithelial odorant application is indicated by the magenta bar. After transection of both olfactory nerves the regions on longer respond to the odorant mixture stimulation

(CeA: H, lower graph; LA: I, lower graph). Central amygdala (**CeA**). Lateral amygdala (**LA**). Olfactory bulb (**OB**). Preoptic area (**POA**). Ventricle (**V**). Anterior (**a**). Posterior (**p**). Dorsal (**d**). Ventral (**v**).

In the second experiment, I imaged both regions with higher magnification (subpallium: n = 4; pallium: n = 3) to ascertain the responding structures were individual neurons. I measured a total of 10 responding cells in the subpallium and 98 responding cells in the pallium that reacted at all three stimulation time points after odorant application. I here show two example neurons of the subpallium (Figure 24 A and B) and pallium (Figure 24 C and D).

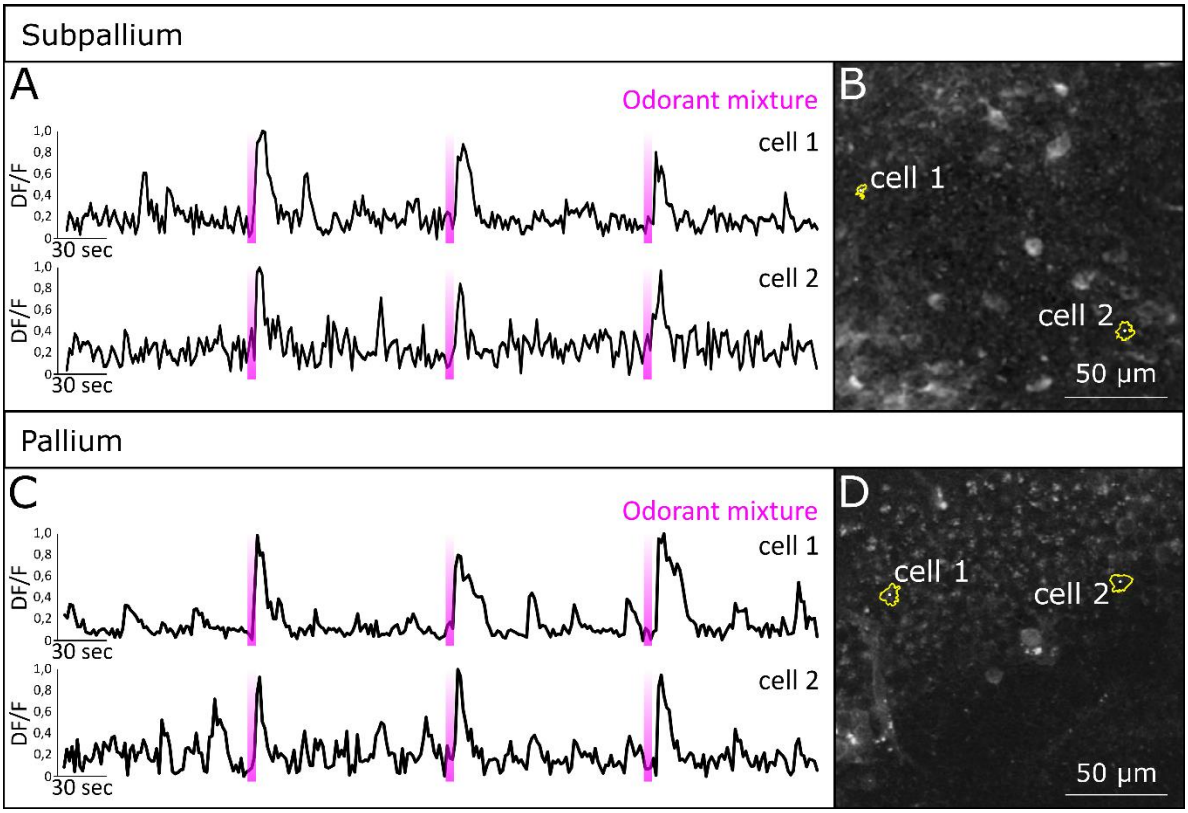

Figure 24: Odorant-induced changes in Ca^{2+}-dependent fluorescence of individual neurons of the subpallium and pallium. A and C Increase of Ca^{2+}-dependent fluorescence after three epithelial stimulations with an odorant mixture in single neurons of the subpallium (A) and pallium (C). The magenta bar indicates the time period of the odorant mixture application. Neurons shown in A and C are highlighted in **B** and **C**.

Discussion

β-tubulin heterodimers are essential components of microtubules which form part of the cytoskeleton in eukaryotic cells (Kapitein & Hoogenraad, 2015; Knossow et al., 2020; Ludueña et al., 1977; Ludueña & Banerjee, 2008; Sullivan, 1988; Wade, 2009). In developing and adult neurons, microtubules support the accurate structure of axons, dendrites and synapses and enable the trafficking of vesicles (Lasser et al., 2018). Isotypes of β-tubulin occur in different tissues or different subtypes of cells from the same tissue (Eddé et al., 1981; Moura Neto et al., 1983; Sullivan & Cleveland, 1986). The neuron-specific β-tubulin isotype of *Xenopus laevis* is class II β-tubulin, which is widely expressed in the nervous system (Bieker & Yazdani-Buicky, 1992; Dworkin-Rastl et al., 1986; Moody et al., 1996; Oschwald et al., 1991). The promoter of class II β-tubulin (*tubb2b*) is used to establish transgenic frog lines for studies of the nervous system (Horb et al., 2019; Love et al., 2011; Offner et al., 2020), but a detailed description of its activity pattern at cellular resolution has not been performed yet. Therefore, this work was set out to provide a first deeper investigation of the *tubb2b*-dependent fluorescence expression pattern in the forebrain of larval *Xenopus laevis* to enable a precise use of *tubb2b* promoter-driven transgenic frogs.

tubb2b-dependent fluorescence is limited to specific cells in the forebrain of larval *Xenopus laevis*

To begin with, it is essential to state that I can confirm that the *tubb2b* promoter is active in neurons, which was also mentioned for its protein class II β-tubulin (Moody et al., 1996). In the forebrain of premetamorphic *Xenopus laevis* larvae I observed that *tubb2b* is not active in all neurons but rather specific to certain regions and subtypes of neurons, on which I go into detail in the OB exclusively. According to this observation, transgenic *tubb2b* promoter-driven frog lines cannot be considered for the use as a pan-neuronal marker and instead has to be used carefully for studies of the nervous system.

Stainings with different antibodies against well-known markers for the main *Xenopus laevis* forebrain regions like Pax7, CR, TH and the use of a transgenic *pax6* promoter-driven frog line (Bandín et al., 2013, 2014; Boyd & Delaney, 2002; González et al.,

1994; Milán & Puelles, 2000; Morona & González, 2013) revealed, that *tubb2b*-dependent fluorescence is absent in: TH- and CR-positive neurons in the OB, *pax6*-positive neurons in the CeA, Mp and Lp, CR-positive neurons and fibers of the Th and Pax7-positive neurons in p3 of the diencephalon. Nevertheless, *tubb2b* is active in all main forebrain regions and I found *tubb2b*-dependet fluorescence in ORNs of the MOE and their axons in the OB, neurons in the OB and AOB mitral cell layer, fibers of the EBOS, neurons of the basal ganglia, pallium, amygdaloid complex, POA, Hyp, prethalamus, Th and fibers of the optic nerve (summarized in Figure 25). To measure the approximate cell density *tubb2b*-positive cells in comparison to postmitotic HuC/D-positive cells, I performed cell counting in the OB as an example region. Only 24.4 % of all mature neurons of the OB are *tubb2b*-postive, which clearly demonstrates again that the activity of the *tubb2b* promoter is not pan-neuronal.

One explanation of this circumstance could be the genome of the frog. *Xenopus laevis* is one of the few allotetraploid species with four sets of chromosomes. Having more than two sets of chromosomes (polyploidy) is a rare condition in higher vertebrates, but very common in amphibians (Bisbee et al., 1977; Evans et al., 2004; Kobel & Du Pasquier, 1986; Session et al., 2016). We cannot exclude that the four chromosome sets potentially lead to a mosaic expression of the genome-inserted transgene. Should this be the case, it would explain why the calculated density of *tubb2b*-postive cells in the OB corresponds to ¼ of the total mature neurons. This implies that the promotor could be inactive or silenced in three of the four chromosome sets.

Another explanation could be the varying expression patterns of genes and proteins during the development of the animal. In this work, I focused on the premetamorphic larvae ranging from stage 48 to 52 (ca. 7 to 17 days after fertilization at 22-24°C; Nieuwkoop & Faber, 1994). Therefore, only a snapshot of the overall gene expression in the *Xenopus laevis* forebrain is shown here and it is possible, that in adult frog the activity pattern of the *tubb2b* promoter looks entirely different. A good example for the varying expression pattern of a β-tubulin protein during development is the zebrafish class I β-tubulin (zβ1; Oehlmann et al., 2004). In the zebrafish *Danio rerio*, zβ1 is restricted to the nervous system, like class II β-tubulin in the frog *Xenopus laevis* (Bieker & Yazdani-Buicky, 1992; Moody et al., 1996; Oehlmann et al., 2004; Oschwald et al., 1991). In zebrafish larvae, zβ1 is restricted to peripheral and central nervous system regions that contain early differentiating neurons. Later in their development,

zβ1 decreases and its expression gets limited to some proliferative zones in the brain and the olfactory epithelium. One of those proliferative zones is the OB (Oehlmann et al., 2004). A role of β-tubulin proteins in neuronal differentiation and neurogenesis is not uncommon and is reported in mice, rat and even *Xenopus laevis* (Joshi & Cleveland, 1989; Latremoliere et al., 2018; Liu et al., 2015; Moody et al., 1996; Oehlmann et al., 2004). Thus, I assume that many of the present *tubb2b*-positive cells in proliferative regions like the Acc, Lp, Mp, Dp, ventral POA and ventral Hyp (D'Amico et al., 2011) are involved in differentiation and neurogenesis which might be a reason why *tubb2b* is not active in all cells of these areas. Interestingly, I also found *tubb2b*-positive cells in regions without proliferative activity, such as the DP and Th (D'Amico et al., 2011), raising the question of whether *tubb2b* in this case has other functions in this context. On the other hand, it could provide an indication, that the DP and Th are not fully developed during that stage of the animal. In order to answer these questions, a comparative study with different larval stages, including the adult frog, would be necessary.

I should also mention, that the expression pattern of β-tubulin proteins can change within individual neurons during development, as it has been shown for different β-tubulin isotypes in single mammalian cells (Guo et al., 2011). In cultured neurons of newborn mice, the expression pattern of β-tubulin II changed during development. After differentiation, β-tubulin II is no longer present in parts of the cell body but starts being expressed in neurites (Guo et al., 2011). Here, β-tubulin II supports the regulation of proper neurite outgrowth (Guo et al., 2011). A study in *Xenopus laevis* also reports of class II β-tubulin being involved in axonal growth and elongation (Moody et al., 1996). This could explain why in some cases I also observed *tubb2b*-dependent fluorescence in axon bundles like the ON, OpN and EBOS. These three structures especially have in common, that their cell bodies are located in peripheral organs and their axons cover a relatively long distance to their target regions (Burd, 1991; Cima & Grant, 1982; Pinelli et al., 2004). Not only does this show *tubb2b* activity in different cellular structures, but also raises the question of whether *tubb2b* might has a special role to enable efficient intracellular transport over long distances.

Structures of the primary olfactory pathway are *tubb2b*-positive

Lifelong neuronal regeneration is an exceptional ability of the vertebrate olfactory system (Calvo-Ochoa et al., 2021; Graziadei & Dehan, 1973; Graziadei & Monti Graziadei, 1983; Steuer et al., 2014; Yu & Wu, 2017). Olfactory sensory neurons undergo constant natural turnover and have the ability to regrow even after an injury (Brann & Firestein, 2014; Graziadei & Monti Graziadei, 1983; Higgs & Burd, 2001; Schwob, 2002). Also in larval *Xenopus laevis*, newborn ORN axons fully reinnervate the OB after 7 weeks of ON injury and calcium imaging experiments show that newly formed glomerular clusters and second order neurons successfully respond to olfactory stimuli again (Hawkins et al., 2017). The presence of *tubb2b*-dependent fluorescence in the vast majority of ORN cell bodies and axonal projections again strongly supports the assumption of *tubb2b* playing a critical role for differentiation and neurogenesis. In the MOE, I observed *tubb2b*-positive ORNs densely packed throughout the entire cavity and their axons terminate in all described glomerular clusters within the OB (projection fields 1-9, α, β, γ, δ; Gaudin & Gascuel, 2005). Although, here too is must be assumed, that not all ORNs are tubb2b-positive.

In addition, I observed that some *tubb2b*-positive axonal projections bypass the glomerular cluster in the OB and terminate in higher brain regions. According to present studies, these fibers are part of the EBOS, which is common in aquatic vertebrates (Demski & Northcutt, 1983; Hofmann & Meyer, 1989; Pinelli et al., 2004; Schmidt et al., 1988; Von Bartheld & Meyer, 1988). EBOS fibers are potentially involved in the perception of pheromones and target regions like the Hyp (Demski & Northcutt, 1983; Schmidt et al., 1988). Some of the observed *tubb2b*-positive fibers project through the anterior commissure into the contralateral OB. These fibers most likely belong to a temperature-sensitive system that is described in *Xenopus laevis* larvae and innervate the γ-glomerulus in the contralateral OB (Kludt et al., 2015).

tubb2b-dependent fluorescence is not present in interneurons of the OB but in olfactory PNs

Within the OB, I observed a large number of *tubb2b*-positive cells which are located in the mitral cell layer. In the anuran amphibian OB, cell layers are not clearly disjunct like

in mammals and an assignment of different cell types to certain bulbar layers is challenging (Kosaka & Kosaka, 2016; Nagayama et al., 2014; Nezlin & Schild, 2000; Scalia et al., 1991a). To overcome this limitation, I performed antibody stainings against known proteins to label specific OB cell types. I chose an antibody against TH to label dopaminergic interneurons of the glomerular and external plexiform layer and an antibody against CR to visualize a subset of PNs and interneurons of the granule cell layer (Boyd & Delaney, 2002; Castro et al., 2008; González et al., 1994; Morona & González, 2013; Porteros et al., 1997). Interestingly I found neither both TH- and *tubb2b*-postive nor both CR- and *tubb2b*-positive neurons. This eliminates the possibility, that the present *tubb2b*-postive cells are dopaminergic TH-immunoreactive interneurons or granule cells.

Another protein that is specifically expressed in certain OB neurons is Pax6, which is present in the periglomerular layer and internal granule cell layer (Bandín et al., 2014). Pax6 is described to be located in a subset of dopaminergic interneurons, which also express TH (Bandín et al., 2014). After several unsuccessful trials to label the Pax6 protein with an antibody to recreate the findings of the Bandín et al., 2014 paper (Bandín et al., 2014), I used a transgenic *Xenopus laevis* line in which both *tubb2b* and *pax6* drive the expression of a fluorescent protein instead. In this line *tubb2b* drives the expression of red fluorescent protein Katushka and *pax6* drives the expression of green fluorescent protein GFP. Similar to the results of the Bandín et al., 2014 paper I found *pax6*-dependent fluorescence in the periglomerular layer where it most probably is present in the dopaminergic interneurons mentioned earlier. Different to the observation of Bandín et al., 2014, I detected no *pax6*-dependent fluorescence in the granule cell layer but instead in the mitral cell layer. At this position, I also found *tubb2b*-dependent fluorescence and a few cells that were both *pax6*- and *tubb2b*-positive. This raises the questions, if *pax6* is active in a subset of PNs, what differs between *pax6*-postive versus *pax6*- and *tubb2b*-positive cells and why are the observations between the Pax6 Protein expression pattern of the Bandín et al., 2014 paper different from the *pax6* promoter activity pattern. To answer these questions, a more thorough investigation of the NBT-Katushka pax6-GFP transgenic line in comparison to several antibody stainings is necessary.

Despite that fact that it is difficult to clearly assign a certain cell type to the *tubb2b*-positive cells in the OB, I am able to narrow down the selection considerably through

my observations. Due to the absence of *tubb2b*-dependent fluorescence in interneurons, I conclude that *tubb2b* is most likely active in PNs. Whether *tubb2b* is active in the entirety of PNs in the OB or only in a subset of PNs still remains unknown.

tubb2b-dependent fluorescence occurs in all main telencephalic regions and in parts of the diencephalon

Besides the OB, *tubb2b*-positive cells are present throughout the entire telencephalon and parts of the diencephalon. *tubb2b*-postive cells are present in parts of the basal ganglia, amygdaloid complex and pallium (summarized in Figure 25). Two *tubb2b*-positve components of the basal ganglia are the Acc and Str (Marín, González, et al., 1997; Marín, Smeets, et al., 1997). Both Acc and Str receive input from several sensory systems, like olfactory system, visual or auditory system but also visceral input, like cardiovascular, respiratory and gastrointestinal information (Marín, González, et al., 1997). These visceral inputs are integrated to the basal ganglia by the extended amygdala which consists of parts of the amygdaloid complex and the BST (Alheid et al., 1995; Marín, González, et al., 1997; Moreno et al., 2012), which are also *tubb2b*-positive. The amygdaloid complex composes of the AA, MeA, LA and CeA (Moreno & González, 2003, 2004, 2005; Swanson & Petrovich, 1998) and I found *tubb2b*-dependent fluorescence in all of these regions. Both MeA and BST also share a similar function as the teleost habenula, which is involved in controlling fear responses (Agetsuma et al., 2010; Lee et al., 2010; Miyasaka et al., 2014). The CeA is the main component of integration within the amygdaloid complex and controls cardiovascular, respiratory and gastrointestinal functions (Jolkkonen & Pitkänen, 1998; Moreno & González, 2005). The LA is located in the ventral pallium (Vp; (Moreno & González, 2004) and together with the MeA described as the main terminal processing center of the olfactory system (Moreno et al., 2005; Moreno & González, 2004).

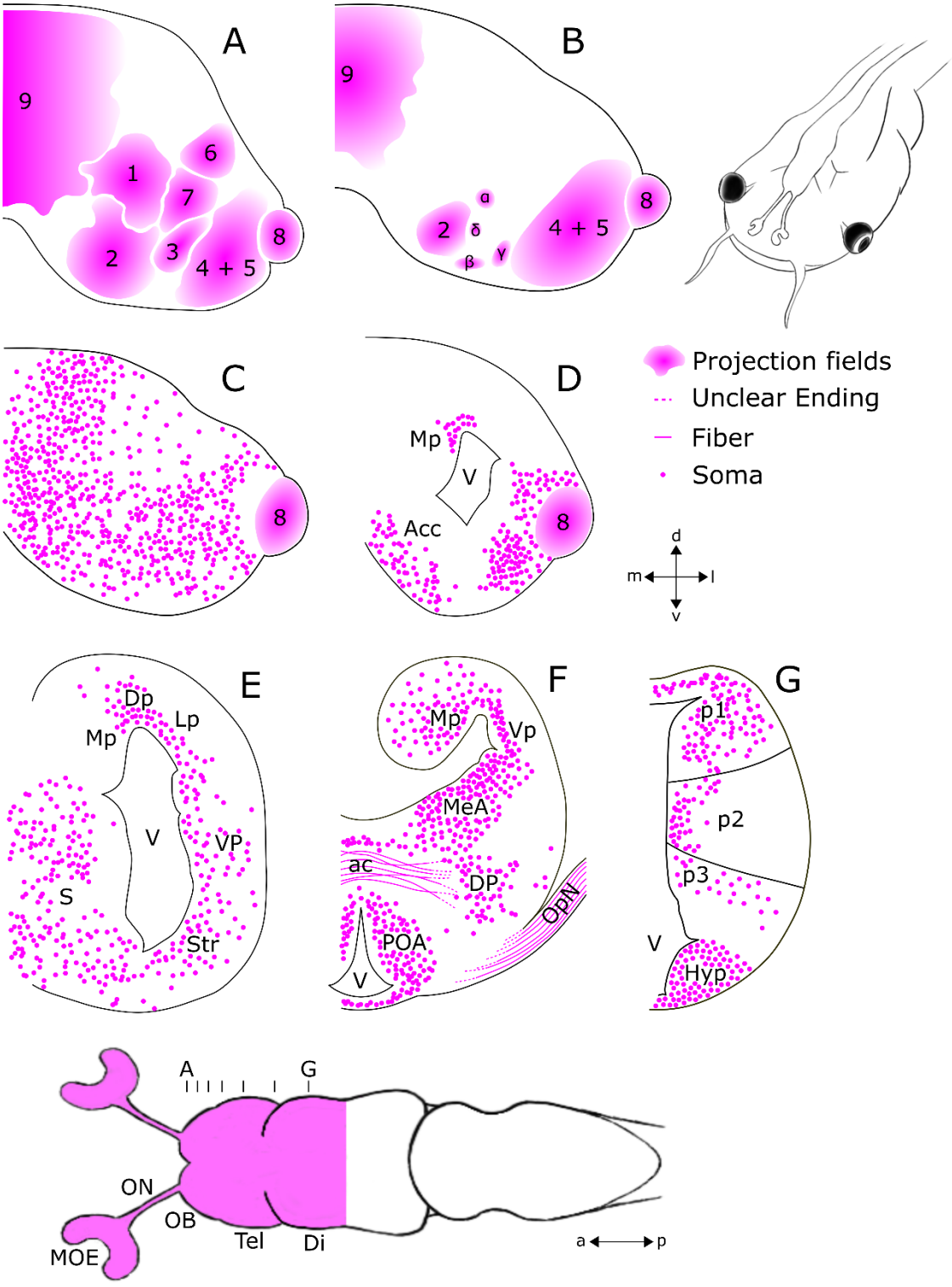

Figure 25: Schematic overview of the premetamorphic *Xenopus laevis* forebrain with approximate positions of *tubb2b*-positive structures. Coronal sections of the whole larval forebrain with approximate positions of A - G shown in the scheme of the forebrain (lower image; ventral view). The positions and density of the cells shown for each region are presented based on observation and not via quantitative analysis. **A and B** Coronal section of the glomerular layer of the OB (one brain hemisphere) showing *tubb2b*-dependent

fluorescence in axonal terminals of olfactory sensory neurons (**1-9 and α, β, γ, δ**) and vomeronasal neurons (**8;** (Gaudin & Gascuel, 2005). **C and D** Coronal section through the main and accessory OB showing *tubb2b*-dependent fluorescence cells in the mitral cells layer as well as the nucleus accumbens (**Acc**) and medial pallium (**Mp**). **E** Section of the intermediate telencephalon with *tubb2b*-positive cells in the septum (**S**), striatum (**Str**), ventral pallium (**Vp**), lateral pallium (**Lp**), dorsal pallium (**Dp**) and medial pallium (**Mp**). **F** Section of the posterior telencephalon with *tubb2b*-positive fibers in the anterior commissure (**ac**) and optic nerve (**OpN**) and *tubb2b*-positive cells in the preoptic area (**POA**), dorsal pallidum (**DP**), medial amygdala (**MeA**), Vp and Mp. **G** Section of the posterior telencephalon and diencephalon. *tubb2b*-dependent fluorescence in cells of the hypothalamus (**Hyp**) and prosomeres 1-3 (**p1-p3**). Main olfactory epithelium (MOE). Olfactory nerve (ON). Olfactory bulb (OB). Telencephalon (Tel). Diencephalon (Di). Anterior (a). Posterior (p). Dorsal (d). Ventral (v). Medial (m). Lateral (l).

Other *tubb2b*-positive regions are the DP, POA and Hyp. Together with the posterior tubercle and the Str, the DP is involved in regulating different motor functions in the frog similar to the nigrostriatal pathway in mammals (Hoke et al., 2007). The Hyp regulates general functions of the body, behavioral patterns and acts as a control unit for endocrine functions (Bruce, 2009; Domínguez et al., 2013, 2014).

Within the diencephalon, I detected *tubb2b*-dependent fluorescence in p1-p3 and in the Th, which are a relay station for sensory information processing, except olfactory stimuli (Bandín et al., 2015; Jones, 2007).

My results indicate that *tubb2b*-positive cells are present is numerous regions that process or forward sensory information and input to maintain important body functions like cardiovascular, respiratory and gastrointestinal processes. The *tubb2b* promoter not only appears to be crucial for these cells, but it also serves as a reliable marker to label these brain regions in future studies.

Transgenic *tubb2b* promoter-driven *Xenopus laevis* lines and their use for studies of olfactory PNs in larval *Xenopus laevis*

In the past years, more transgenic lines of *Xenopus laevis* became available including *tubb2b* promoter-driven lines NBT-Katushka γ-cry Venus [Xla.Tg(tubb2b:Katushka;

cryga:Venus)^{EXCR}; (Love et al., 2011)], tubb2b-GCaMP6s Rno.elas-GFP [Xla.Tg(tubb2b:GCaMP6s; Rno.elas:GFP)^{NXR}; (Horb et al., 2019)] or pax6-GFP CMV-DsRED [Xla.Tg(pax6:GFP;CMV:DsRED)^{Papal}; (Hartley et al., 2001)]. As the results of my study demonstrate, the *tubb2b* promoter is specifically active in brain regions and structures of sensory systems like the olfactory system, which is a great advantage to address difficult research questions. In the larval olfactory system of *Xenopus laevis*, very little is known about the secondary pathway of olfactory information processing and basic information about PNs and terminal processing centers remain largely unexplored. Fortunately, *tubb2b* promoter-driven *Xenopus* lines proved to be a valuable tool for addressing important questions. As mentioned above, larval transgenic NBT-Katushka γ-cry Venus *Xenopus laevis* show *tubb2b*-dependent fluorescence in cells of the mitral cell layer of the OB, that are most likely PNs. In this work, this information enabled me to specifically target the PN population for single cell electroporations and bulk injections into separate cell groups, to gain information about their morphology and axonal projection patterns to target regions in the forebrain. Within the forebrain, the NBT-Katushka γ-cry Venus transgenic line helped to identify the individual brain regions. In adult *Xenopus*, main target regions of the olfactory system are the MeA and LA (Marín, González, et al., 1997; Marín, Smeets, et al., 1997; Moreno et al., 2005; Moreno & González, 2003, 2004; Swanson & Petrovich, 1998). Olfactory stimuli may also reach the Acc and Str via the LA (Marín, González, et al., 1997). This work shows the widespread activity of *tubb2b* in all of these regions. That allowed us to use a *tubb2b* promoter-driven line that expressed a genetically encoded calcium indicator GCaMP6s for functional experiments, in order to visualize brain regions that respond to olfactory stimulation. Of course it must be taken into account, that there could be odorant-induced responses in *tubb2b*-negative regions, which are not mentioned in this study. Further experiments with different approaches to label all larval brain regions for functional imaging would be necessary to find this out in the future.

3D reconstruction of lateral and medial OB PNs reveals differences in the number of dendritic tufts

In larvae of *Xenopus laevis*, olfactory PNs are only sparsely described. It is reported, that *Xenopus* PNs have a mitral cell-like morphology with one to multiple primary

dendrites, that can innervate one or more glomeruli (Nezlin et al., 2003; Nezlin & Schild, 2000; Offner et al., 2023; Weiss et al., 2021a; Weiss et al., 2021b). The cell bodies of *Xenopus* PNs are located in the external plexiform layer close to the glomeruli, similar to PNs in other amphibians (Byrd & Burd, 1991; Nezlin et al., 2003; Nezlin & Schild, 2000). In late tadpole stages after metamorphosis, PNs of the newly formed dorsal glomerular cluster differ morphologically from ventral OB PNs (Weiss et al., 2021b). Dorsal OB PNs show a higher number of dendrites that arise from the soma and possess more dendritic tufts with a smaller tuft volume, compared to ventral OB PNs (Weiss et al., 2021b).

In the ventral OB of *Xenopus laevis* larvae, the primary olfactory pathway is segregated into two distinct odor-processing streams, which remain present even after metamorphosis (Gliem et al., 2013; Weiss et al., 2021b). These streams are sharply segregated into lateral and medial glomerular clusters in the OB and differ functionally from each other (Gliem et al., 2013; Weiss et al., 2020a). By now, no study intended to analyze the PNs directly connected to these two streams. This work was set out to investigate the lateral and medial PNs in more detail and to gain general information about the axonal projection pattern and target brain regions of the ventral PN population.

I found that the overall structure of lateral and medial PNs of the ventral OB in larval *Xenopus laevis* is similar to mammalian mitral cells (Imamura et al., 2020; Nagayama et al., 2014). Each PN had at least one primary dendrite with one dendritic tuft, several secondary dendrites and an axon that connects to higher brain regions. Unlike in mammals, in larval *Xenopus* ventral OB PNs often possess more than one dendritic tuft, which is common in other vertebrates (Dryer & Graziadei, 1994; Imamura et al., 2020; Nagayama et al., 2014; Nezlin et al., 2003; Weiss et al., 2021a; Weiss et al., 2021b). Similar results have been obtained in a recent study that investigates the morphology of lateral PNs in the ventral OB of larval *Xenopus* (Offner et al., 2023). Offner et al., 2023 show a distribution of one to five dendritic tufts in lateral PNs. Most of them show one dendritic tuft (42,6%) and two dendritic tufts (37,7%) while three to five is less common (Three: 13,1%, four: 4,9%, five: 1,6%; Offner et al., 2023). In this study I observed a similar distribution with 60% of lateral PNs showing one dendritic tuft, 33,3% with two dendritic tufts and 6,7% with three dendritic tufts, confirming that one to multiple dendritic tufts are present in lateral PNs of the ventral OB. Due to the

much smaller sample size in comparison to the study from Offner et al., 2023 (present study: n = 15 lateral PNs; Offner et al., 2023: n = 61), I only show a fraction of the whole lateral PN population, which could be a reason why I only found a maximum of three dendritic tufts per cell, in contrast to up to five dendritic tufts per cell shown by Offner et al., 2023 (Offner et al., 2023). Surprisingly, I observed a different distribution in the number of dendritic tufts in the population of medial PNs, which has more similarities to the distribution observed in the postmetamorphic dorsal OB (Weiss et al., 2021b). I observed that most PNs possessed two dendritic tufts (64,3%), while one dendritic tuft was rather rare (21,4%). The amount of cells with three dendritic tufts was a bit higher than in the lateral PN population (14,3%), but still lower than the amount of cell with one or two dendritic tufts. Also, due to the small sample size a higher number of dendritic tufts per cell could be possible as well.

A study conducted in zebrafish addresses this topic and suggested that cells with multiple dendritic tufts have a different odor processing strategy than cells with one dendritic tuft (Braubach & Croll, 2021). Hence it could be possible that medial PN in ventral OB differ from lateral PN in their odor processing logic. I assume this could be linked to the lateral and medial odor processing streams.

Lateral and medial PNs share similar dendritic tree structures

Morphological and electrophysiological studies in frogs show that the complexity of the dendritic tree can vary among PNs and propose a similar division into different PN subtypes, like in mammals (Jiang & Holley, 1992; Nagayama et al., 2014; Scalia et al., 1991b, 1991a; Weiss et al., 2021b). A study conducted in the frog *Rana ridibunda* describes two morphologically distinct PN subgroups based on the structure of the dendritic tree (Jiang & Holley, 1992). One group of PNs has more broad and wide ranging dendrites, the second group is located more distant from the glomerular layer and a more linear structure (Figure 7; Jiang & Holley, 1992). To compare the dendritic tree of lateral and medial PNs I counted the number of stems that arise from the soma, extraglomerular branches and blunt endings (Blunt endings give information about the amount of secondary dendrites without tufts). If a cell has a high number of soma stems, branching points and blunt endings, it is very likely that this cell has a

widespread and complex dendritic tree. Accordingly, fewer soma stems, branching points and blunt endings indicate a less complex but more linear structure.

In this work I found no difference of lateral PNs to medial PNs in all of these aspects. Both lateral and medial PNs share an average number of two stems from the soma, eight branching points and eight blunt endings. In both groups, the distribution of cells with a linear structure versus cells with a wide structure seems to be similar. One soma stem, four branching points and two blunt endings were the lowest numbers I found for both cell groups. The highest numbers were 4 soma stems, 16 branching points and 17 blunt endings. Both linear and wide structured PN seem to be present in the lateral and medial PN population equally and I found no indication, that one PN population is different due to the structure of the dendritic tree.

Besides the structure of the dendritic tree, I discovered two interesting observations during this analysis. Within the medial PN population it seems that medial PNs dive into two separate groups that differ in the number of branching points and blunt endings (Figure 18 A and B, yellow). To find out whether they differ significantly I performed several statistical tests, but all failed to distinguish them as two separate groups. I still assume that a presence of two groups can be possible here, but the small sample size in this work was most probably not enough to proof a significant difference. Specifically analyzing the medial PN population separately and with a higher sample size in total will be necessary to proof this in the future.

Although vertebrate olfactory PNs vary in their morphology, some structural elements are consistent. One of those is the presence of an axon and one primary dendrite that both arise from the soma (Dryer & Graziadei, 1994). This immediately suggests that the presence of two stems from the soma must be the most likely phenotype of PNs. Nevertheless, I observed one cell with only one stem that arises from the soma (see Supplementary Figure 2). I assume that in this case the dye could have been not properly diffused within the cell, causing that the axon was net stained enough for visualization, or the cell body of the neighboring cell is covering the axon, making it unable to see.

During evolution, early amphibians developed additional basal dendrites which are also present to this day in reptiles and mammals. While the primary dendrite connects the cell to a glomerulus, basal dendrites contact other mitral cells to enable lateral communication (Dryer & Graziadei, 1994; G. M. G. Shepherd, 1979). Dryer &

Graziadei, 1994 show an evolutionary trend of olfactory PNs in which primary dendrites are reduced form lower to higher vertebrates while basal dendrites emerge (Dryer & Graziadei, 1994). Because I found cells showing three or four soma stems, I assume that these contain additional basal dendrites. This could improve the communication with neighboring PNs ventrally and laterally.

Axons of lateral and medial PNs target similar structures in the posterior telencephalon with different projection patterns

The anuran telencephalon is divided into a dorsally located pallium and ventrally located subpallium (Hoffman, 1963; Northcutt, 1974) that both contain important brain regions for sensory information processing like the basal ganglia and the amygdaloid complex (Marín, González, et al., 1997; Marín, Smeets, et al., 1997; Moreno et al., 2005; Moreno & González, 2003, 2004, 2005). In adult *Xenopus laevis*, the LA and MeA have been described to be the terminal processing centers of the olfactory system (Moreno et al., 2005) and projections from the OB to regions in the pallium have also been observed in other frog species (Northcutt & Royce, 1975). So far, no study has been conducted to analyze the terminal olfactory processing centers in *Xenopus* tadpoles. According to this and the availability of NBT-Katushka γ-cry Venus transgenic *Xenopus* line, which shows expression of red fluorescent Katushka in parts of the basal ganglia and amygdaloid complex, the following experiment was set out to study axonal projections of OB PNs and find potential target regions in the telencephalon. Here, I specially focus on the comparison of lateral and medial olfactory processing stream consistently.

To visualize axonal projections of lateral in comparison to medial PNs, I injected Calcein AM dye into the lateral and medial PN population separately. In both cases I found that PNs axons project to the subpallium and parts of the ventral pallium in the posterior telencephalon, which includes parts of the amygdaloid complex such as the MeA, CeA and LA (Marín, González, et al., 1997; Marín, Smeets, et al., 1997; Moreno & González, 2003, 2004, 2005). This suggests that similar to the adult frog, larval *Xenopus* OB neurons potentially target the MeA and LA as well. Due to its position, the CeA could also be a direct target region of olfactory PN axons. This suggests a conserved information processing pathway in both larval and adult *Xenopus laevis*.

Despite similar terminal regions, I observed that lateral and medial PN axons take different routes through the telencephalon. Lateral PN axons form two separate fiber bundles that fuse in the intermediate telencephalon until it arrives at the level of the amygdaloid complex. In comparison, medial PN axons form two separate fiber bundles as well, but stay separate until both bundles arrive in the posterior telencephalon. Different routes of olfactory PN axons are not uncommon, but in most cases axons of different routes also target different brain regions. This has been observed in zebrafish and mouse (Igarashi et al., 2012; Miyasaka et al., 2009, 2014; Nagayama et al., 2010). In larval *Xenopus* it seems that both lateral and medial PN axon target the same regions in the telencephalon, which is why I assume that the different routes observed in this study emerge due to limitations in the space of the telencephalon and the location of other brain regions in this area. In addition, I observed that both lateral and medial PN axons travel only laterally through the lateral olfactory tract. I found no evidence of a medial olfactory tract in larval *Xenopus laevis,* which is described in other species (Eisthen & Polese, 2007).

Calcium imaging experiments in the posterior telencephalon manifest the functional connection of the CeA and LA with the larval olfactory system

In amphibians, the information on odor representation in higher brain regions is very limited. Many studies in amphibians, especially in larval *Xenopus laevis,* show functional experiments in the olfactory epithelium or OB (Czesnik et al., 2003; Gliem et al., 2013; Hawkins et al., 2017; Junek et al., 2010; Kauer, 1974; Offner et al., 2023; Rhodes & Amo, 2022; Weiss et al., 2021b) and in the past, odorant-induced responses of cortical neurons have only been shown with electrophysiological studies (Duchamp-Viret et al., 1996). With the use of transgenic tubb2b-GCaMP6s Rno.elas-GFP (*tubb2b*-promoter driven) *Xenopus* larvae for calcium imaging experiments (Chen et al., 2013; Horb et al., 2019) Offner and colleagues, 2020 report odorant-induced activity for the first time in larval higher brain regions (Offner et al., 2020). With the opportunity to use GCaMP6s expressed under the *tubb2b* promoter in this transgenic line, I planned a more thorough investigation for this work, to study odorant-induced responses in the forebrain of larval *Xenopus laevis*. Based on my tracing experiments which are explained above, I decided to focus on measurements in the posterior

telencephalon, which I assume contain potential target regions of PN axons. Since I observed that both lateral and media PN axons terminate in the same regions of the posterior telencephalon, analyzed my results as a summary of all ventral PNs of the main OB. In the posterior pallium, I observed odorant-induced responses in the LA. Similar to adult *Xenopus* (Moreno et al., 2005; Moreno & González, 2004) it can be one of the main higher olfactory processing centers in the larvae as well. In adult *Xenopus* the second olfactory processing center is the MeA (Moreno et al., 2005). Unexpectedly, in my experiments I found odorant-induced activity in the CeA instead. This could be an indication that the olfactory circuitry of adult and larval *Xenopus* differs partly. Measurements of single cortical neurons although show, that in the LA a much higher number of cells is activated by the epithelial odorant stimulation in comparison to the CeA. For this reason, I propose the LA as the main target region for olfactory information in the larval *Xenopus laevis* forebrain.

Conclusion

In summary, this work shows a detailed investigation of the expression pattern of *tubb2b*-dependent fluorescence in the forebrain of larval *Xenopus laevis,* which enabled the first deeper study of the secondary olfactory pathway in *Xenopus* tadpoles.

In this work, I not only confirm the activity of the *tubb2b* promoter in neurons, but also show its specificity to certain brain regions and subtypes of neurons in the premetamorphic forebrain. I was able to create a detailed map of the *tubb2b* activity pattern, that is essential for future studies that use *tubb2b* promoter driven transgenic *Xenopus laevis* tadpoles. With the knowledge about the *tubb2b* activity pattern in the larval forebrain it was possible to approach investigations of olfactory PNs and their target brain regions for the first time.

I was able to specifically inject single PNs related to the medial and lateral glomerular clusters, which allowed a thorough comparison of morphological structures. Even though the number of cells in this experiment was rather small it was possible to find that medial PNs possess a higher number of dendritic tufts compared to lateral PNs.

Using the *tubb2b* promoter driven *Xenopus* tadpoles additionally enabled precise bulk injections into the medial PN population separately from the lateral PN population, in

order to compare their axonal projection patterns. I observed that both PN populations target similar regions in the posterior telencephalon, which most probably belong to the amygdaloid complex. On their way to the posterior telencephalon medial PN axons take a slightly different route than lateral PN axons.

In a final step, I was able to find two brain regions in the posterior telencephalon with functional calcium imaging experiments, that responded to epithelial odorant mixture application. The use of transgenic *tubb2b* promoter driven tadpoles that express the genetically encoded calcium indicator GCaMP6s made it possible to identify the lateral amygdala and central amygdala as target regions for olfactory information.

Taken together, this study shows a detailed investigation of *tubb2b* activity in the larval *Xenopus laevis* forebrain and provides first insights into the secondary olfactory pathway with the terminal processing centers of the olfactory system. Overall, my results show indications that the secondary olfactory pathway of adult and larval *Xenopus laevis* slightly differ and lay the groundwork for future investigations of the larval olfactory system.

References

Ache, B. W., & Young, J. M. (2005). *Olfaction: Diverse species, conserved principles.* In *Neuron* 48(3), 417–430. https://doi.org/10.1016/j.neuron.2005.10.022

Agetsuma, M., Aizawa, H., Aoki, T., Nakayama, R., Takahoko, M., Goto, M., Sassa, T., Amo, R., Shiraki, T., Kawakami, K., Hosoya, T., Higashijima, S. I., & Okamoto, H. (2010). The habenula is crucial for experience-dependent modification of fear responses in zebrafish. *Nature Neuroscience*, *13*(11), 1354–1356. https://doi.org/10.1038/nn.2654

Alheid, G., de Olmos, J. S., & Beltramino, C. A. (1995). Amygdala and extended amygdala. In G. Paxinos (Ed.), *The rat nervous system* (2nd ed., pp. 495–578). San Diego: Academic Press.

Bandín, S., Morona, R., & González, A. (2015). Prepatterning and patterning of the thalamus along embryonic development of *Xenopus laevis*. *Frontiers in Neuroanatomy*, *9*, 1–21. https://doi.org/10.3389/fnana.2015.00107

Bandín, S., Morona, R., López, J. M., Moreno, N., & González, A. (2014). Immunohistochemical analysis of Pax6 and Pax7 expression in the CNS of adult *Xenopus laevis*. *Journal of Chemical Neuroanatomy*, *57–58*, 24–41. https://doi.org/10.1016/j.jchemneu.2014.03.006

Bandín, S., Morona, R., Moreno, N., & González, A. (2013). Regional expression of pax7 in the brain of *Xenopus laevis* during embryonic and larval development. *Frontiers in Neuroanatomy*, *7*, 1–22. https://doi.org/10.3389/fnana.2013.00048

Baxi, K. N., Dorries, K. M., & Eisthen, H. L. (2006). Is the vomeronasal system really specialized for detecting pheromones? *Trends in Neurosciences*, *29*(1), 1–7. https://doi.org/10.1016/j.tins.2005.10.002

Bieker, J. J., & Yazdani-Buicky, M. (1992). The multiple β-tubulin genes of *Xenopus*: Isolation and developmental expression of a germ-cell isotype β-tubulin gene. *Differentiation*, *50*(1), 15–23. https://doi.org/10.1111/j.1432-0436.1992.tb00481.x

Bisbee, C. A., Baker, M. A., Wilson, A. C., Hadji-Azimi, I., & Fischberg, M. (1977). Albumin phylogeny for clawed frogs (*Xenopus*). *Science*, *195*(4280), 785–787. https://doi.org/10.1126/science.65013

Boyd, J. D., & Delaney, K. R. (2002). Tyrosine hydroxylase-immunoreactive interneurons in the olfactory bulb of the frogs *Rana pipiens* and *Xenopus laevis*. *Journal of Comparative Neurology*, *454*(1), 42–57. https://doi.org/10.1002/cne.10428

Brann, J. H., & Firestein, S. J. (2014). A lifetime of neurogenesis in the olfactory system. *Frontiers in Neuroscience*, *8*(128), 1–11. https://doi.org/10.3389/fnins.2014.00182

Braubach, O., & Croll, R. P. (2021). The glomerular network of the zebrafish olfactory bulb. *Cell and Tissue Research*, *383*(1), 255–271. https://doi.org/10.1007/s00441-020-03394-4

Brox, A., Puelles, L., Ferreiro, B., & Medina, L. (2004). Expression of the genes Emx1, Tbr1, and Eomes (Tbr2) in the telencephalon of *Xenopus laevis* confirms the existence of a ventral pallial division in all tetrapods. *Journal of Comparative Neurology*, *474*(4), 562–577. https://doi.org/10.1002/cne.20152

Bruce, L. L. (2009). Evolution of the hypothalamus in amniotes. In M. D. Binder, N. Hirokawa, & U. Windhorst (Eds.), *Encyclopedia of neuroscience* (pp. 1363–1367). Springer, Berlin, Heidelberg. https://doi.org/https://doi.org/10.1007/978-3-540-29678-2

Burd, G. D. (1991). Development of the olfactory nerve in the African clawed frog*, Xenopus laevis I. Normal development*. *304*(1), 123–134. https://doi.org/doi: 10.1002/cne.903040109.

Byrd, C. A., & Burd, G. D. (1991). Development of the olfactory bulb in the clawed frog, *Xenopus laevis*: A morphological and quantitative analysis. *Journal of Comparative Neurology*, *314*(1), 79–90. https://doi.org/10.1002/cne.903140108

Calvo-Ochoa, E., Byrd-Jacobs, C. A., & Fuss, S. H. (2021). Diving into the streams and waves of constitutive and regenerative olfactory neurogenesis: insights from zebrafish. *Cell and Tissue Research*, *383*(1), 227–253. https://doi.org/10.1007/s00441-020-03334-2

Castro, A., Becerra, M., Anadón, R., & Manso, M. J. (2008). Distribution of calretinin during development of the olfactory system in the brown trout, *Salmo trutta fario*: Comparison with other immunohistochemical markers. *Journal of Chemical Neuroanatomy*, *35*(4), 306–316. https://doi.org/10.1016/j.jchemneu.2008.03.005

Chen, T. W., Wardill, T. J., Sun, Y., Pulver, S. R., Renninger, S. L., Baohan, A., Schreiter, E. R., Kerr, R. A., Orger, M. B., Jayaraman, V., Looger, L. L., Svoboda, K., & Kim, D. S. (2013). Ultrasensitive fluorescent proteins for imaging neuronal activity. *Nature*, *499*(7458), 295–300. https://doi.org/10.1038/nature12354

Cima, C., & Grant, P. (1982). Development of the optic nerve in *Xenopus laevis*. I. Early development and organization. *Journal of Embryology and Experimental Morphology*, *72*, 225–249.

Czesnik, D., Rössler, W., Kirchner, F., Gennerich, A., & Schild, D. (2003). Neuronal representation of odourants in the olfactory bulb of *Xenopus laevis* tadpoles. *European Journal of Neuroscience*, *17*(1), 113–118. https://doi.org/10.1046/j.1460-9568.2003.02448.x

D'Amico, L. A., Boujard, D., & Coumailleau, P. (2011). Proliferation, migration and differentiation in juvenile and adult *Xenopus laevis* brains. *Brain Research*, *1405*, 31–48. https://doi.org/10.1016/j.brainres.2011.06.032

Daume, D., Offner, T., Hassenklöver, T., & Manzini, I. (2022). Patterns of tubb2b promoter-driven fluorescence in the forebrain of larval *Xenopus laevis*. *Frontiers in Neuroanatomy*, *16*(July), 1–13. https://doi.org/10.3389/fnana.2022.914281

Davidson, L. A., & Lowery, L. A. (2022). Imaging methods in *Xenopus* cells, embryos, and tadpoles. In *Cold Spring Harbor Protocols*. https://doi.org/10.1101/pdb.top105627

Demski, L. S., & Northcutt, R. G. (1983). The terminal nerve: A new chemosensory system in vertebrates? *Science*, *220*(4595), 435–437. https://doi.org/10.1126/science.6836287

Dittrich, K., Kuttler, J., Hassenklöver, T., & Manzini, I. (2016). Metamorphic remodeling of the olfactory organ of the African clawed frog, *Xenopus laevis*. *Journal of Comparative Neurology*. https://doi.org/10.1002/cne.23887

Domínguez, L., González, A., & Moreno, N. (2014). Characterization of the hypothalamus of *Xenopus laevis* during development. II. The basal regions. *Journal of Comparative Neurology*, *522*(5), 1102–1131. https://doi.org/10.1002/cne.23471

Domínguez, L., Morona, R., González, A., & Moreno, N. (2013). Characterization of the hypothalamus of *Xenopus laevis* during development. I. The alar regions. *Journal of Comparative Neurology*, *521*(4), 725–759. https://doi.org/10.1002/cne.23222

Dryer, L., & Graziadei, P. P. C. (1994). Mitral cell dendrites: a comparative approach. *Anatomy and Embryology*, *189*(2), 91–106. https://doi.org/10.1007/BF00185769

Duchamp-Viret, P., Palouzier-Paulignan, B., & Duchamp, A. (1996). Odor coding properties of frog olfactory cortical neurons. *Neuroscience*, *74*(3), 885–895. https://doi.org/10.1016/0306-4522(96)00194-7

Dworkin-Rastl, E., Kelley, D. B., & Dworkin, M. B. (1986). Localization of specific mRNA sequences in *Xenopus laevis* embryos by in situ hybridization. *J Embryol Exp Morphol*, *91*, 153–168.

Eddé, B., Jeantet, C., & Gros, F. (1981). One β-tubulin subunit accumulates during neurite outgrowth in mouse neuroblastoma cells. *Biomedical and Biophysical Research Communications*, *103*(3), 1035–1043. https://doi.org/10.1016/0006-291x(81)90913-x.

Eisthen, H. L. (2002). Why are olfactory systems of different animals so similar? In *Brain, Behavior and Evolution* (Vol. 59, Issues 5–6, pp. 273–293). Karger. https://doi.org/10.1159/000063564

Eisthen, H. L., & Polese, G. (2007). Evolution of vertebrate olfactory subsystems. In *Evolution of nervous systems* (pp. 355–406). Elsevier. https://doi.org/https://doi.org/10.1159/000113336

Evans, B. J., Kelley, D. B., Tinsley, R. C., Melnick, D. J., & Cannatella, D. C. (2004). A mitochondrial DNA phylogeny of African clawed frogs: Phylogeography and

implications for polyploid evolution. *Molecular Phylogenetics and Evolution*, *33*(1), 197–213. https://doi.org/10.1016/j.ympev.2004.04.018

Farbman, A. I. (1992). *Cell biology of olfaction*. Cambridge University Press.

Fuller, C. L., Yettaw, H. K., & Byrd, C. A. (2006). Mitral cells in the olfactory bulb of adult zebrafish (*Danio rerio*): Morphology and distribution. *Journal of Comparative Neurology*, *499*, 218–230. https://doi.org/10.1002/cne.21091

Gaudin, A., & Gascuel, J. (2005). 3D atlas describing the ontogenic evolution of the primary olfactory projections in the olfactory bulb of *Xenopus laevis*. *Journal of Comparative Neurology*, *489*(4), 403–424. https://doi.org/10.1002/cne.20655

Giovannucci, A., Friedrich, J., Gunn, P., Kalfon, J., Brown, B. L., Koay, S. A., Taxidis, J., Najafi, F., Gauthier, J. L., Zhou, P., Khakh, B. S., Tank, D. W., Chklovskii, D. B., & Pnevmatikakis, E. A. (2019). Caiman an open source tool for scalable calcium imaging data analysis. *ELife*, *8*, 1–45. https://doi.org/10.7554/eLife.38173

Gliem, S., Syed, A. S., Sansone, A., Kludt, E., Tantalaki, E., Hassenklöver, T., Korsching, S. I., & Manzini, I. (2013). Bimodal processing of olfactory information in an amphibian nose: odor responses segregate into a medial and a lateral stream. *Cellular and Molecular Life Sciences : CMLS*, *70*(11), 1965–1984. https://doi.org/10.1007/s00018-012-1226-8

González, A., Marín, O., Tuinhof, R., & Smeets, W. J. A. J. (1994). Ontogeny of catecholamine systems in the central nervous system of anuran amphibians: An immunohistochemical study with antibodies against tyrosine hydroxylase and dopamine. *Journal of Comparative Neurology*, *346*(1), 63–79. https://doi.org/10.1002/cne.903460105

Graziadei, P. P. C., & Dehan, R. S. (1973). Neuronal regeneration in frog olfactory system. *Journal of Cell Biology*, *59*(2), 525–530. https://doi.org/10.1083/jcb.59.2.525

Graziadei, P. P. C., & Monti Graziadei, A. G. (1983). Regeneration in the olfactory system of vertebrates. *American Journal of Otolaryngology--Head and Neck Medicine and Surgery*, *4*(4), 228–233. https://doi.org/10.1016/S0196-0709(83)80063-5

Guo, J., Qiang, M., & Ludueña, R. F. (2011). The distribution of β-tubulin isotypes in cultured neurons from embryonic, newborn, and adult mouse brains. *Brain Research*, *1420*, 8–18. https://doi.org/10.1016/j.brainres.2011.08.066

Haberly, L. B., & Price, J. L. (1977). The axonal projection patterns of the mitral and tufted cells of the olfactory bulb in the rat. *Brain Research*, 152–157.

Hansen, A., Reiss, J. O., Gentry, C. L., & Burd, G. D. (1998). Ultrastructure of the olfactory organ in the clawed frog, *Xenopus laevis*, during larval development and metamorphosis. *Journal of Comparative Neurology*, *398*(2), 273–288. https://doi.org/10.1002/(SICI)1096-9861(19980824)398:2<273::AID-CNE8>3.0.CO;2-Y

Hartley, K. O., Hardcastle, Z., Friday, R. V., Amaya, E., & Papalopulu, N. (2001). Transgenic *Xenopus* embryos reveal that anterior neural development requires continued suppression of BMP signaling after gastrulation. *Developmental Biology*, *238*(1), 168–184. https://doi.org/10.1006/dbio.2001.0398

Hassenklöver, T., & Manzini, I. (2014). The olfactory system as a model to study axonal growth patterns and morphology in vivo. *Journal of Visualized Experiments*, *92*, 1–9. https://doi.org/10.3791/52143

Hawkins, S. J., Weiss, L., Offner, T., Dittrich, K., Hassenklöver, T., & Manzini, I. (2017). Functional reintegration of sensory neurons and transitional dendritic reduction of mitral/tufted cells during injury-induced recovery of the larval *Xenopus* olfactory circuit. *Frontiers in Cellular Neuroscience*, *11*, 380. https://doi.org/10.3389/fncel.2017.00380

He, H. Y., Lin, C. Y., & Cline, H. T. (2022). In vivo time-lapse imaging and analysis of dendritic structural plasticity in *Xenopus laevis* tadpoles. In *Cold Spring Harbor Protocols*. https://doi.org/10.1101/PDB.PROT106781

Higgs, D. M., & Burd, G. D. (2001). Neuronal turnover in the *Xenopus laevis* olfactory epithelium during metamorphosis. *Journal of Comparative Neurology*, *433*(1), 124–130. https://doi.org/10.1002/cne.1130

Hoffman, H. H. (1963). The olfactory bulb, accessory olfactory bulb, and hemisphere of some anurans. *Journal of Comparative Neurology*, *120*(2), 317–368. https://doi.org/10.1002/cne.901200208

Hofmann, M. H., & Meyer, D. L. (1989). Central projections of the nervus terminalis in four species of amphibians. *Brain, Behavior and Evolution*, *34*(5), 301–307. https://doi.org/10.1159/000116515

Hoke, K. L., Ryan, M. J., & Wilczynski, W. (2007). Functional coupling between substantia nigra and basal ganglia homologues in amphibians. *Behav Neurosci*, *121*(6), 1393–1399. https://doi.org/10.1037/0735-7044.121.6.1393.

Horb, M., Wlizla, M., Abu-Daya, A., McNamara, S., Gajdasik, D., Igawa, T., Suzuki, A., Ogino, H., Noble, A., Nicolas, M., Lafond, T., Boujard, D., Audic, Y., Guillet, B., Kashiwagi, A., Kashiwagi, K., Suzuki, N., Tazawa, I., Ochi, H., … Guille, M. (2019). *Xenopus* resources: Transgenic, inbred and mutant animals, training opportunities, and web-based support. *Frontiers in Physiology*, *10*, 387. https://doi.org/10.3389/fphys.2019.00387

Igarashi, K. M., Ieki, N., An, M., Yamaguchi, Y., Nagayama, S., Kobayakawa, K., Kobayakawa, R., Tanifuji, M., Sakano, H., Chen, W. R., & Mori, K. (2012). Parallel mitral and tufted cell pathways route distinct odor information to different targets in the olfactory cortex. *Journal of Neuroscience*, *32*(23), 7970–7985. https://doi.org/10.1523/JNEUROSCI.0154-12.2012

Imai, T. (2014). Construction of functional neuronal circuitry in the olfactory bulb. *Seminars in Cell and Developmental Biology*, *35*, 180–188. https://doi.org/10.1016/j.semcdb.2014.07.012

Imamura, F., Ito, A., & LaFever, B. J. (2020). Subpopulations of Projection Neurons in the Olfactory Bulb. *Frontiers in Neural Circuits*, *14*, 1–19. https://doi.org/10.3389/fncir.2020.561822

Jiang, T., & Holley, A. (1992). Morphological variations among output neurons of the olfactory bulb in the frog (*Rana ridibunda*). *Journal of Comparative Neurology*, *320*(1), 86–96. https://doi.org/10.1002/cne.903200106

Jolkkonen, E., & Pitkänen, A. (1998). Intrinsic connections of the rat amygdaloid complex: Projections originating in the central nucleus. *Journal of Comparative Neurology*, *395*(1), 53–72. https://doi.org/10.1002/(SICI)1096-9861(19980525)395:1<53::AID-CNE5>3.0.CO;2-G

Jones, E. G. (2007). *The thalamus* (2nd ed.). Cambridge University Press.

Joshi, H. C., & Cleveland, D. W. (1989). Differential utilization of β-tubulin isotypes in differentiating neurites. *Journal of Cell Biology*, *109*(2), 663–673. https://doi.org/10.1083/jcb.109.2.663

Junek, S., Kludt, E., Wolf, F., & Schild, D. (2010). Olfactory Coding with Patterns of Response Latencies. *Neuron*, *67*(5), 872–884. https://doi.org/10.1016/j.neuron.2010.08.005

Kapitein, L. C., & Hoogenraad, C. C. (2015). Building the neuronal microtubule cytoskeleton. *Neuron*, *87*(3), 492–506. https://doi.org/10.1016/j.neuron.2015.05.046

Katsetos, C. D., Frankfurter, A., Christakos, S., Mancall, E. L., Vlachos, I. N., & Urich, H. (1993). Differential localization of class III, beta-tubulin isotype and calbindin-D28k defines distinct neuronal types in the developing human cerebellar cortex. *J Neuropathol Exp Neurol* ., *52*(6), 655–666. https://doi.org/10.1097/00005072-199311000-00013.

Katsetos, C. D., Herman, M. M., & Mörk, S. J. (2003). Class III β-tubulin in human development and cancer. *Cell Motility and the Cytoskeleton*, *55*(2), 77–96. https://doi.org/10.1002/cm.10116

Kauer, J. S. (1974). Response patterns of amphibian olfactory bulb neurones to odour stimulation. *The Journal of Physiology*, *243*(3), 695–715. https://doi.org/10.1113/jphysiol.1974.sp010772

Kludt, E., Okom, C., Brinkmann, A., & Schild, D. (2015). Integrating temperature with odor processing in the olfactory bulb. *Journal of Neuroscience*, *35*(20), 7892–7902. https://doi.org/10.1523/JNEUROSCI.0571-15.2015

Knossow, M., Campanacci, V., Khodja, L. A., & Gigant, B. (2020). The mechanism of tubulin assembly into microtubules: Insights from structural studies. *IScience*, *23*(9), 101511. https://doi.org/10.1016/j.isci.2020.101511

Kobel, H. R., & Du Pasquier, L. (1986). Genetics of polyploid *Xenopus*. *Trends in Genetics*, *2*, 310–315. https://doi.org/10.1016/0168-9525(86)90286-6

Kosaka, T., & Kosaka, K. (2016). Neuronal organization of the main olfactory bulb revisited. *Anatomical Science International*, *91*(2), 115–127. https://doi.org/10.1007/s12565-015-0309-7

Lasser, M., Tiber, J., & Lowery, L. A. (2018). The role of the microtubule cytoskeleton in neurodevelopmental disorders. *Frontiers in Cellular Neuroscience*, *12*, 165. https://doi.org/10.3389/fncel.2018.00165

Latremoliere, A., Cheng, L., DeLisle, M., Wu, C., Chew, S., Hutchinson, E. B., Sheridan, A., Alexandre, C., Latremoliere, F., Sheu, S.-H., Golidy, S., Omura, T., Huebner, E. A., Fan, Y., Whitman, M. C., Nguyen, E., Hermawan, C., Pierpaoli, C., Tischfield, M. A., … Engle, E. C. (2018). Neuronal-specific TUBB3 is not required for normal neuronal function but is essential for timely axon regeneration. *Cell Rep.*, *24*(7), 1865–1879. https://doi.org/10.1016/j.cel.rep.2018.07.029

Lee, A., Mathuru, A. S., Teh, C., Kibat, C., Korzh, V., Penney, T. B., & Jesuthasan, S. (2010). The habenula prevents helpless behavior in larval zebrafish. *Current Biology*, *20*(24), 2211–2216. https://doi.org/10.1016/j.cub.2010.11.025

Lee, M. K., Rebhun, L. I., & Frankfurter, A. (1990). Posttranslational modification of class III β-tubulin. *Proceedings of the National Academy of Sciences of the United States of America*, *87*(18), 7195–7199. https://doi.org/10.1073/pnas.87.18.7195

Lee, M. K., Tuttle, J. B., Rebhun, L. I., Cleveland, D. W., & Frankfurter, A. (1990). The expression and posttranslational modification of a neuron-specific β-tubulin isotype during chick embryogenesis. *Cell Motility and the Cytoskeleton*, *17*(2), 118–132. https://doi.org/10.1002/cm.970170207

Liu, Y., Wang, C., Destin, G., & Szaro, B. G. (2015). Microtubule-associated protein tau promotes neuronal class II β-tubulin microtubule formation and axon elongation in embryonic *Xenopus laevis*. *European Journal of Neuroscience*, *41*(10), 1263–1275. https://doi.org/10.1111/ejn.12848

Lodovichi, C. (2021). Topographic organization in the olfactory bulb. *Cell and Tissue Research*, *383*(1), 457–472. https://doi.org/10.1007/s00441-020-03348-w

Love, N. R., Thuret, R., Chen, Y., Ishibashi, S., Sabherwal, N., Paredes, R., Alves-Silva, J., Dorey, K., Noble, A. M., Guille, M. J., Sasai, Y., Papalopulu, N., & Amaya, E. (2011). pTransgenesis: A cross-species, modular transgenesis resource. *Development*, *138*(24), 5451–5458. https://doi.org/10.1242/dev.066498

Ludueña, R. F., & Banerjee, A. (2008). The tubulin superfamily. In T. Fojo (Ed.), *Cancer drug discovery and development: The role of microtubules in cell biology, neurobiology, and oncology* (pp. 177–191). Humana Press. https://doi.org/10.1002/3527603808.ch2

Ludueña, R. F., Shooter, E. M., & Wilson, L. (1977). Structure of the tubulin dimer. *The Journal of Biological Chemistry*, *252*(20), 7006–7014.

Mann, H. B., & Whitney, D. R. (1947). On a test of whether one of two random variables is stochastically larger than the other. *The Annals of Mathematical Statistics*, *18*(1), 50–60. https://doi.org/10.1214/aoms/1177730491

Manzini, I. (2015). From neurogenesis to neuronal regeneration: The amphibian olfactory system as a model to visualize neuronal development in vivo. *Neural Regeneration Research*, *10*(6), 872–874. https://doi.org/10.4103/1673-5374.158334

Manzini, I., Frasnelli, J., & Croy, I. (2014). How we smell and what it means to us: basic principles of the sense of smell. *HNO*, *62*(12), 846–852. https://doi.org/10.1007/s00106-014-2925-2

Manzini, I., & Schild, D. (2010). Olfactory coding in larvae of the African clawed frog *Xenopus laevis*. In A. Menini (Ed.), *The Neurobiology of Olfaction*. Boca Raton (FL): CRC Press/Taylor & Francis.

Manzini, I., Schild, D., & Di Natale, C. (2022). Principles of odor coding in vertebrates and artificial chemosensory systems. *Physiological Reviews*, *102*(1), 61–154. https://doi.org/10.1152/PHYSREV.00036.2020

Marín, O., González, A., & Smeets, W. J. A. J. (1997). Basal ganglia organization in amphibians: Afferent connections to the striatum and the nucleus accumbens. *The Journal of Comparative Neurology*, *378*(1), 16–49. https://doi.org/10.1002/(sici)1096-9861(19970203)378:1<16::aid-cne2>3.0.co;2-n.

Marín, O., Smeets, W. J. A. J., & González, A. (1997). Basal ganglia organization in amphibians: Catecholaminergic innervation of the striatum and the nucleus accumbens. *Journal of Comparative Neurology*, *378*(1), 50–69. https://doi.org/10.1002/(sici)1096-9861(19970203)378:1<50::aid-cne3>3.0.co;2-j.

Measey, J. (2016). Overland movement in African clawed frogs (*Xenopus laevis*): A systematic review. *PeerJ*. https://doi.org/10.7717/peerj.2474

Milán, F. J., & Puelles, L. (2000). Patterns of calretinin, calbindin, and tyrosine-hydroxylase expression are consistent with the prosomeric map of the frog diencephalon. *Journal of Comparative Neurology*, *419*(1), 96–121. https://doi.org/10.1002/(SICI)1096-9861(20000327)419:1<96::AID-CNE6>3.0.CO;2-V

Miyasaka, N., Arganda-Carreras, I., Wakisaka, N., Masuda, M., Sümbül, U., Seung, H. S., & Yoshihara, Y. (2014). Olfactory projectome in the zebrafish forebrain revealed by genetic single-neuron labelling. *Nature Communications*, *5*, 3639. https://doi.org/10.1038/ncomms4639

Miyasaka, N., Morimoto, K., Tsubokawa, T., Higashijima, S. I., Okamoto, H., & Yoshihara, Y. (2009). From the olfactory bulb to higher brain Centers: Genetic visualization of secondary olfactory pathways in zebrafish. *Journal of Neuroscience*, *29*(15), 4756–4767. https://doi.org/10.1523/JNEUROSCI.0118-09.2009

Moody, S. A. (1989). Quantitative lineage analysis of the origin of frog primary motor and sensory neurons from cleavage stage blastomeres. *Journal of Neuroscience*, *9*(8), 2919–2930. https://doi.org/10.1523/jneurosci.09-08-02919.1989

Moody, S. A., Miller, V., Spanos, A., & Frankfurter, A. (1996). Developmental expression of a neuron-specific β-tubulin in frog (*Xenopus laevis*): A marker for growing axons during the embryonic period. *Journal of Comparative Neurology*, *364*(2), 219–230. https://doi.org/10.1002/(SICI)1096-9861(19960108)364:2<219::AID-CNE3>3.0.CO;2-8.

Moreno, N., & González, A. (2003). Hodological characterization of the medial amygdala in anuran amphibians. *Journal of Comparative Neurology*, *466*(3), 389–408. https://doi.org/10.1002/cne.10887

Moreno, N., & González, A. (2004). Localization and connectivity of the lateral amygdala in anuran amphibians. *Journal of Comparative Neurology*, *479*(2), 130–148. https://doi.org/10.1002/cne.20298

Moreno, N., & González, A. (2005). Central amygdala in anuran amphibians: Neurochemical organization and connectivity. *Journal of Comparative Neurology*, *489*(1), 69–91. https://doi.org/10.1002/cne.20611

Moreno, N., Morona, R., López, J. M., Domínguez, L., Joven, A., Bandín, S., & González, A. (2012). Characterization of the bed nucleus of the stria terminalis in the forebrain of anuran amphibians. *Journal of Comparative Neurology*, *520*(2), 330–363. https://doi.org/10.1002/cne.22694

Moreno, N., Morona, R., López, J. M., Dominguez, L., Muñoz, M., & González, A. (2008). Anuran olfactory bulb organization: Embryology, neurochemistry and hodology. *Brain Research Bulletin*, *75*(2–4), 241–245. https://doi.org/10.1016/j.brainresbull.2007.10.027

Moreno, N., Morona, R., López, J. M., Muñoz, M., & González, A. (2005). Lateral and medial amygdala of anuran amphibians and their relation to olfactory and vomeronasal information. *Brain Research Bulletin*, *66*(4–6), 332–336. https://doi.org/10.1016/j.brainresbull.2005.05.017

Morona, R., & González, A. (2013). Pattern of calbindin-D28k and calretinin immunoreactivity in the brain of *Xenopus laevis* during embryonic and larval development. *Journal of Comparative Neurology*, *521*(1), 79–108. https://doi.org/10.1002/cne.23163

Moura Neto, V., Mallat, M., Jeantet, C., & Prochiantz, A. (1983). Microheterogeneity of tubulin proteins in neuronal and glial cells from the mouse brain in culture. *The EMBO Journal*, *2*(8), 1243–1248.

Nagayama, S., Enerva, A., Fletcher, M. L., Masurkar, A. V., Igarashi, K. M., Mori, K., & Chen, W. R. (2010). Differential axonal projection of mitral and tufted cells in the mouse main olfactory system. *Frontiers in Neural Circuits*, *4*, 1–8. https://doi.org/10.3389/fncir.2010.00120

Nagayama, S., Homma, R., & Imamura, F. (2014). Neuronal organization of olfactory bulb circuits. *Frontiers in Neural Circuits*, *8*, 89. https://doi.org/10.3389/fncir.2014.00098

Nezlin, L. P., Heermann, S., Schild, D., & Rössler, W. (2003). Organization of glomeruli in the main olfactory bulb of *Xenopus laevis* tadpoles. *Journal of Comparative Neurology*. https://doi.org/10.1002/cne.10709

Nezlin, L. P., & Schild, D. (2000). Structure of the olfactory bulb in tadpoles of *Xenopus laevis*. *Cell and Tissue Research*, *302*(1), 21–29. https://doi.org/10.1007/s004410000208

Nieuwkoop, P. D., & Faber, J. (1994). *Normal table of Xenopus laevis (Daudin): a systematical and chronological survey of the development from the fertilized egg till the end of metamorphosis*. Garland Science.

Northcutt, R. G. (1974). Some histochemical observations on the telencephalon of the bullfrog, *Rana catesbeiana shaw*. *Journal of Comparative Neurology*, *157*(4), 379–389. https://doi.org/10.1002/cne.901570403

Northcutt, R. G., & Royce, G. J. (1975). Olfactory bulb projections in the bullfrog *Rana catesbeiana*. *J. Morphol.*, *145*(3), 251–267. https://doi.org/10.1002/jmor.1051450302.

Oehlmann, V. D., Berger, S., Sterner, C., & Korsching, S. I. (2004). Zebrafish beta tubulin 1 expression is limited to the nervous system throughout development, and in the adult brain is restricted to a subset of proliferative regions. *Gene Expression Patterns*, *4*(2), 191–198. https://doi.org/10.1016/j.modgep.2003.09.001

Offner, T., Daume, D., Weiss, L., Hassenklöver, T., & Manzini, I. (2020). *Whole-brain calcium imaging in larval Xenopus* (Issue 12). Cold Spring Harbor Protocols. https://doi.org/10.1101/pdb.prot106815

Offner, T., Weiss, L., Daume, D., Berk, A., Inderthal, T. J., Manzini, I., & Hassenklöver, T. (2023). Functional odor map heterogeneity is based on multifaceted glomerular connectivity in larval *Xenopus* olfactory bulb. *Isci*, 26(9), 107518. http://doi.org/10.1016/j.isci.2023.107518.

Oka, Y. (1992). Gonadotropin-releasing hormone (GnRH) cells of the terminal nerve as a model neuromodulator system. *Neuroscience Letters*, *142*(2), 119–122. https://doi.org/10.1016/0304-3940(92)90353-9

Oschwald, R., Richter, K., & Grunz, H. (1991). Localization of a nervous system-specific class II β-tubulin gene in *Xenopus laevis* embryos by whole-mount in situ hybridization. *International Journal of Developmental Biology*, *35*(4), 399–405.

Pedregosa, F., Grisel, O., Weiss, R., Passos, A., Brucher, M., Varoquax, G., Gramfort, A., Michel, V., Thirion, B., Grisel, O., Blondel, M., Prettenhofer, P., Weiss, R., Dubourg, V., & Brucher, M. (2011). Scikit-learn: Machine Learning in

Python. *Journal of Machine Learning Research*, *12*, 2825–2830. https://doi.org/10.5555/1953048.2078195

Peng, H., Ruan, Z., Long, F., Simpson, J. H., & Myers, E. W. (2010). V3D enables real-time 3D visualization and quantitative analysis of large-scale biological image data sets. *Nature Biotechnology*, *28*(4), 348–353. https://doi.org/10.1038/nbt.1612

Pinelli, C., D'Aniello, B., Polese, G., & Rastogi, R. K. (2004). Extrabulbar olfactory system and nervus terminalis FMRFamide immunoreactive components in *Xenopus laevis* ontogenesis. *Journal of Chemical Neuroanatomy*, *28*(1–2), 37–46. https://doi.org/10.1016/j.jchemneu.2004.06.001

Pnevmatikakis, E. A., & Giovannucci, A. (2017). NoRMCorre: An online algorithm for piecewise rigid motion correction of calcium imaging data. *Journal of Neuroscience Methods*, *291*, 83–94. https://doi.org/10.1016/j.jneumeth.2017.07.031

Porteros, A., Arévalo, R., Weruaga, E., Crespo, C., Briñón, J. G., Alonso, J. R., & Aijón, J. (1997). Calretinin immunoreactivity in the developing olfactory system of the rainbow trout. *Developmental Brain Research*, *100*(1), 101–109. https://doi.org/10.1016/S0165-3806(97)00037-0

Preibisch, S., Saalfeld, S., & Tomancak, P. (2009). Globally optimal stitching of tiled 3D microscopic image acquisitions. *Bioinformatics*, *25*(11), 1463–1465. https://doi.org/10.1093/bioinformatics/btp184

Reiss, J. O., & Burd, G. D. (1997a). Cellular and molecular interactions in the development of the *Xenopus* olfactory system. *Seminars in Cell and Developmental Biology*, *8*(2), 171–179. https://doi.org/10.1006/scdb.1996.0138

Reiss, J. O., & Burd, G. D. (1997b). Metamorphic remodeling of the primary olfactory projection in *Xenopus*: Developmental independence of projections from olfactory neuron subclasses. *Journal of Neurobiology*, *32*(2), 213–222. https://doi.org/10.1002/(SICI)1097-4695(199702)32:2<213::AID-NEU6>3.0.CO;2-B

Reiss, J. O., & Eisthen, H. L. (2008). Comparative anatomy and physiology of chemical senses in amphibians. In J. G. M. Thewissen (Ed.), *Sensory evolution on the threshold: Adaptations in secondary aquatic vertebrates* (pp. 42–63). https://doi.org/https://doi.org/10.1525/california/9780520252783.003.0004

Rhodes, H. J., & Amo, M. (2022). Electrophysiological responses to conspecific odorants in *Xenopus laevis* show potential for chemical signaling. *PLoS ONE*, *17*, 1–14. https://doi.org/10.1371/journal.pone.0273035

Richter, K., Grunz, H., & Dawid, I. B. (1988). Gene expression in the embryonic nervous system of *Xenopus laevis*. *Proceedings of the National Academy of Sciences of the United States of America*, *85*(21), 8086–8090. https://doi.org/10.1073/pnas.85.21.8086

Scalia, F. (1972). The projection of the accessory olfactory bulb in the frog. *Brain Research*, *36*(2), 409–411. https://doi.org/10.1016/0006-8993(72)90745-7

Scalia, F., Gallousis, G., & Roca, S. (1991a). A note on the organization of the amphibian olfactory bulb. *Journal of Comparative Neurology*, *305*(3), 435–442. https://doi.org/10.1002/cne.903050307

Scalia, F., Gallousis, G., & Roca, S. (1991b). Differential projections of the main and accessory olfactory bulb in the frog. *Journal of Comparative Neurology*, *305*(3), 443–461. https://doi.org/10.1002/cne.903050308

Schindelin, J., Arganda-Carrera, I., Frise, E., Verena, K., Mark, L., Tobias, P., Stephan, P., Curtis, R., Stephan, S., Benjamin, S., Jean-Yves, T., Daniel, J. W., Volker, H., Kevin, E., Pavel, T., & Albert, C. (2012). Fiji: an open-source platform for biological-image analysis. *Nature Methods*, *9*(7), 676–682. https://doi.org/10.1038/nmeth.2019.Fiji

Schmidt, A., Naujoks-Manteuffel, C., & Roth, G. (1988). Olfactory and vomeronasal projections and the pathway of nervus terminalis in ten species of salamanders. *Cell and Tissue Research*, *251*, 45–50.

Schwob, J. E. (2002). Neural regeneration and the peripheral olfactory system. *Anatomical Record*, *269*(1), 33–49. https://doi.org/10.1002/ar.10047

Scott, J. W., McBride, R. L., & Schneider, S. P. (1980). The organization of projections from the olfactory bulb to the piriform cortex and olfactory tubercle in the rat. *Journal of Comparative Neurology*, *194*(3), 519–534. https://doi.org/10.1002/cne.901940304

Session, A. M., Uno, Y., Kwon, T., Chapman, J. A., Toyoda, A., Takahashi, S., Fukui, A., Hikosaka, A., Suzuki, A., Kondo, M., van Heeringen, S. J., Quigley, I., Heinz, S., Ogino, H., Ochi, H., Hellsten, U., Lyons, J. B., Simakov, O., Putnam, N., … Rokhsar, D. S. (2016). Genome evolution in the allotetraploid frog *Xenopus laevis*. *Nature*, *538*(7625), 336–343. https://doi.org/10.1038/nature19840.

Shepherd, G. M. (1972). Synaptic organization of the mammalian olfactory bulb. *Physiological Reviews*, *52*(4), 864–917. https://doi.org/10.1152/physrev.1972.52.4.864

Shepherd, G. M. G. (1979). *The synaptic organization of the brain*.

Steuer, E., Schaefer, M. L., & Belluscio, L. (2014). Using the olfactory system as an in vivo model to study traumatic brain injury and repair. *Journal of Neurotrauma*, *31*(14), 1277–1291. https://doi.org/10.1089/neu.2013.3296

Sullivan, K. F. (1988). Structure and utilization of tubulin isotypes. *Ann. Rev. Cell Biol.*, *4*, 687–716. https://doi.org/10.1146/annurev.cb.04.110188.003351.

Sullivan, K. F., & Cleveland, D. W. (1986). Identification of conserved isotype-defining variable region sequences for four vertebrate β tubulin polypeptide classes. *Proceedings of the National Academy of Sciences of the United States of America*, *83*(12), 4327–4331. https://doi.org/10.1073/pnas.83.12.4327

Swanson, L., & Petrovich, G. (1998). What is the amygdala? *Trends in Neurosciences*, *21*(8), 323–331. https://doi.org/10.1016/s0166-2236(98)01265-x.

Von Bartheld, C. S., & Meyer, D. L. (1988). Central projections of the nervus terminalis in lampreys, lungfishes, and bichirs. *Brain, Behavior and Evolution*, *32*(3), 151–159. https://doi.org/10.1159/000116542

Wade, R. H. (2009). On and around microtubules: An overview. *Molecular Biotechnology*, *43*(2), 177–191. https://doi.org/10.1007/s12033-009-9193-5

Weiss, L., Offner, T., Hassenklöver, T., & Manzini, I. (2018). Dye electroporation and imaging of calcium signaling in *Xenopus* nervous system. In *Xenopus: Methods and Protocols* (Vol. 1865, pp. 217–231). https://doi.org/10.1007/978-1-4939-8784-9_15

Weiss, L., Jungblut, L. D., Pozzi, A. G., O'Connell, L. A., Hassenklöver, T., & Manzini, I. (2020a). Conservation of glomerular organization in the main olfactory bulb of anuran larvae. *Frontiers in Neuroanatomy*, *14*, 44. https://doi.org/10.3389/fnana.2020.00044

Weiss, L., Jungblut, L. D., Pozzi, A. G., Zielinski, B. S., O'Connell, L. A., Hassenklöver, T., & Manzini, I. (2020b). Multi-glomerular projection of single olfactory receptor neurons is conserved among amphibians. *Journal of Comparative Neurology*, *528*(13), 2239–2253. https://doi.org/10.1002/cne.24887

Weiss, L., Manzini, I., & Hassenklöver, T. (2021a). Olfaction across the water–air interface in anuran amphibians. *Cell and Tissue Research*, *383*(1), 301–325. https://doi.org/10.1007/s00441-020-03377-5

Weiss, L., Segoviano Arias, P., Offner, T., Hawkins, S. J., Hassenklöver, T., & Manzini, I. (2021b). Distinct interhemispheric connectivity at the level of the olfactory bulb emerges during *Xenopus laevis* metamorphosis. *Cell and Tissue Research*, *386*(3), 491–511. https://doi.org/10.1007/s00441-021-03527-3

Wirsig-Wiechmann, C. R., Wiechmann, A. F., & Eisthen, H. L. (2002). What defines the nervus terminalis? Neurochemical, developmental, and anatomical criteria. *Progress in Brain Research*, *141*, 45–58. https://doi.org/10.1016/S0079-6123(02)41083-7

Yu, C. R., & Wu, Y. (2017). Regeneration and rewiring of rodent olfactory sensory neurons. *Experimental Neurology*, *287*(3), 395–408. https://doi.org/10.1016/j.expneurol.2016.06.001

Zeppilli, S., Ackels, T., Attey, R., Klimpert, N., Ritola, K. D., Boeing, S., Crombach, A., Schaefer, A. T., & Fleischmann, A. (2021). Molecular characterization of projection neuron subtypes in the mouse olfactory bulb. *ELife*, *10*, 1–29. https://doi.org/10.7554/eLife.65445

Supplementary Figures

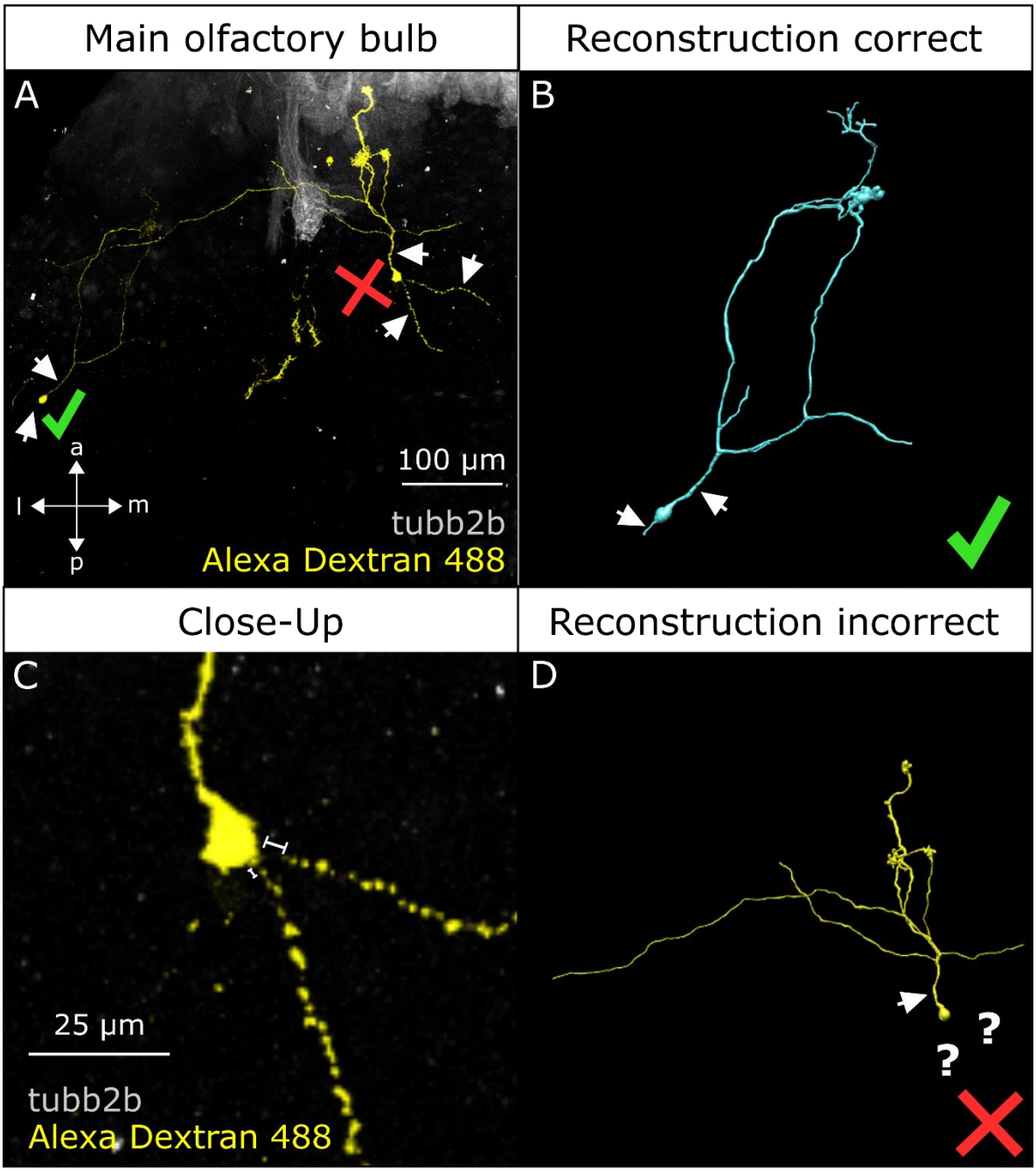

Supplementary Figure 1: Medial and lateral olfactory PNs in the OB of larval *Xenopus laevis* and their corresponding 3D reconstructions using Vaa3D. A Maximum projection of the OB (left brain hemisphere) of transgenic NBT-Katushka γ-cry Venus tadpoles with one labelled lateral and one medial single PN. The lateral PN (green check) contains two stems (white arrows) from the soma and the medial PN (red cross) contains three stems (white arrows) from the soma. **B** Corresponding 3D reconstruction of the lateral PN showing that the cell was reconstructed correctly with all two stems that arise from the soma. **C** Close-Up of the medial PN´s soma with its three stems from the soma. Two stems show apoptotic blebbing and are not connected to the soma anymore (white distance indicator). **D** Corresponding 3D reconstruction of the medial PN missing two stems from the soma and for this reason is considered incorrect. Anterior (**a**). Posterior (**p**). Lateral (**l**). Medial (**m).**

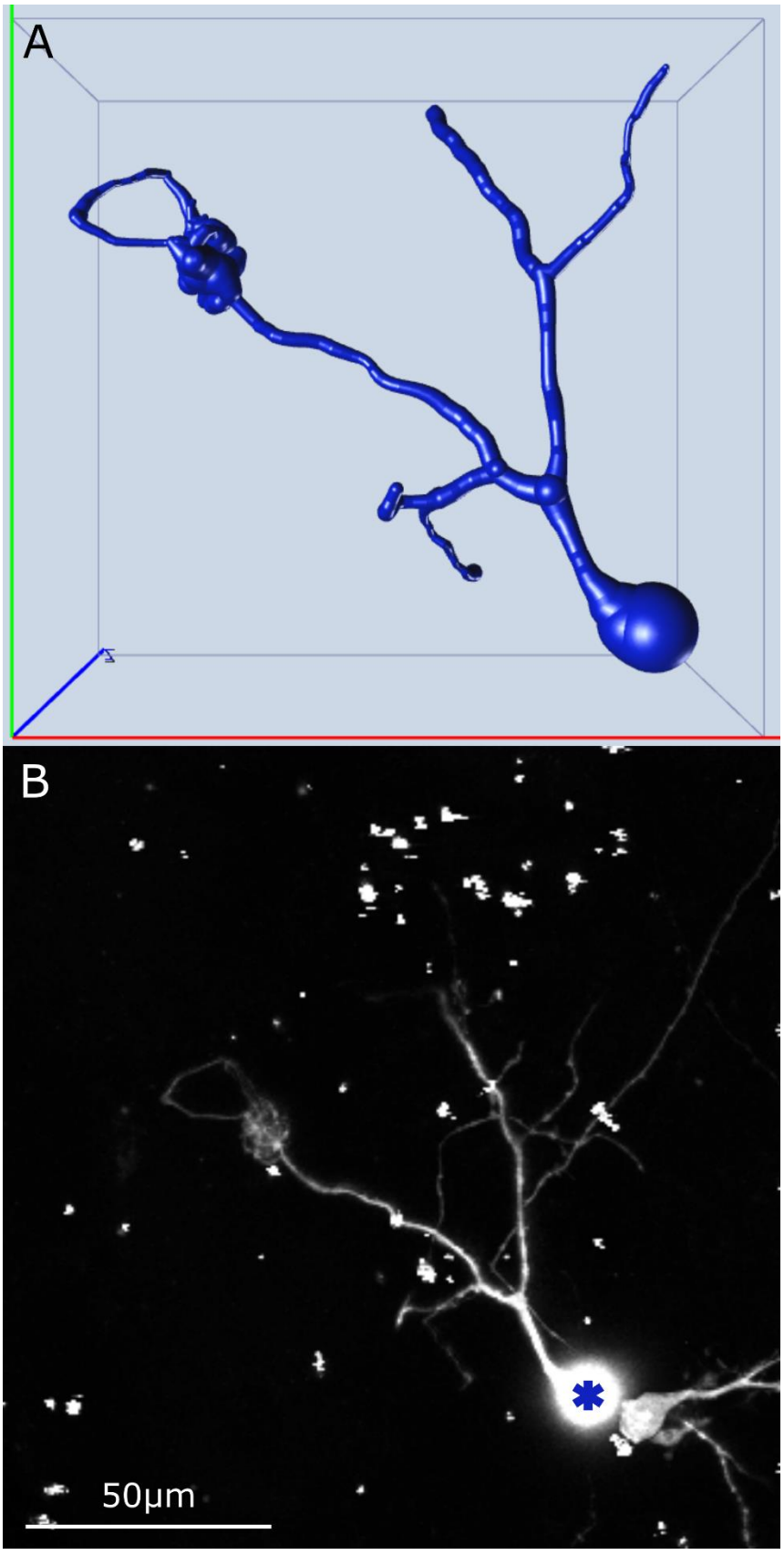

Supplementary Figure 2: Lateral PN with only one stem arising from the soma. A Reconstruction of the neuron displayed below, showing only one stem that arises from the soma. **B** Microscopic image of a lateral PN with only one soma stem (dark blue asterisk).

List of figures

List of tables

Affidavit

I hereby confirm that my thesis entitled "*Visualization of the secondary olfactory pathway in tubb2b promoter-driven transgenic Xenopus laevis larvae*" is the result of my own work. I did not receive any help or support from commercial consultants. All sources and materials applied are listed and specified in the thesis.

Furthermore, I confirm that this thesis has not yet been submitted as part of another examination process neither in identical nor in similar form.

Hiermit erkläre ich an Eides statt, die vorliegende Dissertation mit dem Titel „*Visualisierung der sekundären olfaktorischen Bahn in tubb2b Promoter-gesteuerten transgenen Xenopus laevis Larven*" eigenständig, d.h. insbesondere selbstständig und ohne Hilfe eines kommerziellen Promotionsberaters, angefertigt und keine anderen als die von mir angegebenen Quellen und Hilfsmittel verwendet zu haben.

Ich erkläre außerdem, dass die Dissertation weder in gleicher noch in ähnlicher Form bereits in einem anderen Prüfungsverfahren vorgelegen hat.

Gießen, 15. August 2024 _____

Daniela Daume

Acknowledgments

An dieser Stelle möchte ich zuerst die Gelegenheit nutzen und mich bei Prof. Ivan Manzini bedanken, dass er mir die Möglichkeit gegeben hat in seiner Arbeitsgruppe meine Doktorarbeit zu schreiben. Ebenso möchte ich mich bei Thomas Hassenklöver für die Unterstützung während meiner Zeit in der Arbeitsgruppe bedanken. Ich bin wirklich froh diese berufliche Möglichkeit gehabt zu haben und freue mich umso mehr, dass ich dadurch so viele wundervolle Menschen kennenlernen durfte.

Die letzten 5 Jahren waren mitunter die schwerste Zeit die ich bisher in meinem Leben erleben durfte. Nicht nur die Covid-Pandemie, die jeden von uns sehr belastet hat, auch die Diagnose zweier chronischer Krankheiten und der Abschied einer geliebten Person haben meine Zeit als Doktorandin sehr überschattet. Umso mehr möchte ich deshalb in dieser Danksagung bewusst auf die schönen Momente zurückschauen und allen danken, die mich in dieser Zeit immer wieder unterstützt haben und mir zur Seite standen.

Beginnen möchte ich dabei mit meiner Familie, insbesondere meiner Mama Ulrike, meinen Papa Uli und meinem Bruder Darwin. Ich bin so unglaublich dankbar in einer so tollen Familie groß geworden zu sein und so viel Unterstützung erfahren zu haben. Ich habe euch alle unglaublich lieb und danke euch, dass ihr immer für mich da seid! Auch wenn Sie nicht mehr bei uns sein kann und diese Sätze lesen, möchte ich mich trotzdem auch bei meiner Oma bedanken und mich an die Zeit mit ihr erinnern. Bis zum Schluss hast du dich immer um mich gesorgt und gefragt wie meine Arbeit läuft. Es wäre schön gewesen, wenn ich dir noch stolz davon hätte erzählen können, dass ich es endlich geschafft habe sie fertig zu schreiben. Natürlich möchte ich mich auch bei Addy, meiner Gote Helga, meinem Onkel Martin, Cousin Manuel und seiner Frau Marice und Baby Mia bedanken, die mir auf jedem Weg zur Seite standen. Zu meiner Familie zähle ich auch meine beste Freundin Isi, mit der ich seit Kindertagen meine Zeit verbringe und die mich ebenso immer unterstützt hat. Danke, dass du immer für mich da bist!

Before I even started my doctoral thesis, I by accident found my Mexican sister when we both did our master thesis in the Manzini lab, which I now count to my family as well. You were the best roommate I ever had and I am so happy to have you as my friend. Thank you, Paola, for all your love and support over the last years! Während

meines Studiums konnte ich ebenfalls viele tolle Menschen kennen lernen, doch bei einer möchte ich mich hier besonders bedanken. Danke Marie, für viele schöne Momente zusammen und deine Unterstützung auf diesem langen Weg!

During my time in the Manzini lab, I also got to know many incredible colleagues, that I now count as my friends. Special thanks go to Lukas Weiss, Thomas Offner, Sara Joy Hawkins, Lukas Wichmann, Kati Dittrich, Joscha Alt, Melina Kahl, Michelle Endres & Yvonne Gärtner for so many beautiful moments together. Through ups and downs, we all always supported each other, which made us stronger as a group. I miss the days with all of you and hope we can meet again from time to time in the future. Außerdem möchte ich mich bei Joscha, Johannes, Mirjam und Prof. Reinhard Lakes-Harlan aus unserer Nachbararbeitsgruppe bedanken, die immer mit Rat und Hilfe zur Seite standen und mit denen wir immer eine schöne Zeit hatten. In meiner Zeit als Doktorandin durfte ich außerdem vier tolle Bachelorstudentinnen betreuen, auf die ich sehr stolz bin. Wir hatten eine schöne Zeit zusammen und ihr habt eure Arbeiten wirklich sehr gut gemacht. In dieser Zeit war ich besonders froh Hanne Jeckel und ihren Freund Lennart Schulte kennengelernt zu haben. Vielen Dank für eure Unterstützung und die vielen schönen Abende in der Boulderhalle zusammen mit Luki. In meinem letzten Jahr im Institut durfte ich außerdem noch Christina Anding kennen lernen, dich sich mit Herzblut um unsere froggies und fishies gekümmert hat. Schon nach kurzer Zeit fanden wir viele gemeinsame Interessen heraus und es entstand eine tolle Freundschaft, die ich bis heute schätze. Danke, dass du immer für mich da warst und wir uns immer gegenseitig unterstützen!

Aber in all dieser schweren Zeit, in der ich irgendwann dachte das es keine guten Dinge mehr geben wird, lernte ich eine Person kennen, die so viel Licht ins Dunkle gebracht hat, dass ich wieder nach vorne schauen konnte und so unglaublich viel Halt und Liebe fand. Ich möchte mich deshalb ganz besonders bei meinem Freund Joshi bedanken, denn ohne deine Unterstützung wäre ich nie so weit gekommen. Du hast mich immer wieder aufgebaut, wenn ich dachte, dass ich es nicht weiter schaffe und hast nie aufgehört an mich zu glauben. Ich bin so unendlich glücklich, dass wir uns kennengelernt haben und ich liebe dich über alles!

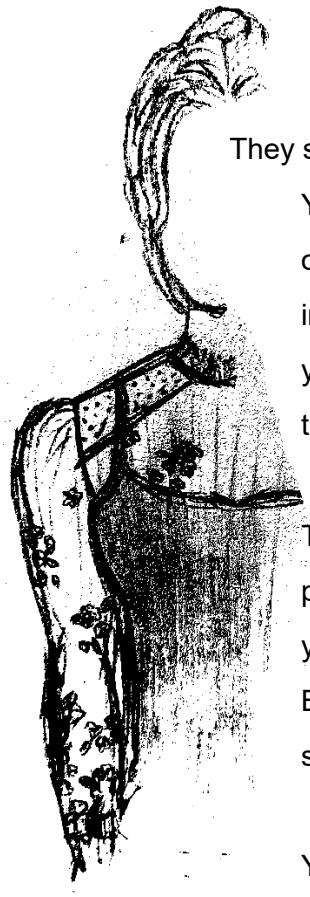

They say,
Your healing begins
on a day you look
in the mirror and
you don't recognize
the person staring back.

They are not the
person you have known
your whole life.
But an empty, withering
shadow.

You wonder where
that person has gone
and about the ache
that has pushed them
so far away.

And so you promise
this broken version
of yourself that
you'll find a way back,
just little steps day by day.

Courtney Peppernell